UNIVERSITY OF CALIFORNIA, SAN DIEGO

SAN DIEGO STATE UNIVERISTY

The Development and Characterization of N-Heterocyclic Carbene Based Catalysts

A dissertation submitted in partial satisfaction of the

requirements for the degree Doctor of Philosophy

in

Chemistry

by

Zephen Gregory Specht

Committee in charge:

University of California, San Diego

Professor Yitzhak Tor, Co-Chair
Professor Richard Herz
Professor Clifford Kubiak

San Diego State University

Professor Douglas Grotjahn, Chair
Professor Mikael Bergdahl
Professor Asfaw Beyene

2012

The Dissertation of Zephen Gregory Specht is approved, and it is acceptable in quality and form for publication on microfilm and electronically:

_____

_____

_____

_____

_____

Co-Chair

_____

Chair

University of California, San Diego

San Diego State University

2012

TABLE OF CONTENTS

LIST OF ABBREVIATIONS

Å	angstrom, 1×10^{-10} m
°C	degrees Celsius
^{13}C-NMR	carbon-13 nuclear magnetic resonance
calcd	calculated
Cp	cyclopentadienyl
Cp*	pentamethyl cyclopentadienyl
d	doublet
δ	chemical shift in ppm
DCM	dichloromethane, methylene chloride
DMF	dimethylformamide
DMSO	dimethylsulfoxide
dd	doublet of doublets
eq	equivalent
EtOAc	ethyl acetate
g	grams
h	hours
^{1}H-NMR	proton nuclear magnetic resonance
Hz	Hertz
*i*Pr	isopropyl
IR	infrared
*t*Bu	*tert*-butyl
J	coupling constant

Kcal	kilocalories
M	molar
m	multiplet
mm	millimeter
Me	methyl
MeOH	methanol
mg	milligrams
MHz	megahertz
min	minutes
mL	milliliters
mmol	millimoles
mol	moles
^{15}N-NMR	nitrogen-15 nuclear magnetic resonance
NHC	*N*-heterocyclic carbene
NMP	*N*-methyl-2-piperidone
p.	page
Ph	phenyl
q	quartet
rt	room temperature
σ	sigma
s	singlet
t	triplet
THF	tetrahydrofuran

TMS	trimethylsilyl
TOF	turnover frequency
TON	turnover number
VT	variable tempature

LIST OF FIGURES

LIST OF GRAPHS

LIST OF SCHEMES

LIST OF TABLES

ACKNOWLEDGEMENTS

I would like to acknowledge Professor Douglas Grotjahn for his support as the chair of my committee. Through multiple drafts and many long nights, his guidance has proved to be invaluable. Dr. LeRoy Lafferty was instrumental in helping to acquire the 2D NMR data for many of the compounds with in my research. The x-ray crystallography structures, which greatly added to the understanding of how sterics affected the chelating nitrogen atom on the iridium metal center, were solved by Arnold Rheingold, Curtis Moore, Antonio G. DiPasquale, and James Golen. The Raman spectra obtained for the iridium complexes was made possible with the help of Dr. David Pullman.

I would also like to acknowledge the support of all of the teachers and administration in the UCSD Socrates program for giving me a chance to learn more about how to effectively teach and communicate science. In particular I am grateful to Duke Riley, chemistry teacher at Eastlake High School, without whom my work in the Socrates program would not have been possible. It is their support that helped me in an immeasurable way.

Chapter 1, in part, is a reprint of the material as it appears in *Chemistry--A European Journal*, **2011**, *17*(24), 6606-6609 (Specht, Zephen G.; Cortes-Llamas, Sara A.; Tran, Hai N.; van Niekerk, Christoffel J.; Rancudo, Khing T.; Golen, James A.; Moore, Curtis E.; Rheingold, Arnold L.; Dwyer, Tammy J.; Grotjahn, Douglas B.). The dissertation author was the primary investigator and author of this paper. Chapter 1, in part, also contains a reprint of the material as it appears in the *Journal of the American Chemical Society*, **2011**, *133*, 19024–19027

submitted by authors Douglas B. Grotjahn, Derek B. Brown, Jessica K. Martin, David C. Marelius, Marie-Caline Abadjian, Hai N. Tran, Gregory Kalyuzhny, Kenneth S. Vecchio, Zephen G. Specht, Sara A. Cortes-Llamas, Valentin Miranda-Soto, Christoffel van Niekerk, Curtis E. Moore, and Arnold L. Rheingold. The dissertation author was not the primary investigator or author of this paper. Chapter 1, in part, has also been submitted for publication of the material as it may appear in *European Journal of Inorganic Chemistry*, **2012**, submitted by authors Specht, Zephen; Grotjahn, Douglas; Moore, Curtis; and Rheingold, Arnold. The dissertation author was the primary investigator and author of this paper.

In chapter 3, the work on developing metal-free catalysts for the esterification of triglycerides was done with the help of Arianna Pérez. Also in chapter 4, the work on developing catalysts with N-heterocyclic carbene ligands was carried out with the help of Khoi Le.

Chapter 4, in part, contains material as it may appear in an article which has been submitted for publication to the *Journal of Chemical Education*, **2012**, by authors Specht, Zephen; Raley, Duke. The dissertation author was the primary investigator and author of this paper.

VITA

2000-2001	Laboratory Technician at Monsanto, DeKalb, Illinois
2002	Bachelors of Science, Northern Illinois University
2002-2004	Teaching Assistant, Department of Chemistry and Biochemistry, Northern Illinois University
2004	Master of Science, Northern Illinois University
2004-2006	Research Assistant at Siplast, Arkadelphia, Arkansas
2006-2012	Teaching Assistant, Department of Chemistry and Biochemistry, San Diego State University
2008	Summer Intern at Pfizer, La Jolla, California
2009	Teaching Assistant, Department of Chemistry and Biochemistry, University of California, San Diego
2010-2011	NSF GK-12 Recipient, Socrates Fellow at the University of California, San Diego
2012	Doctor of Philosophy, University of California, San Diego

PUBLICATIONS

“Spectral Fingerprints of Bacterial Strains by Laser-Induced Breakdown Spectroscopy” Kim, T.; Specht, Z. G.; Vary, P. S.; Lin, C. T., *Journal of Physical Chemistry B*, **2004**, *108*, 5477-5482.

“Enabling Bifunctionality and Hemilability of N-Heteroaryl NHC Complexes” Specht, Zephen G.; Cortes-Llamas, Sara A.; Tran, Hai N.; van Niekerk, Christoffel J.; Rancudo, Khing T.; Golen, James A.; Moore, Curtis E.; Rheingold,

Arnold L.; Dwyer, Tammy J.; Grotjahn, Douglas B. *Chemistry--A European Journal,* **2011***, 17*, 6606-6609.

“Evolution of Iridium-Based Molecular Catalysts during Water Oxidation with Ceric Ammonium Nitrate “ Grotjahn, Douglas B.; Brown, Derek B.; Martin, Jessica K.; Marelius, David C.; Abadjian, Marie-Caline; Tran, Hai N.; Kalyuzhny, Gregory; Vecchio, Kenneth S.; Specht, Zephen G.; Cortes-Llamas, Sara A.; Valentin Miranda-Soto, Christoffel van Niekerk, Curtis E. Moore, and Arnold L. Rheingold*, Journal of the American Chemical Society*, **2011**, *133,* 19024-19027.

PRESENTATIONS

“Synthesis and Characterization of Bifunctional N-Heterocyclic Carbene Complexes” Specht, Zephen; Lev, Daniel A.; Grotjahn, Douglas B.; DiPasquale, Antonio G. From Abstracts, 41st Western Regional Meeting of the American Chemical Society, San Diego, CA, United States, October 9-13, **2007**.

“Synthesis, Characterization, and Catalytic Properties of Bifunctional N-Heterocyclic Carbene Complexes” Specht, Zephen; Lev, Daniel A.; Grotjahn, Douglas B.; Rheingold, Arnold L.; DiPasquale, Antonio G. Abstracts of Papers, 236th ACS National Meeting, Philadelphia, PA, United States, August 17-21, **2008**.

“N-heterocyclic Carbenes with Functional Ligands for the Oppenauer-type Oxidation of Alcohols” Zephen Specht, Daniel A. Lev, Hai Tran, Sara Cortes, Khing Rancudo, Christoff van Niekerk, Douglas B. Grotjahn, and Arnold Rheingold, Curtis Moore, Antonio G. DiPasquale, VII Simposio Internacional: Investigación Química en la Frontera, Tijuana, B.C., November 17-19, **2009.**

“Novel N-pyridyl imidazolidene carbenes coordinated to iridium” Zephen Specht, Douglas Grotjahn, Curtis E. Moore, Arnold L. Rheingold, 243rd ACS National, San Diego, CA, March 25-29, **2012**.

ABSTRACT OF THE DESSERTATION

The Development and Characterization of N-Heterocyclic Carbene Based Catalysts

by

Zephen Gregory Specht

Doctor of Philosophy in Chemistry

University of California, San Diego, 2012
San Diego State University, 2012

Professor Douglas Grotjahn, Chair

Professor Yitzhak Tor, Co-Chair

The following body of work is a compilation of five years of research at San Diego State University as well as one year spent working as a fellow in the GK-12 program through the Socrates program at the University of California, San Diego. During that time I focused on creating iridium NHC complexes that featured nitrogen containing ring substituents that showed the possibility of acting as a pendant base. The two heterocyclic substituents on which I focused were derivatives of pyridine and pyrimidine groups attached to an NHC ligand. The ability of the nitrogen to coordinate to the metal center was controlled through the use of sterically bulky groups adjacent to the nitrogen atoms of the pyridine and pyrimidine rings. The resulting metal complexes were studied for their structure,

dynamics, and catalytic activity using a variety of experimental systems, with the notable success of cyclizing primary and secondary amines onto alkenes in an intramolecular fashion.

For the future work, the two projects that I developed for my assistants, Khoi Le and Ariana Perez, will be covered. For Khoi Le the research goal is to develop tridentate ligands based on my previous NHC research with bi-dentate ligands. These complexes will then be tested for their ability to reduce glycerin, a common by product of saponification, into more commercially interesting molecules. Ariana Perez was tasked with developing nitrogen containing ring systems as metal free catalysts for the refinement of triglycerides into methyl esters for the production of bio-diesel. Her work was based on literature reports of DMAP working as an efficient nucleophilic catalyst.

Finally the work that I did as an NSF GK-12 fellow will be covered as well. During that time I was developing my skills in communication and implementing several new laboratory experiments aimed at improving high school students understanding of basic chemistry. Of particular note, I worked on two laboratory experiments that helped to develop the students understanding of electron orbitals and molecular shapes as dictated through bonding. This experience proved to be a great opportunity to not only refine my teaching abilities, but also to see chemistry from a different perspective.

CHAPTER 1 – Research Overview and Background

The following body of work is a compilation of research done during my six years of research at San Diego State University as well as my time spent working as a fellow in the GK-12 program through the Socrates program at the University of California, San Diego. During this time I worked on developing novel N-heterocyclic carbene (NHC) ligands that featured nitrogen containing heterocyclic substituents that could either coordinate to a metal center or dissociate. In this respect the (heteroaryl)NHC complexes would have a type of pendant base, which may help in the transfer of protons and allow for increased catalytic activity in certain reactions. In my final year of graduate school I was also involved in establishing projects and mentoring for two undergraduate students, Ariana Perez and Khoi Le, both of whom are working on developing bio-renewable technologies.

Catalysts allow for the lowering of energetic barriers to reactions, which can make chemical processes lower in cost or even allow for other chemical reactions to be possible at all. A large part of the global economy relies on catalysts, estimated at about 900 billion US dollars annually.[1] It has also been estimated that about 90% of all chemical products produced commercially involve catalysts in some way.[2] Examples include polymer synthesis using Ziegler–Natta catalysts, Fischer–Tropsch synthesis, the Haber-Bosch fixation of atmospheric nitrogen, or the Grubbs catalyst for metathesis.[3-5] The importance of catalysis in science can also be measured by the number of Nobel Prizes given recently for work in synthesis; to Knowles, Noyori and Sharpless for their work on

chirally catalyzed hydrogenation reactions (2001); to Chauvin, Grubbs, and Schrock for the development of the metathesis method in organic synthesis (2005); and the recent recognition of Heck, Negishi and Suzuki for palladium-catalyzed cross couplings in organic synthesis (2010).[6]

Two common ways of altering a catalyst's reactivity are either to change its steric or electronic properties. One example of this is the evolution of Buchwald's palladium catalysts with biphenyl phosphine ligands, which are primarily used in coupling chemistry such as Suzuki-Miyaura cross-coupling reactions and amination reactions.[7] The general structure of the catalyst ligands is shown in Figure 1 and summarizes the several areas of the ligand that influence the performance of the catalyst. With respect to control over sterics, the alkyl groups attached to the phosphorus atom (where binding of the palladium atom takes place) aid in the determination of the rate of reductive elimination. The steric demand of the second phenyl ring of the phosphine ligand also helps lowering the oxygen sensitivity of the catalyst. Electronically the ligand can be tuned at several positions, where the most notable position is at the R groups on P. For R = alkyl, electron density is increased at the phosphorus and this helps to increase the rate of substrate oxidative addition to the palladium catalyst.

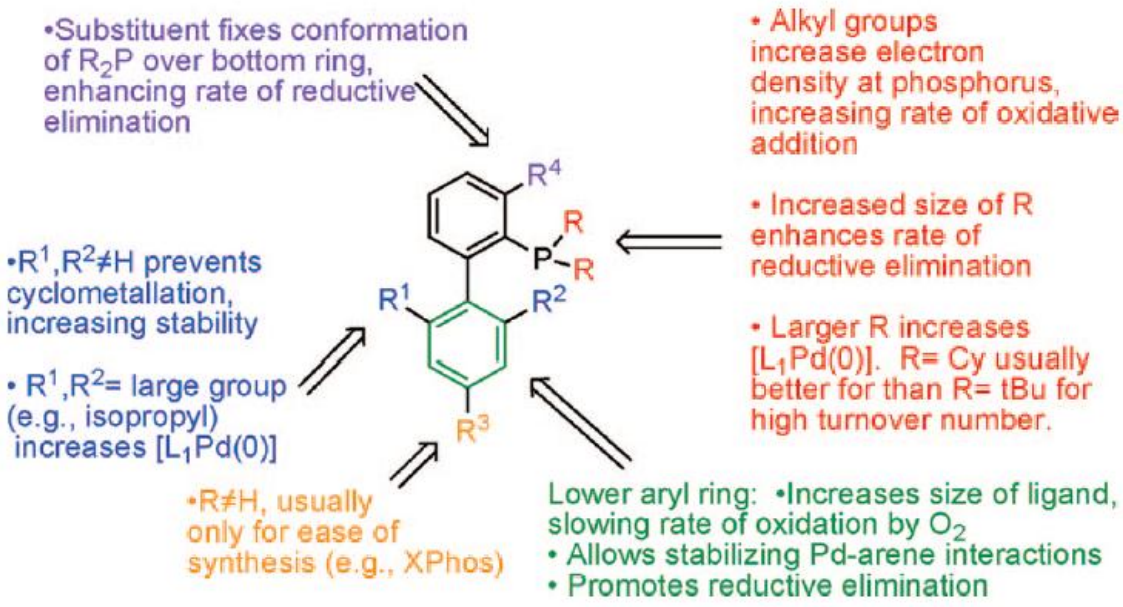

Figure 1. Diagram of how substitutions on the phosphine ligand affect the reactivity of Buchwald's palladium catalysts; image taken from Martin and Buchwald.[7]

Another approach to developing catalytically interesting systems is to use a co-catalyst or a complex that has an interactive secondary structure that can increase the catalyst's effectiveness. Examples of use of secondary interactions can be found in the pioneering work done by Kumada who studied the influence of remote pendant functional groups on directing nucleophilic attacks on allyl-palladium intermediates.[8] Figure 2 shows two possible ways in which enantioselectivity could be achieved during a nucleophilic attack on an allyl-palladium compound: (A) use of a chiral ligand that produces chiral product through sterics, and (B) a chiral ligand that uses a pendant group to electrostatics direct the formation of chiral product. A few examples of the use of a pendant group, in this case as a base, are the Noyori catalysts that were designed for the enantioselective hydrogenation of ketones, aldehydes, and imines.[9-10] These

ruthenium-based catalysts are thought to work by transferring a hydride from the metal center along with a proton from an adjacent amine group to the ketone containing compound. For these reactions it is clear that the ruthenium catalyst requires a ligand, like a 1,2-diamine, in order to help transfer a hydrogen atom to the incoming ketone group or the reaction will become sluggish at best.

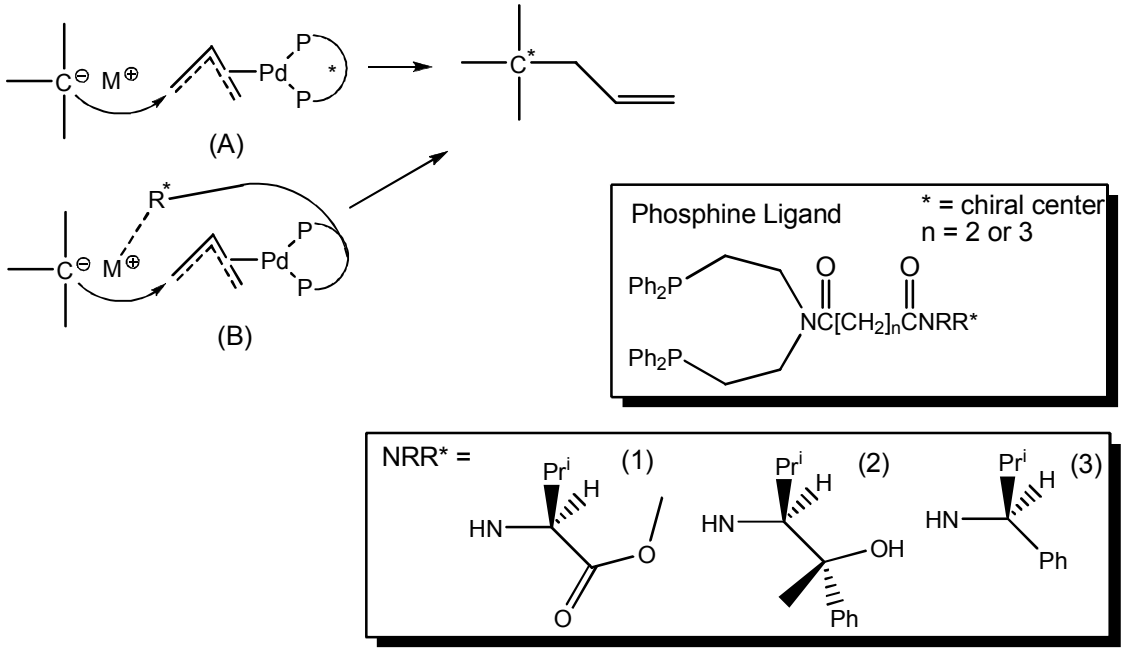

Figure 2. Diagram of the phosphine ligands that were designed by Kumada[8] to have chiral groups (1-3) that could have an influence on the cation of an incoming molecule (shown in B).

The development of bifunctional catalysts has also been explored within the Grotjahn group, with the emphasis before this thesis work being on phosphine ligands. In particular there are two catalytic reactions of great interest; *anti*-Markovnikov alkyne hydration and alkene isomerization.[11-15] Figure 3 depicts the transformation of an alkyne group into an aldehyde using a ruthenium catalyst which has phosphine ligands with imidazolyl or pyridyl groups that can

act as pendant bases.[16] In Figure 4 another ruthenium based catalyst is shown to facilitate alkene isomerization through the use of a single phosphine ligand with an imidazole ring attached to it.[17] The basic nitrogen atom in the imidazole ring is thought to transfer protons from and to coordinated alkene and allyl intermediates as the alkene group is moved.

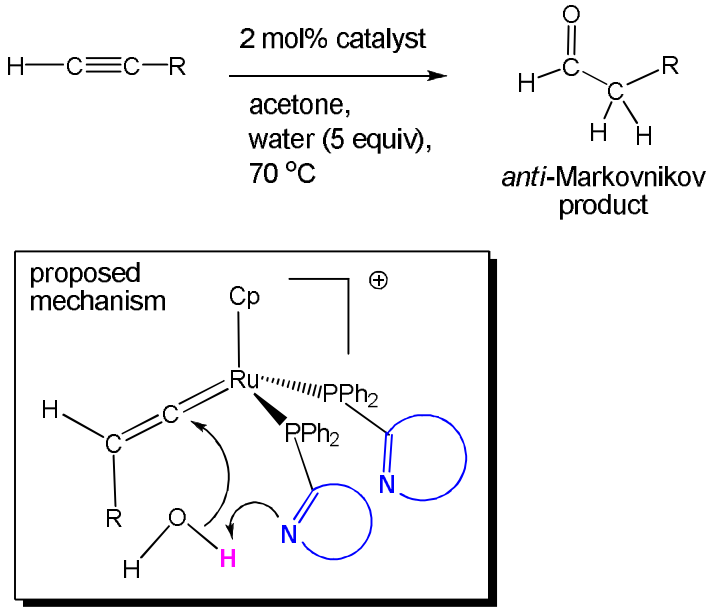

Figure 3. The *anti*-Markovnikov alkyne hydration reaction is shown along with one key step of the proposed catalytic mechanism.[16]

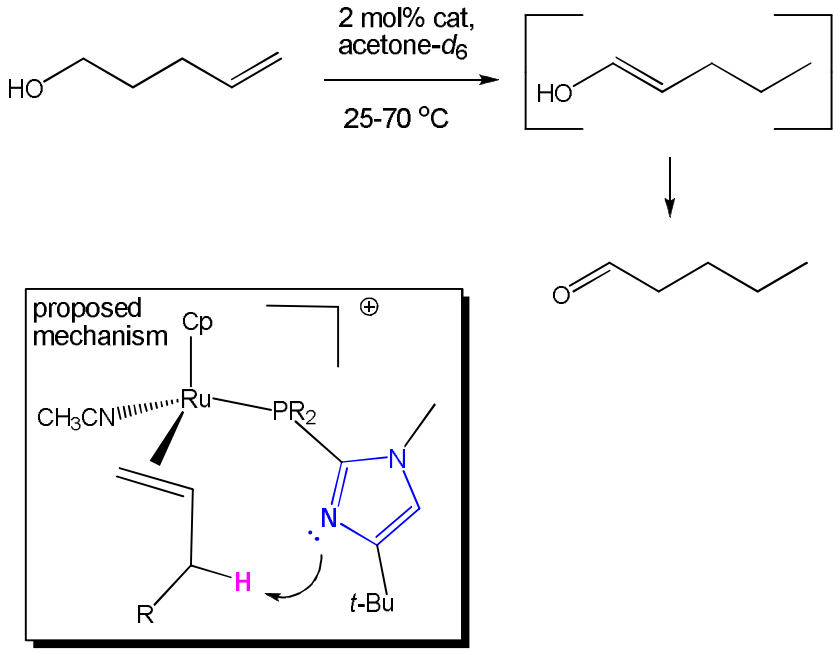

Figure 4. Alkene isomerization reaction is shown using a ruthenium catalyst with a phosphine imidazole ligand which uses the unhindered nitrogen atom to act as a pendant base for proton transfer.[17]

With the knowledge of how to develop successful phosphine ligand-based bifunctional catalysts in hand, the next step was to design a more robust family of catalysts, hopefully lacking the air sensitivity shown by the CpRu-phosphine species just mentioned. Since Arduengo isolated the first stable NHC in 1991[18-19] the study of stable carbenes[20-23] and their ability to carry out catalytic reactions[24-27] have attracted a good deal of attention. Those NHCs that are bound to a metal center have provided an alternative to tertiary phosphines in homogeneous catalysis due to their strong σ-donating ability and poor back bonding.[23, 28-35] Compared to their phosphine counterparts, NHC complexes in general also show a higher stability to air and moisture, as well as a greater thermal stability in oxidizing acidic conditions.[31, 35] The carbene-metal complexes have been shown

to be extremely versatile and stable catalysts for a wide range of reactions including olefin metathesis,[36-44] transfer hydrogenation,[45-48] hydroformylation,[49-50] hydrosilylation,[51-52] C-C coupling reactions,[53-69] and polymerization reactions.[70]

As discussed above, electronic and steric optimization of the catalytic site(s) is possible through ligand design. In contrast, further improvement of catalyst performance through NHC functionalization has been studied using a variety of NHC ligands bearing substituents such as pyridine,[33, 71-86] pyrimidine ligands[51, 87-89], pyrazole,[60, 90-93] pyridazine,[94] ester, keto, ether,[95] oxazoline,[52, 96-98] amine,[99-101] imine,[102-104] amido,[105-107] and thioether[108-112] donor functions. Unlike phosphines, which tend to bond strongly to metals, the lone pair of electrons on nitrogen, oxygen, or sulfur in these ligands generally form weak bonds with transition metals.[113] This may allow for an active site on the metal center in question to be turned “on and off” given the right conditions,[114-117] although pendant ligand basicity was not the subject of study in the examples above.

Even though the *possible* role of a pendant pyrimidine (cite 2009 Gnanamgari) or aliphatic amine (cite Jimenez 2008) on an NHC has been discussed, it appears as if these studies have not been able to demonstrate the ability of a pendant base to aid in the transfer of protons. If anything, researchers either add coordinating substituents simply to increase coordination number (and perhaps overall complex stability, through the chelate effect) or to increase coordination number but add a hemilabile, weakly coordinated ligand to facilitate catalysis.

In contrast, my research was focused on determining if a chelating nitrogen containing ring system, which is part of an NHC ligand, could be created that would act as a pendant base for proton transfer during catalytic reactions. The additional advantage in creating a catalyst with a pendant base is that during the addition of a C-H or X-H sigma bond of an incoming molecule (Figure 5, right) the catalyst would not undergo a change in formal oxidation state, which could be a rate limiting step in an overall catalytic cycle.[118-119] A series of NHC based ligands were proposed because NHC have been shown to form very stable carbon-metal bonds due to their strong sigma donating character.[120] In order to design the optimum pendant base the plan was to adjust both the steric around the chelating nitrogen as well as the electronic nature of the nitrogen group. The general idea (Figure 5) shows the pendant base could not only serve to transfer protons, but also prevent the metal from going through a change in oxidation state.

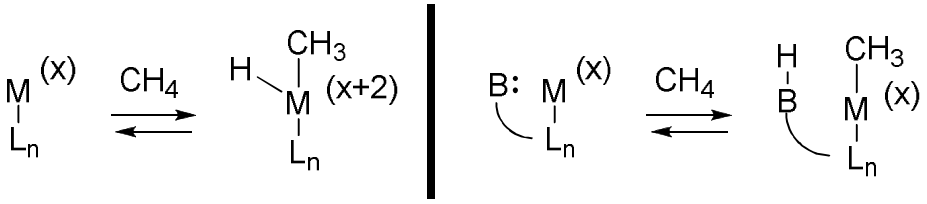

Figure 5. The general idea behind designing a series of pendant bases on a strong NHC ligand, enabling more stable catalysts that will not change their oxidation state (x) during a catalytic cycle.

Using the general idea of catalysts with pendant bases, or basic nitrogen atoms, the groundwork was laid for designing the two projects for Khoi Le and Ariana Perez. For Khoi Le the research goal has been to develop tridentate ligands based on coupling 2,2'-bipyridine to a imidazole ring and subsequently

form an NHC bound to a metal center. These complexes will then be tested for their ability to convert glycerin, a common by product of saponification, into more commercially interesting molecules, such as 3-hydroxypropanal and propane-1,3-diol. Ariana Perez was tasked with developing nitrogen-containing heterocycles as metal free catalysts for the refinement of triglycerides into methyl esters for the production of bio-diesel. Her work was based on literature reports of DMAP working as an efficient nucleophilic catalyst.

While in the middle of my research work with Dr. Grotjahn I also spent a year in the NSF GK-12 program. During that time I was developing my skills in communication and implementing several new lab experiments aimed at improving high school students' understanding of basic chemistry. My mentor, Duke Raley, was extremely helpful in developing my abilities to both explain existing lesson plans and lectures, as well as develop new laboratory experiments for the students to try. Of particular note, I worked on two lab experiments that helped to develop the students understanding of electron orbitals and molecular shapes as dictated through bonding.

CHAPTER 2 – Iridium Complexes with NHC Ligands Featuring Pyrimidine Pendant Groups

The overall research objective of this thesis is the development of complexes that are able to act as better catalysts by using bifunctional ligands, as described in Chapter 1. Scheme 1 outlines the basic idea behind changing the steric bulk of a pendant base substituent. The chelating nitrogen group, depicted here as part of a ring system that could be either a pyrimidine, pyridine, or imidazole ring, is part of an NHC ligand attached to a transition metal. The chelation of the nitrogen atom is depicted as being weak and allows for the insertion of another molecule, where by the proton on the incoming molecule will be attacked to the nitrogen atom as the molecule binds to the metal. An example of how important sterics can be for determining chelating effects can be seen in the work by Hintermann (2009) using ruthenium catalysts.[121] Figure 5 outlines the difference that changing the steric around the chelating nitrogen atoms has resulted in alkyne hydration catalysts which are at most 5 times faster with the addition of *tert*-butyl groups adjacent to the chelating nitrogen atoms.

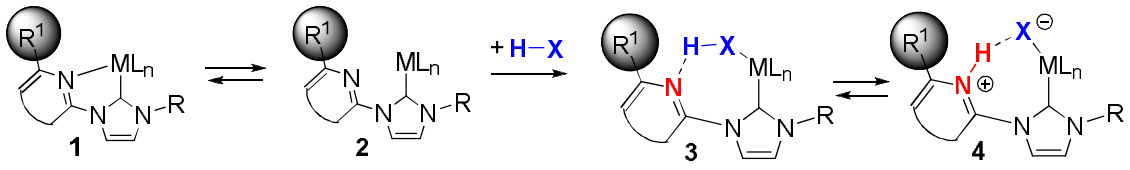

Scheme 1. Proposed interconversions of (heteroaryl)NHC complexes.

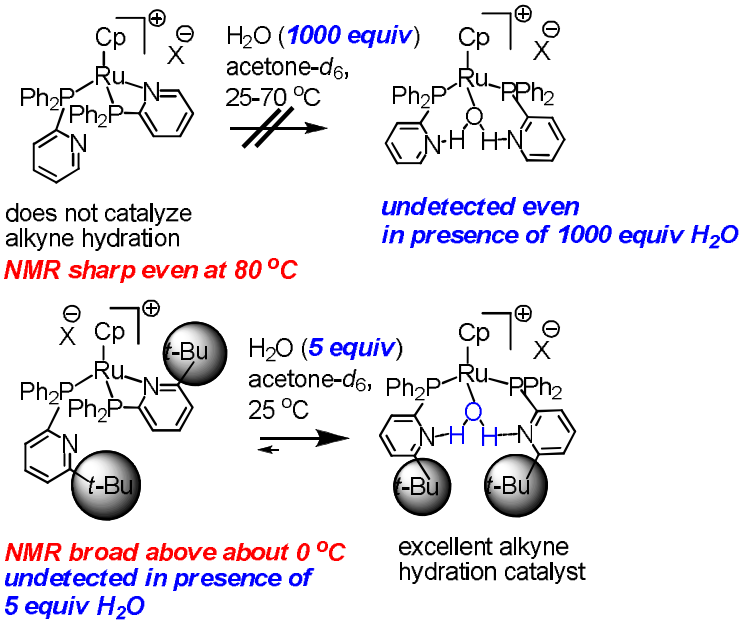

Figure 6. The importance of pendant base substituents on structure and the opening of chelates as demonstrated with ruthenium based catalysts, Grotjahn (2008).[122]

Specifically, the goals were to use NHC based ligands due to their more robust nature relative to phosphine ligands, adding a weakly chelating side group that could act as a pendant base. A series of NHC ligands were proposed in order to vary the basicity, sterics and electronics of the ligands and the effects of these parameters on the catalytic properties of the corresponding Cp*Ir complexes. The proposed series of ligands is outlined in figure 6, all on Cp*Ir fragments. Complexes **5a**-**c** will be the focus of chapter 2, while complexes **5w**-**z** will be covered in chapter 3. Complex **6**, featuring an (imidazolyl)NHC ligand, was developed by Hai Tran,[123] a fellow researcher in the Grotjahn group during his M.S. thesis research and is included here merely for comparative purposes.

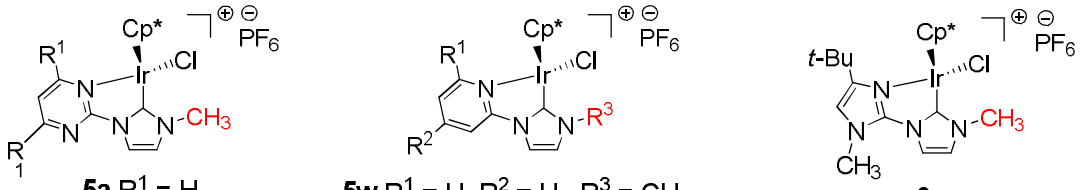

5a R^1 = H
5b R^1 = Ph
5c R^1 = *t*-Bu

5w R^1 = H, R^2 = H, R^3 = CH_3
5x R^1 = *t*-Bu, R^2 = H, R^3 = CH_3
5y R^1 = *t*-Bu, R^2 = H, R^3 = 6-tBu-Pyr
5z R^1 = *t*-Bu, R^2 = *t*-Bu, R^3 = CH_3

6
**created by Hai Tran*

Figure 7. Diagram of the targeted complexes for study showing the variability in pendant heteroaryl rings (pyrimidine, to pyridine, and finally to imidazole) and the increase in steric bulk around the chelating nitrogen groups (hydrogen to *tert*-butyl groups).

Based on the proposed list of changes to the NHC ligand the role of steric bulk around the chelating nitrogen atoms will be studied as well as the change in electronics as the rings are varied between pyrimidine, pyridine, and imidazole. Another factor that may be considered are the different basicities of the parent N-heterocyclies; literature pK_a values for the conjugate acids are 1.3 for pyrimidine,[124] 5.2 for pyridine,[125] and 7.9 for imidazole.[126] All other things being equal, on (heteroaryl)NHC ligands it could be assumed that the heteroaryl substituents will exhibit a similar order of basicity.

SECTION 2.1 NHC Ligands with Pyrimidyl Substituents

We initiated our studies on creating a pendant base on an NHC ligand utilizing a potentially labile nitrogen atom in Fall 2006 and reported parts of this work at conferences in 2007 and 2008.[124,125] Meanwhile, in early 2009 Crabtree's group.[88, 127-128] reported the complex **5a-Bu** shown in Figure 8, which is very similar to **5a** in figure 7. For **5a-Bu**, no specific evidence for the role of the

pyrimidine nitrogens in catalysis (other than metal-nitrogen coordination) was observed. Moreover, the NMR spectrum of Crabtree's iridium complex was reported to remain sharp in an NMR probe heated up to 110 ^{o}C, indicating that the nitrogen-metal bond remained intact. Significantly, the persistence of sharp NMR signals even at high temperatures would be consistent with de-coordination of the pyrimidine and rotation about the pyrimidine-NHC bond being a process with a high activation barrier. The results of Crabtree supported our hypothesis that in order to fully realize the potential of NHC ligands with pendant heterocyclic bases their ability to chelate with a metal must be decreased. Here we report successful strategies toward achieving this aim, which should be of general application to NHC chemistry.[129]

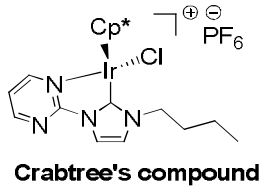

Crabtree's compound

Figure 8. Cp*Ir NHC compound **5a-Bu** reported by Crabtree in 2009, similar to the targeted pyrimidine compound **5a** except for an n-butyl group on the carbene nitrogen atom instead of a methyl group.[88]

SECTION 2.2 Synthesis of Precursors for Chelating (Pyrimidyl)NHC Ligands

NHC iridium complexes are made by first developing imidazolium salts which can be deprotonated to make free carbene, either in a first step or in presence of transition metal. In order to make the requisite imidazolium salts, two different synthetic routes, labeled A and B, were carried out as shown (Scheme 2). Also, because **5a** was judged to be so similar to **5a-Bu**, once the latter

complex, its crystal structure, and lack of evidence for the role of coordinated N as pendant base had been reported, we decided it was not worth making **5a** itself because the effect of having an N-methyl versus N-butyl group on the chemistry was expected to be minor at most.

Coupling of 2-chloropyrimidine with neutral 1-substituted imidazoles (Scheme 2, Route A) is a very direct route, reported by Strassner et al.[87] recently as a way to make imidazolium salts **8-H** and **9-H**. Using **7-Ph,**[130] we made new derivatives **8-Ph** and **9-Ph** in a similar way, but found that using NMP (N-methylpyrrolidinone) was helpful because of the solubilities of reactants and products. It should be noted here that although the iridium complexes using **9-H**[87] and **9-Ph** were not listed as part of the original plan for comparing iridium complexes, these ligands were developed so that the steric effects of the second, non-heteroaryl NHC substituent on chemistry at the iridium center could be tested.

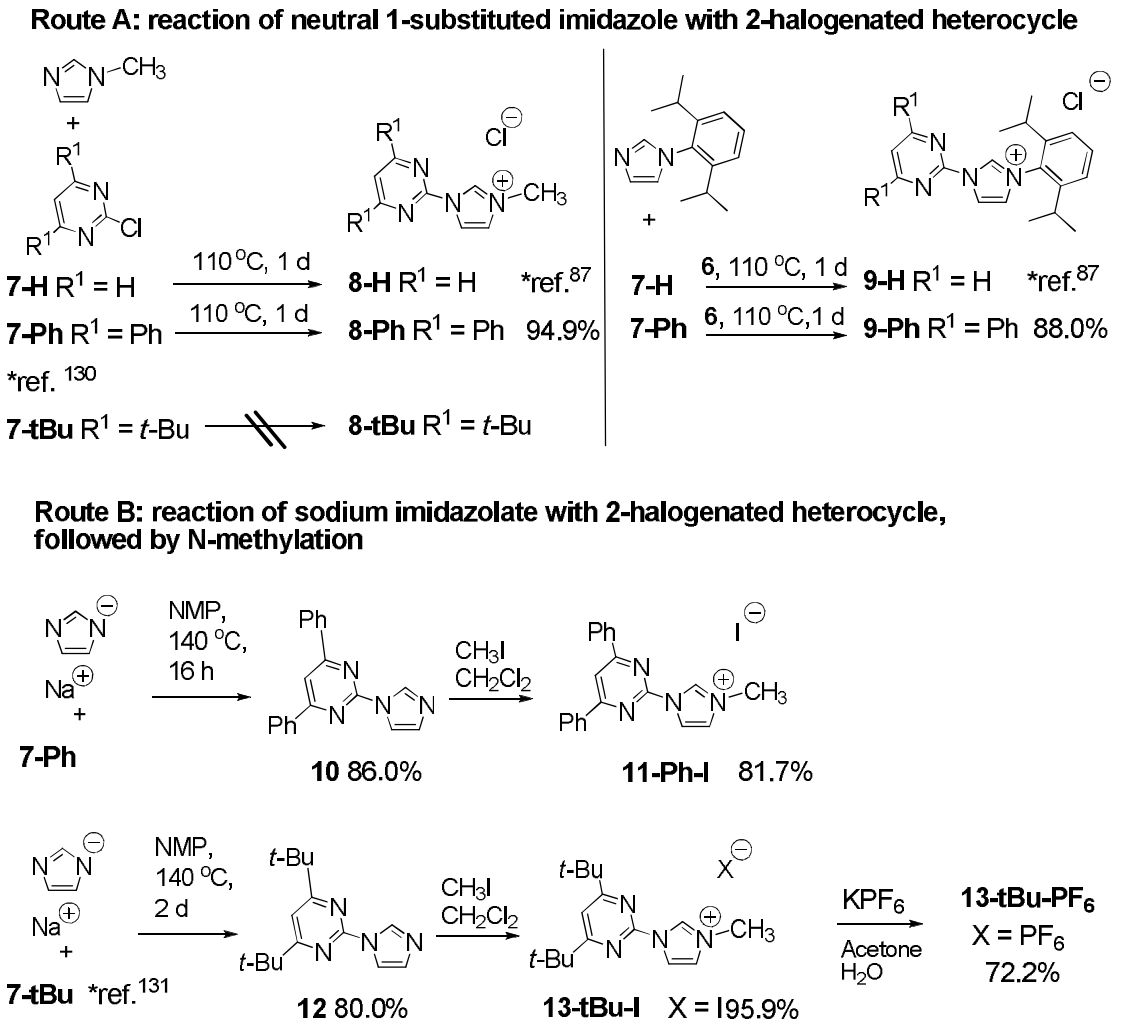

Scheme 2. Synthetic routes for synthesis of precursors for chelating NHC ligands.

Successful synthesis of the di-*tert*-butylated system was achieved using Route B (Scheme 2) starting with deprotonating imidazole with sodium hydride and then adding **7-tBu**[131] to form **12**. Subsequent methylation with methyl iodide gave **13-tBu-I**. Final ion exchange using potassium hexafluorophosphate in methanol gave **13-tBu-PF$_6$**. The salts were characterized by elemental analysis

and NMR spectroscopy. The ^{1}H NMR spectra showed a very low field resonance in the range δ 9-11 ppm characteristic of the NC*H*N imidazolium proton.

SECTION 2.3 Synthesis of (Pyrimidyl)NHC Silver Complexes and Ir(III) Derivatives

Silver was used in order to prevent the NHC from forming unwanted complexes, in the form of silver oxide, was used to form air stable silver NHC following the methods reported by Nolan et al.[132] The (pyrimidyl)NHC silver complexes were isolated in the case of the imidazolium salts where chloride had been exchanged for the hexafluorophosphate anion. Transformations of the imidazolium salts to their corresponding silver-NHC complexes led to downfield shifts of the C-2 carbon from 135-138 ppm to 183-185 ppm, respectively. Interestingly, the imidazolium salt, **13-tBu-PF$_6$**, having the hexafluorophosphate as the counter anion appeared to form bis-carbene complexes with silver. In the case of **13-tBu-PF$_6$**, the ^{13}C NMR signal for the carbene carbon peak bound to silver (^{107}Ag and ^{109}Ag has a spin of ½) gave a set of doublets at 138.7 ppm and 183.8 ppm. The rest of the isolated silver carbene complexes only showed a broad ^{13}C NMR singlet for the carbene carbon. The isolated silver compounds were air stable and only a small amount of degradation was seen upon exposure to light, even after several days. It should also be noted silver carbene of the pyrimidine salt **9-Ph** was previously reported by Strassner[87] and **5a-Bu** along with its silver NHC complex reported by Crabtree.[88]

Transmetallation from the silver carbene complexes of the aforementioned complexes to the $(Cp^*IrCl_2)_2$ was carried out under light and oxygen-free conditions in CH_2Cl_2 or tetrahydrofuran at room temperature to form the iridium carbene complexes. For iridium complexes **5a**, **5b-Cl** (with a chloride anion), and **5c** the silver intermediate were isolated prior to transmetallation with the iridium dimer. The reaction for compounds **13-tBu-PF_6, 8-Ph, 8-H,** and **9-Ph** also had one equivalent of potassium hexafluorophosphate to remove one of the chlorides on the iridium metal. The mixtures were stirred for 12 h, filtered through Celite and concentrated to yield yellowish-orange solids in good to moderate yields. The iridium complexes created from **5b** (with hexafluorophosphate as an anion) was also prepared in two steps, without isolation of intermediate silver carbene complexes,[87, 133] treatment of imidazolium salt with Ag_2O under light and oxygen-free conditions in CH_2Cl_2 at room temperature formed the presumed silver carbene complex in less than 1 h. The $(Cp^*IrCl_2)_2$ was then directly added to silver complex. The reaction for compound **5b** also had one equivalent of potassium hexafluorophosphate. The mixture was stirred for 12 h, then filtered through Celite, concentrated and crystallized to yield yellowish-orange solids in good to moderate yields. Scheme 3 outlines the general methodology for forming the NHC silver intermediates as well as the final iridium complexes. Table 1 shows the yields for the various ligands bound to both silver and iridium. The samples were all characterized by ^1H and ^{13}C NMR and elemental analysis unless noted otherwise.

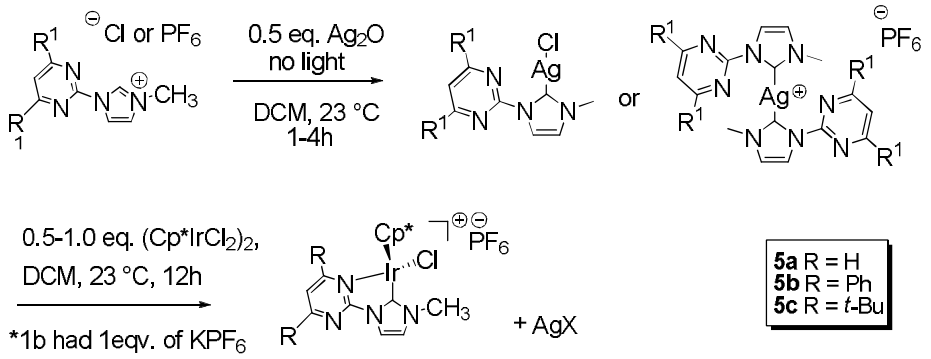

Scheme 3. Synthetic route for Silver NHC complexes that lead to Iridium NHC complexes.

Table 1. Formation of Silver and Iridium (Pyrimidyl)NHC Complexes.[a]

Imidazolium salt	Ag carbene	% Yield	Iridium Complex	% Yield
8-H	**8-H-AgCl**	80.4	**5a**	31.8
8-Ph	**-**	-	**5b**	99.7
8-Ph	**8-Ph-AgCl**	88.9	**5b-Cl**	76.2
9-H	**-**	-	**9-H-Ir**	34.2 (86.9)[b]
9-Ph	**9-Ph-AgCl**	79.0	**9-Ph-Ir**	*
13-tBu-PF6	**13-tBu-Ag**	73.8	**5c**	99.0

[a] Compounds **8-Ph** and **10-Ph** were made without first isolating the silver complex. The iridium complex of **10-Ph** (*) was not isolated due to poor yield and slow formation, presumably due to the steric bulk around the carbene carbon. [b]Compound **10-H-Ir** was first synthesized as with a chloride anion for a yield of 34.2%, then an anion exchange was done using a solution of potassium hexafluorophosphate (2 equivalents) in acetone for a yield of 86.9%.

SECTION 2.4 Crystallographic Studies of (Pyrimidyl)NHC Iridium complexes

The crystal structures for most of the NHC iridium complexes were obtained, with bond distances and torsion angles of interest listed in table 2. The actual crystal structures are shown in figures 9, 10, and 11. The iridium to

carbene carbon distances were all within the expected range. The N-Ir bond length shows an interesting trend increasing from 2.109 Å to 2.266 Å on going from **5a-Bu**[88] to **5b** and to **5c**, most likely due to the increasing steric hindrance on the pyrimidine rings across the series, an effect especially pronounced for **5c**, which has an adjacent *tert*-butyl group. The progressive effect of R group hindrance would also fit with the observation that carbene-iridium-nitrogen angle decreases as the nitrogen atom is forced further away from the iridium atom due to steric hindrance. The torsion angle around the pyrimidine ring relative to the NHC also shows twisting as the steric hindrances on the pyrimidine ring increases, with the angle going from 1.8° in the unhindered pyrimidine ring of **5a-Bu** [88] to 7.8° for the *tert*-butyl hindered pyrimidine ring of **5c**

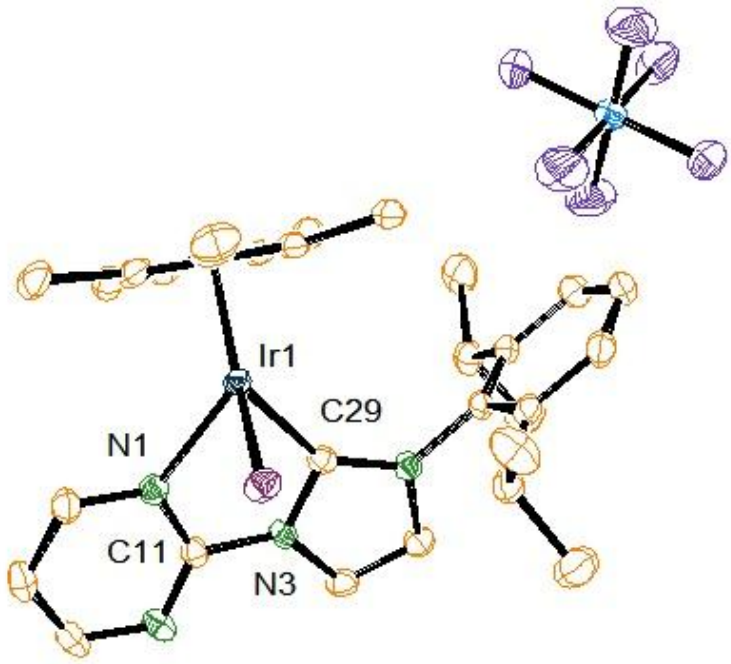

Figure 9. The NHC iridium(III) compound **9-H-Ir** with the pyrimidyl ring substituent bound to the iridium metal. The crystal system was monoclinic with the space group P2(1)/n.

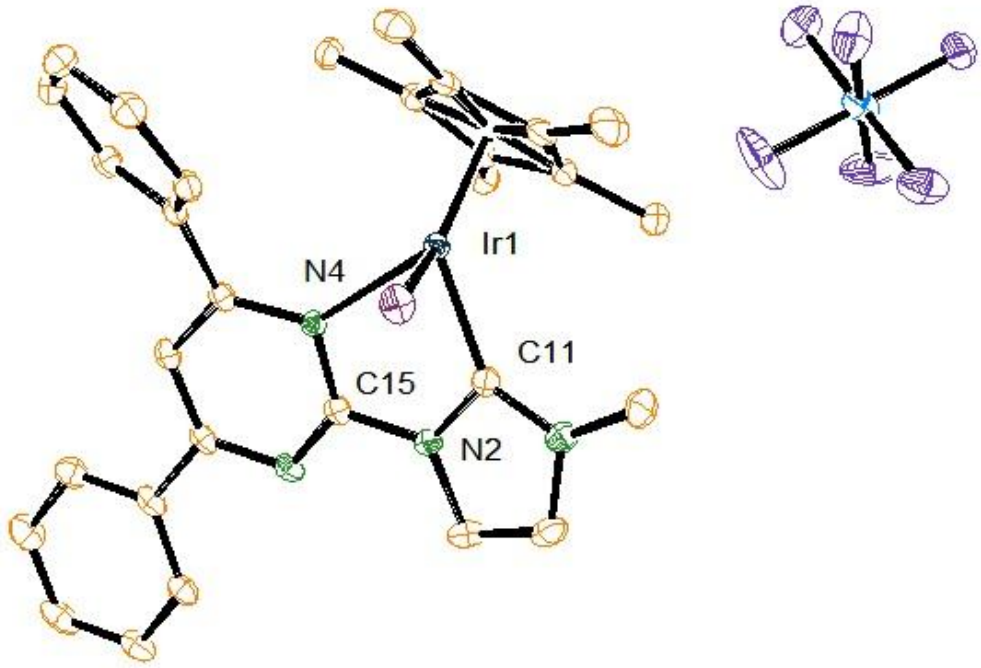

Figure 10. The NHC iridium(III) compound **5b** with the (3,5-di-phenyl)pyrimidyl substituent. The crystal system was monoclinic with the space group P2(1)/c.

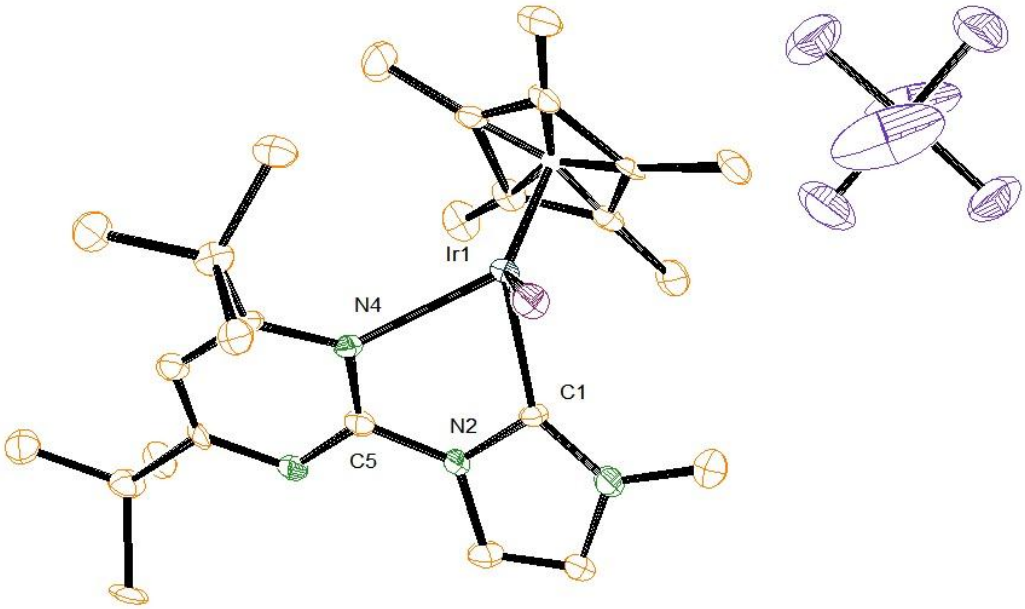

Figure 11. The NHC iridium(III) compound **5c** with the (3,5-di-tert-butyl)pyrimidyl substituent. The crystal system was monoclinic with the space group P2(1)/n.

For comparative purposes, the structure of the rhodium analog of **5c** (**5c-Rh**) was also added to the data in table 2. This rhodium complex was developed by a fellow researcher in the Grotjahn group, Christoff van Niekerk.[129] The key structural difference in the rhodium analog appears to be the slight increase in bond length of the metal to carbene carbon. The apparent shortening of the iridium to C2 bond is most likely due to relativistic effects with the larger third row element.

Table 2. Crystal Structures of (Pyrimidyl)NHC Group 9 Complexes.[a]

Metallated Compound	M-Carbene Distance (Å)	M-N Distance (Å)	Carbene-M-N Angle (°)	C1-N1-C4-N3 Torsion Angle (°)
5a-Bu[88]	2.044(7)	2.109(6)	76.7(3)	1.8
9-H-Ir	2.033(3)	2.113(2)	76.89(10)	3.0
5b	1.996(3)	2.180(2)	76.5(1)	4.1
5c	1.990(7)	2.266(6)	75.4(3)	7.8
5c-Rh[129]	1.998(?)	2.317(?)	74.6(?)	7.4
6	1.947(8)	2.200(6)	76.3(3)	0.2

[a] The M abbreviation in the table's headers stands for metal, since compounds based on iridium and rhodium are being compared.

Because of the change in ring size for compound **6**, the bond angles and torsion angles may not be applicable for comparison. However, the bond length of the nitrogen to iridium is of great significance, 2.200 Å, since it lies between that of complexes **5b** and **5c**. This is significant because at room temperature pyrimidine ring in **5a-Bu**[88] and **5b** is bound tightly to the metal center and does

not allow for free rotation about the NHC to pyrimidine bond, unlike in complex **5c**. Also included in this discussion of sterics is the molecular structure of imidazolium salt **10-Ph** in figure 12. Presumably due to the large amount of steric hindrance around the C2 atom of the imidazolium ring, the iridium trans-metalation reaction was unsuccessful.

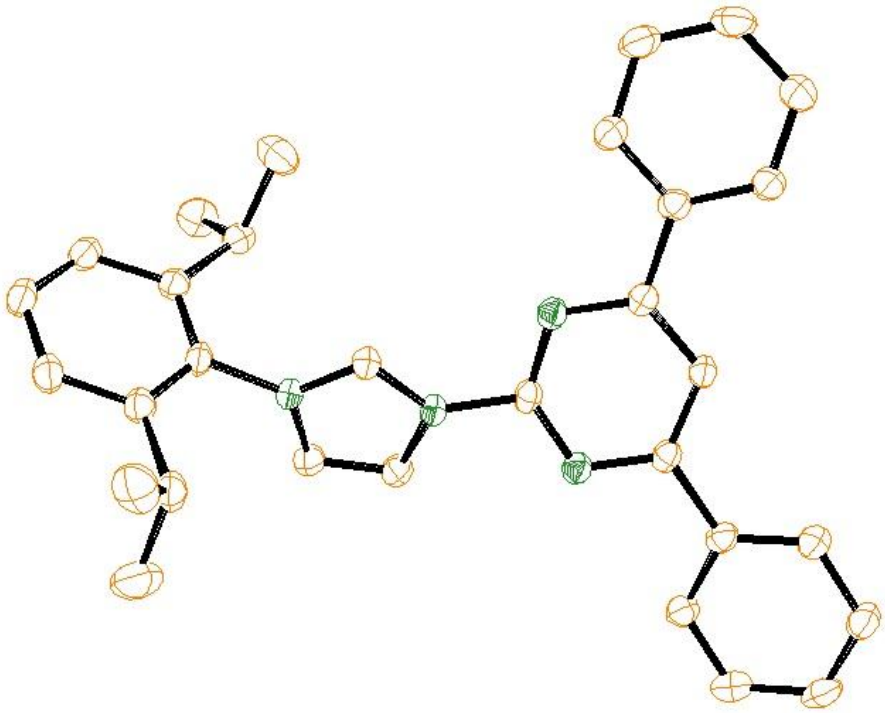

Figure 12. 1-(2,6-diisopropylphenyl)-3-(4,6-diphenylpyrimidin-2-yl)-1H-imidazol-3-ium chloride, **10-Ph**, after recrystallizing from a solution of CH_2Cl_2 with the diffusion of pentane. The crystal system was triclinic with the space group P-1.

SECTION 2.5 Determining Strength of Pendant Nitrogen Chelation

One of the most interesting aspects of designing the NHC iridium complexes in scheme 1 was to try and measure the energy of activation for breaking the metal-chelate bond. The primary goal of this work is to try and determine how much sterics around the chelating nitrogen will affect the lability of the pendant ligand. The NHC ligands with pyrimidyl substituents offer a unique

opportunity due to the possibility of fluxionality, as shown in figure 10. Quantification of ligand dynamics for the pyrimidine based iridium NHC complexes was obtained by variable-temperature NMR experiments.

The case of **5a-Bu**[88] required EXSY in the range of 110-135 ^{o}C, whereas for **5c** and **5c**-**Rh** line-shape analyses of ^{1}H NMR spectra between –40 and +30 ^{o}C sufficed. Figure 13 illustrates that how at 203 K the nitrogen atoms do not show a free exchange and the t-butyl groups show two distinct peaks. This proton spectra shows the ground state of the structure, just like the observed x-ray crystallographic structure predicted in figure 9. However, at room temperature the pyrimidine ligand with t-butyl groups can freely switch between being bound at either nitrogen. The lowered activation energies clearly show the dramatic effects of phenyl or *t*-butyl groups on the strength of the metal-nitrogen bond. The difference in free energies between the related structures appears to be directly influenced by the steric effects that additional groups on the pyrimidine rings can impart. This result also holds true for the rhodium-coupled complex, **5c-Rh**.

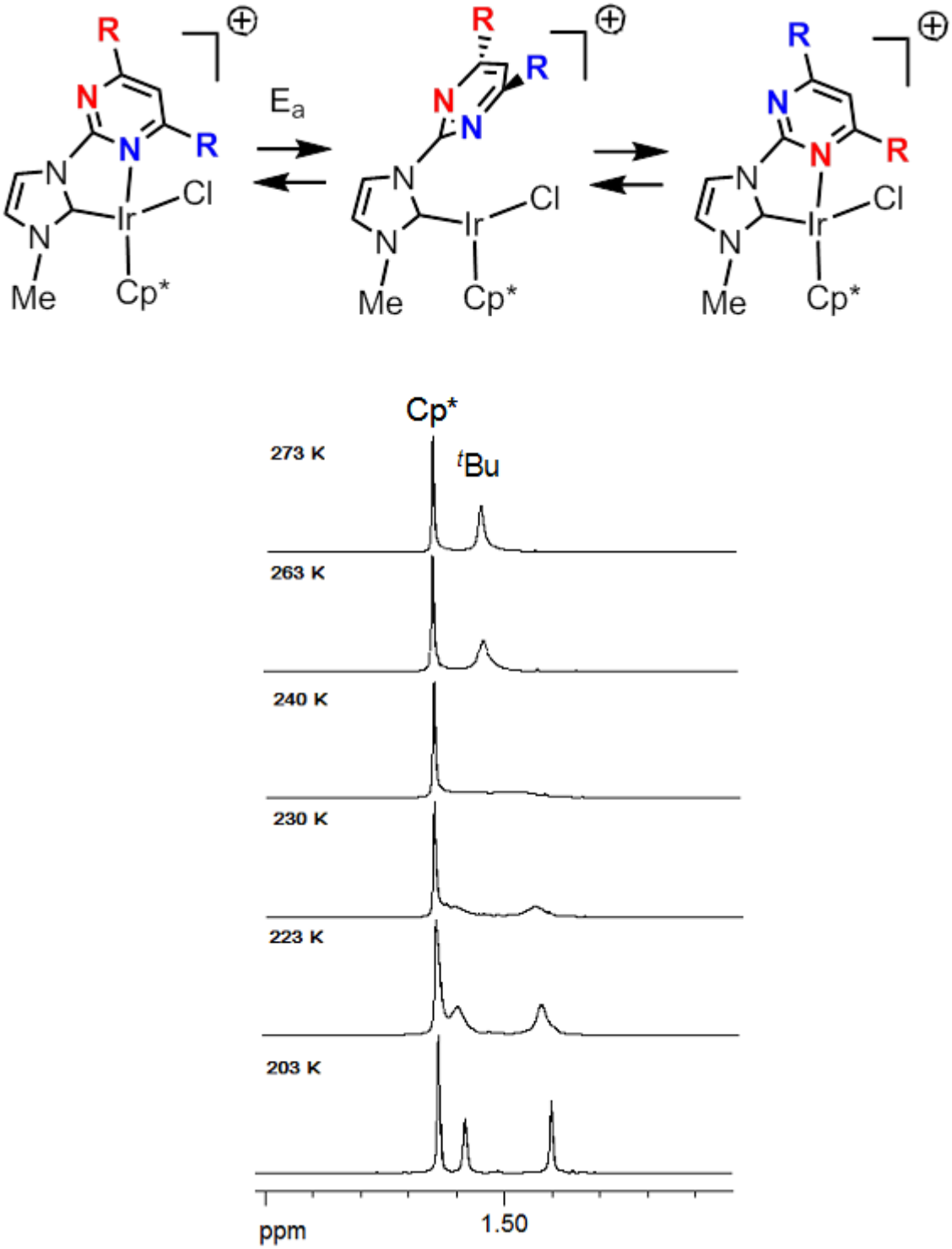

Figure 13. The temperature controlled NMR experiment on **5c** shows that the free rotation of the pyrimidine ring has a ΔH = 12.0 Kcal/mol and ΔS = 0.5 cal/mol.

Variable temperature NMR[134] with 15 mg of compound in 0.7 mL of deuterated solvent was used for the experiments. For **5a-Bu** *d*-DMF was used as the solvent due to the solvent's relatively high boiling point, sample solubility, and lack of a tendency to coordinate. The EXSY ^{1}H NMR experiment was set to run between 110-135 ^{o}C at 5 ^{o}C intervals. For compound **5b** *d*-chloroform was used and the temperature range was 58-75 ^{o}C, in 2 ^{o}C intervals. The EXSY data were then fitted to an Arrhenius plot for the energy of activation calculation and an Eyring plot to find the enthalpy of activation ($\Delta H^{\ddagger}$) and entropy of activation ($\Delta S^{\ddagger}$).[135-136] The data for compounds **5c** and **5c-Rh** were provided by Christoff van Niekerk.[129] As shown in table 3, the E_a values for the compounds **5c** and **5c-Rh** do not change much from iridium to rhodium and are both about 40% that of **5a-Bu**, a remarkable result from the hindrance provided by the ring substituents Likewise, the enthalpies of activation for both **5c** and **5c-Rh** are very close. The difference in entropy of activation is almost 5 cal mol^{-1} K^{-1}, but the uncertainties are rather large so no meaningful conclusion can be drawn.

Table 3. Experimental activation parameters for pyrimidine ring-flip on 5a-Bu, 5b, 5c, and 5c-Rh.[a]

	5a-Bu[88]	**5b**	**5c**[b]	**5c-Rh**[b]
Activation Energy (kcal mol^{-1})	29.6 ± 0.9	22.0 ± 0.3	12.5 ± 0.2	14.3 ± 0.3
$\Delta H^{‡}$ (kcal mol^{-1})	28.9 ± 0.9	21.3 ± 0.3	12.0 ± 0.2	13.8 ± 0.3
$\Delta S^{‡}$ (cal mol^{-1} K^{-1})	12.1 ± 26.3	5.8 ± 12.4	0.5 ± 0.9	5.2 ± 1.1

[a] EXSY experiments for compounds **5b** and **5a-Bu** were performed on a 600 MHz Varian NMR and compounds **5c** and **5c-Rh** were performed on a 500 MHz Varian NMR. [b] The data for compounds **5c** and **5c-Rh** were provided by Christoff van Niekerk.[129]

SECTION 2.6 Reactivity and Catalytic Studies

In order to evaluate the potential of the iridium (pyrimidyl)NHC complexes to engage in ligand binding, shown in scheme 1, the possibility of chelate ring opening was investigated using benzylamine and its ^{15}N labeled derivative.

Preliminary results show that weakening the chelation has significant effects on ligand binding: benzylamine reacted with either **5c** or **6**, forming adducts **5c-BA** and **6-BA** quantitatively. *In contrast, unhindered analog* ***5a-Bu*** *remains completely intact.* Distinctive features of **5c-BA** and **6-BA** include a four-spin system for the $–CH_2NH_2$ unit, with the two NH protons resonating at 6.63 and 4.17 ppm (**5c-BA**), and 3.95 and 7.67 ppm (**6-BA**). Our suspicion was that the downfield NH resonances were due to the proton engaged in hydrogen bonding.

In order to fully characterize hydrogen bonding in the benzylamine adducts, ^{15}N labelled material was used to obtain one-bond H-N coupling information, which might be expected to change as a function of hydrogen

bonding. Moreover, using 2D NMR in the form of ^{1}H-^{15}N gHMBC data, even with natural abundance material we expected to be able to obtain the ^{15}N chemical shift of the pyrimidine nitrogen involved in hydrogen bonding and compare its shift to that of the second nitrogen. Approximately 0.04 mmol of iridium compound with an equal amount of labeled benzylamine dissolved in 0.6 mL of methylene chloride-d_2 for this study, which was done with significant help from Dr. Douglas Grotjahn and is shown below in scheme 4. For the pyrimidyl system of **5c-BA** at 30 ^{o}C, a single set of ^{1}H and ^{13}C NMR peaks for the two *t*-Bu groups suggest free rotation around the heteroaryl-NHC bond; moreover for the pyrimidyl N in the ^{1}H-^{15}N gHMBC spectrum a single peak at -108.5 ppm was seen. In contrast, at -90 ^{o}C, two nitrogen ^{1}H-^{15}N gHMBC crosspeaks were seen at -100.6 and -118.0 ppm, clearly showing an upfield shift of 17.4 ppm which is strong evidence[122, 137] for hydrogen bond acceptance by one pyrimidyl nitrogen. For **6-BA**, as determined by ^{1}H-^{15}N gHMBC correlation on natural abundance material, an upfield ^{15}N chemical shift (by ca. 10 ppm) for the basic imidazolyl nitrogen (-135.3 ppm) relative to values seen for the corresponding imidazolium hexafluorophosphate salt and silver bis(NHC) hexafluorophosphate complex (-125.3 and -121.2 ppm, respectively) was seen. The upfield shift may be considered useful spectroscopic evidence for the intramolecular hydrogen bonding shown.[122, 137]

For **5c-BA-^{15}N** with ^{15}N label at the coordinated nitrogen of the benzylamine, the downfield NH proton resonance at 6.64 ppm showed a one-bond coupling constant $^{1}J_{HN}$ = 72.8 Hz, whereas the upfield NH resonance at

4.17 ppm showed $^{1}J_{HN}$ = 71.3 Hz. The change is significant, though there are cases where donation of a hydrogen bond by an NH either raises or lowers the value of $^{1}J_{HN}$ depending on if there are any shielding effects from neighboring groups.[122, 137-138]

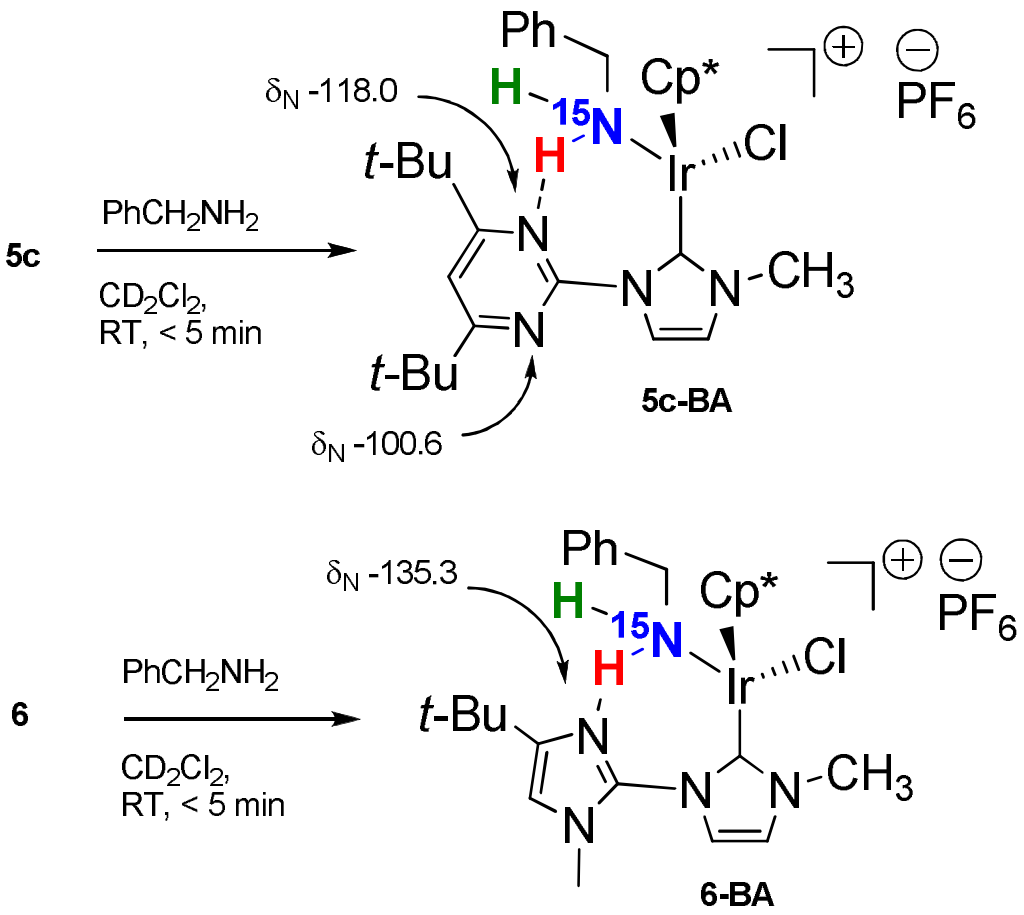

Scheme 4. ^{15}N NMR chemical shift data. The shifts for the heteroaryl nitrogens at natural abundance were derived from ^{1}H-^{15}N gHMBC spectra.

Several different experimental reaction conditions have been tested in order to gauge the performance of the various potential catalysts that have been synthesized. Only the metal complexes that had hexafluorophosphate as an anion were tested, which excluded compounds **5b-Cl** and **10-H-Ir**. These

potential catalysts were then compared to the previously published **5a-Bu**.[88] As a control, the non-NHC starting material $[Cp^*Ir(\mu\text{-}Cl)Cl]_2$ was also examined, particularly because it has been shown to be a good catalyst for various coupling reactions[139] including N-alkylation of amines with alcohols,[140] transfer hydrogenation of quinolines,[140] conversion of alcohols to amides via oximes,[141] and synthesis of substituted indoles.[142]

SECTION 2.6.1 Hydrogen/Deuterium Exchange

The earliest catalytic experiments that were run focused on isotopic labeling through hydrogen-deuterium exchange, based on the work published by Peris.[143] The iridium based NHC compound created by Peris, shown in figure 14, was similar enough to the work that I was pursuing that a few of the early iridium compounds that I made were run in deuteration experiments. Table 4 lists the results obtained from the limited tested that was conducted. The percentages were based on the total possible dueteration possible given a ratio of deuterium present in the solvent, which for these experiments was heavy water, to the compound being methanol-*d*. Unfortunitly, none of the catalysts tested at the time performed as well as the Peris complex, possibly due to steric interference of the larger NHC around the iridium metal. Based on these preliminary results it was decided that this catalytic route was not a good test of the newly developed iridium complexes and another reaction, Oppenauer-type oxidation, was targeted.

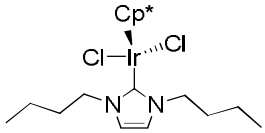

Peris's compound

Figure 14. The iridium based NHC compound created by Peris.[143]

Table 4. Deuteration of simple organic compound using iridium based catalysts.[a]

Substrate	catalyst	% Deuteration	Time (H)
Diethyl ether	Peris Cat.	CH_3, CH_2 > 99	12
Diethyl ether	**5y**	CH_3, CH_2 > 0	24
tert-butylethene	Peris Cat.	vinyl: 90; *t*-Bu: 59	12
tert-butylethene	**5x**	vinyl: 19; *t*-Bu : 18	18
tert-butylethene	**5y**	vinyl: 22; *t*-Bu : 22	16
styrene	Peris Cat.	vinyl > 99; *o* > 99; *m*,*p*: 65	12
styrene	**5b**	vinyl > 18; *o* > 0; *m*,*p*: 0	14
tetrahydrofuran	Peris Cat.	α-CH_2: 25, β-CH_2: 20	12
tetrahydrofuran	**5b**	α-CH_2, β-CH_2: 0	21

[a] The following experiment was run in 2% of catalyst with 8% of silver triflate, 5.7×10^{-5} mol of the organic molecule to be deuterated in 0.6mL (1.5×10^{-2} mol) of methanol-*d*. External standard capillary consisting of a solution of ferrocene in chloroform-*d* (0.16 mg/μL). The reaction was heated at 100°C for the specified time.

The mechanism proposed for this reaction is based on the mechanism that was suggested by Peris and others.[143-144] Scheme 5 shows how the iridium NHC complex created by Peris, in figure 14, is proposed to react catalytically. Scheme 5 shows how the pendent base could improve a deuterium exchange

reaction verses a catalyst like the iridium NHC complex created by Peris in figure 14. As stated earlier, the sterics around the NHC of compound **5b** may have hindered the catalysts ability to catalyze the H/D exchange. However, the Peris compound had smaller, more flexible, butyl groups on the NHC and may have allowed for easier access to the iridium metal during catalysis.

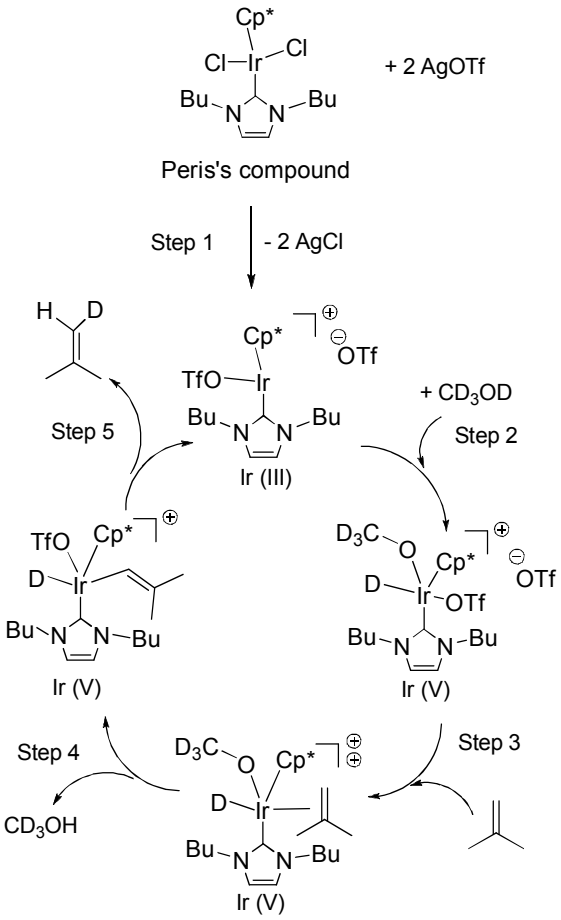

Scheme 5. Proposed catalytic cycle for iridium NHC complex created by Peris.[143]

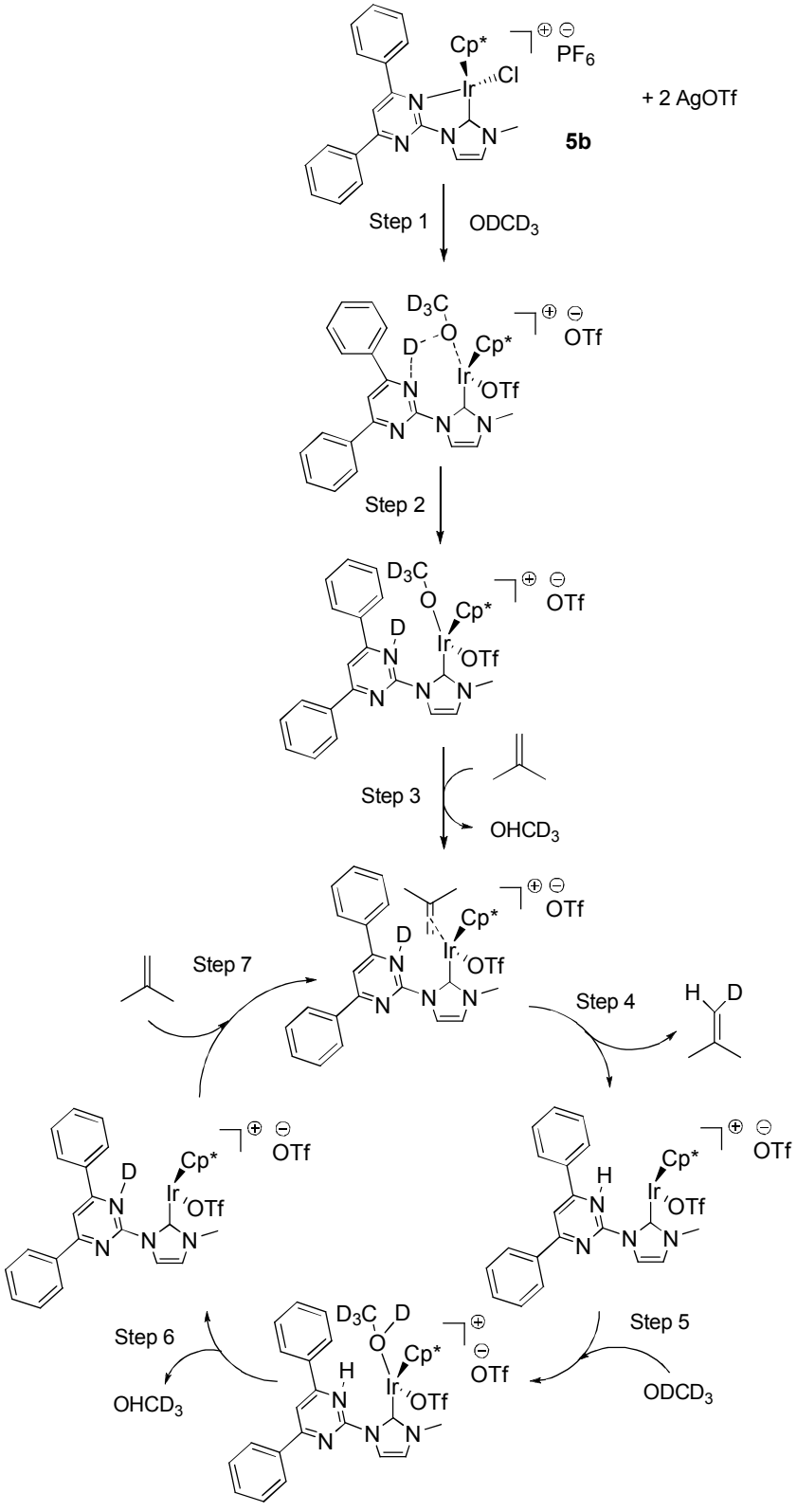

Scheme 6. Proposed catalytic cycle for H/D exchange with **5b**.

SECTION 2.6.2 Oppenauer-type Oxidation

Following the procedure set forth by Yamaguchi *et al.*, the Oppenauer-type oxidation of 1-phenylethanol to acetophenone was examined in the presence of the catalyst precursor (0.50 mol %) and AgOTf (1.0 mol %).[145] Figure 15 outlines the basic reaction and the results are summarized in Table 5. Although the previous report on **5a-Bu**[88] showed moderate catalytic activity without base, entry 2, the catalytic systems employing **5c** showed high catalytic activity, entry 5, in the same conditions within the first 5 h. The rhodium analog, **5c-Rh,** proved to be the second most efficient catalyst tested, with the higher energy of activation one possible reason for its lower efficiency then the iridium complex. In contrast with these results, low yields were observed with the starting material, $[Cp^*Ir(\mu\text{-}Cl)Cl]_2$, entry 1.

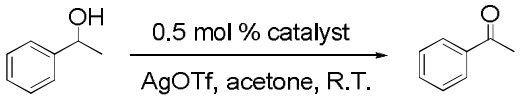

Figure15. Oppenauer-type oxidation of alcohols.

Table 5. Yields of ketone in Figure 11.[a]

Entry	catalyst	5 h (% yield)	24 h (% yield)	48 h (% yield)
1	$[Cp^*Ir(\mu\text{-}Cl)Cl]_2$	2.4	2.7	2.9
2	**5a-Bu**	12.4	51.9	60.4
3	**5b**	1.9	6.9	9.9
4	**5c**	87.7	87.0	85.7
5	**5c-Rh**	34.0	51.2	67.4
6	**6**	16.6	48.8	52.1

[a] 1.00 mmol of 1-phenylethanol, AgOTf (1 mol %), catalyst (0.5 mol %) in 4 mL of acetone at RT. % yields were determined by ^{1}H NMR spectroscopic analysis of aliquots using 1,3,5-trimethoxybenzene as an internal standard.

The proposed mechanism for this reaction for **5c** is based on the mechanistic proposal made by Yamaguchi *et al.*, and is shown in scheme 7. Using the pendant base of the pyrimidine ring eliminates the need for an external base to the reaction, as well as keeping the proton close to the metal center, which may be important for reaction time.

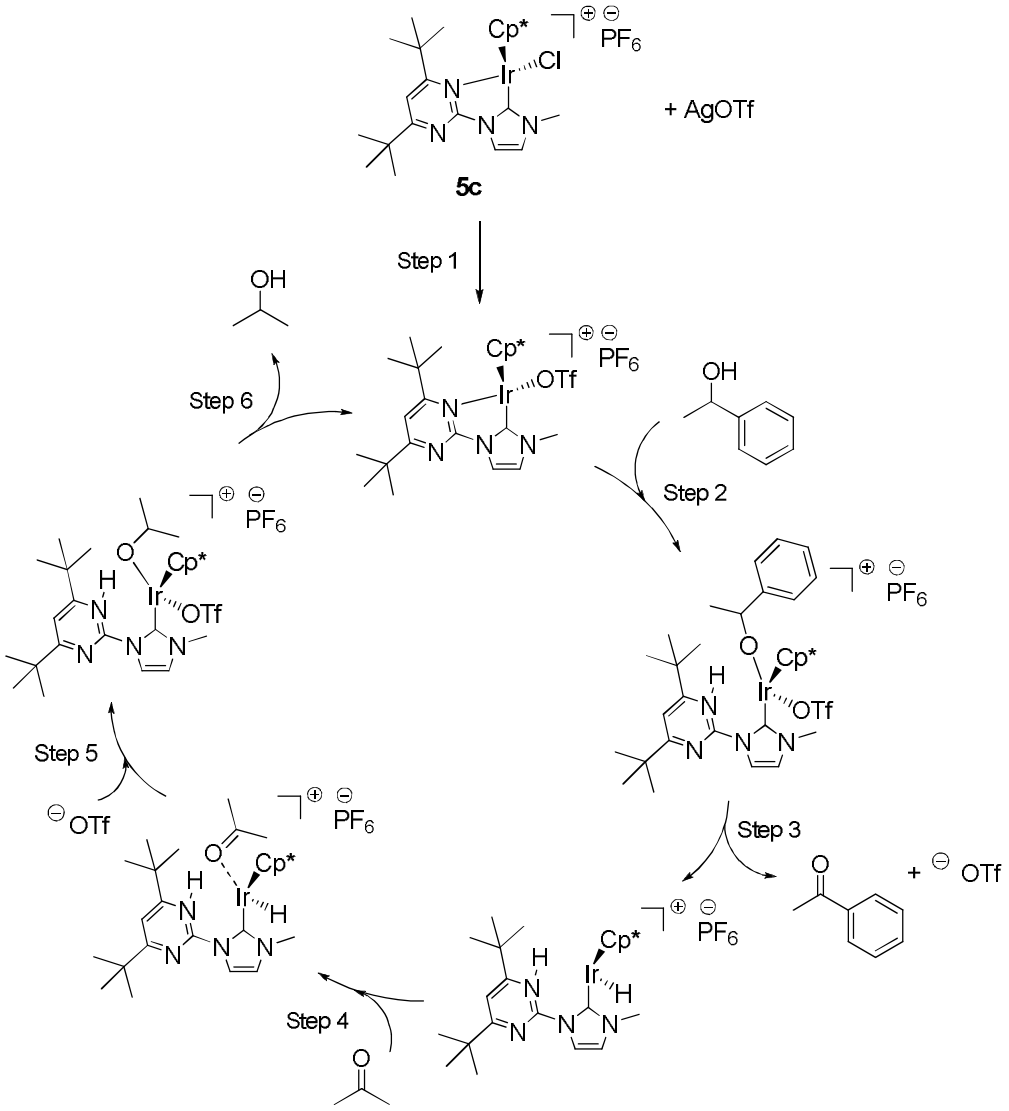

Scheme 7. Proposed mechanism for this reaction for Oppenauer-type oxidation of alcohols with **5c**.

SECTION 2.6.2 Alkylation of Secondary Alcohols with Primary Alcohols

Following the procedure set forth by Gnanamgari *et al.*, the alkylation of secondary alcohols with primary alcohols was examined in the presence of the catalyst precursor (1.0 mol %) and KOH (100.0 mol %) at 110°C.[88] Figure 16 outlines the basic reaction and the results are summarized in Table 6. The

starting material, $[Cp^*Ir(\mu\text{-}Cl)Cl]_2$, showed a surprising amount of catalytic activity for the formation of 1,3-diphenylpropan-1-ol. By comparison **5a-Bu**[88] only showed an increase of 1.4 in catalytic ability. Samples **5c** and **6** showed an increase of nearly two times that of the starting material. Sample **5c** also showed the production of 10% ketone formation, which makes the total product yield equal to 86.5%. As an unexpected result compound **5b** showed an increase in catalytic reactivity of about 2.4 with the second highest percentage of ketone formation.

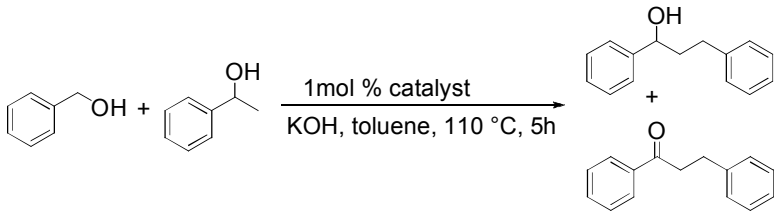

Figure 16. Alkylation of secondary alcohols with primary alcohols.

Table 6. β-Alkylation of 1-phenylethanol with benzyl alcohol[a].

Entry	catalyst	% Alcohol	% Ketone
7	$[Cp^*Ir(\mu\text{-}Cl)Cl]_2$	39.3	0.0
8	**5a-Bu**	55.3	0.0
9	**5b**	93.1	8.6
10	**5c**	76.5	10.0
11	**6**	77.0	0.0

[a] 2.00 mmol of benzyl alcohol and 1-phenylethanol, 2.0 mmol of KOH (100 mol %), 1 mol % catalyst, 0.5 mL of toluene at 110 °C. Yields determined by ^1H NMR spectroscopic analysis of aliquots using 1,3,5-trimethoxybenzene as an internal standard.

The proposed mechanism for this reaction is listed in scheme 8 and is based on the proposed mechanism by both Yamaguchi and Pullarkat.[146-147] In their proposed mechanisms there was always a base added in order to initiate the reaction mechanism. Here I propose that in step one the pendant base removes the proton from the alcohol as the oxygen forms a bond to the iridium, as shown in scheme 8. However, the actual experimental set-up did use potassium hydroxide, which would have over shadowed the possible contributions of the potential pendant base. This may also be a factor for **5b** out performing **5c** and **6** even through **5b** was shown to have a stronger chelating energy and hence make for a less effective pendant base.

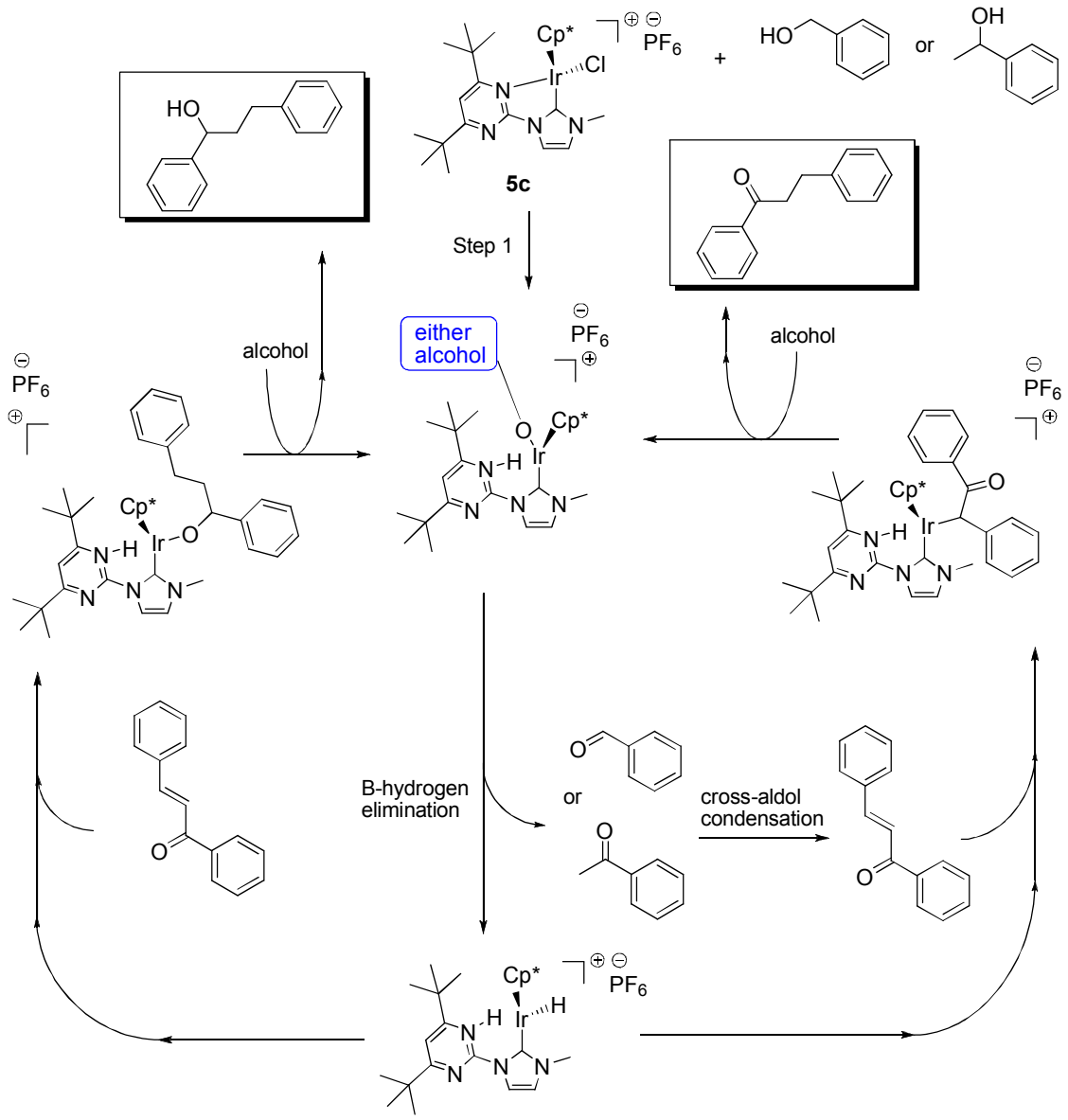

Scheme 8. Proposed mechanism for alkylation of secondary alcohols with primary alcohols, without KOH.

SECTION 2.6.3 N-Alkylation of Amines with Alcohols

Following the procedure was also set forth by Gnanamgari, *et al.*, the N-alkylation of amines with primary alcohols was examined in the presence of the catalyst precursor (1.0 mol %) and sodium bicarbonate (25.0 mol %) at 110°C.[88]

Figure 17 outlines the basic reaction and the results are summarized in Table 7. The starting material, $[Cp^*Ir(\mu\text{-}Cl)Cl]_2$, also showed a surprising amount of catalytic activity for the formation of dibenzylamine. By comparison **5a-Bu**[88] only showed an increase of 1.2 in catalytic ability of amine, though it also shows the highest formation of the imine compound. Complex **5c** showed the largest increase, nearly a 2.7 ratio, of amine formation.

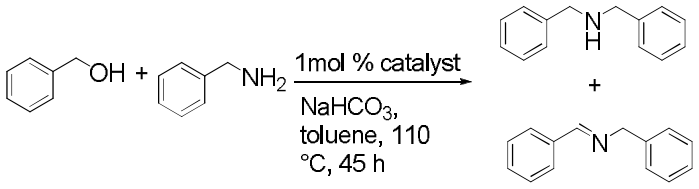

Figure 17. N-Alkylation of amines with alcohols.

Table 7. N-Alkylation of benzylamine with benzyl alcohol.[a]

Entry	catalyst	% Amine	% Imine
12	$[Cp^*Ir(\mu\text{-}Cl)Cl]_2$	31.5	0.0
13	**5a-Bu**	38.8	5.5
14	**5b**	74.3	0.0
15	**5c**	84.1	2.2
16	**6**	44.3	1.4

[a] 1.00 mmol of benzyl alcohol and benzyl amine, 0.5 mmol of $NaHCO_3$, 1 mol % catalyst, 0.5 mL of toluene at 110 °C. Yields determined by ^1H NMR spectroscopic analysis of aliquots using 1,3,5-trimethoxybenzene as an internal standard.

The proposed mechanism for this reaction is listed in scheme 9 is very similar to that of scheme 8. Here the added base in the actual experiment has been left out of the diagram.

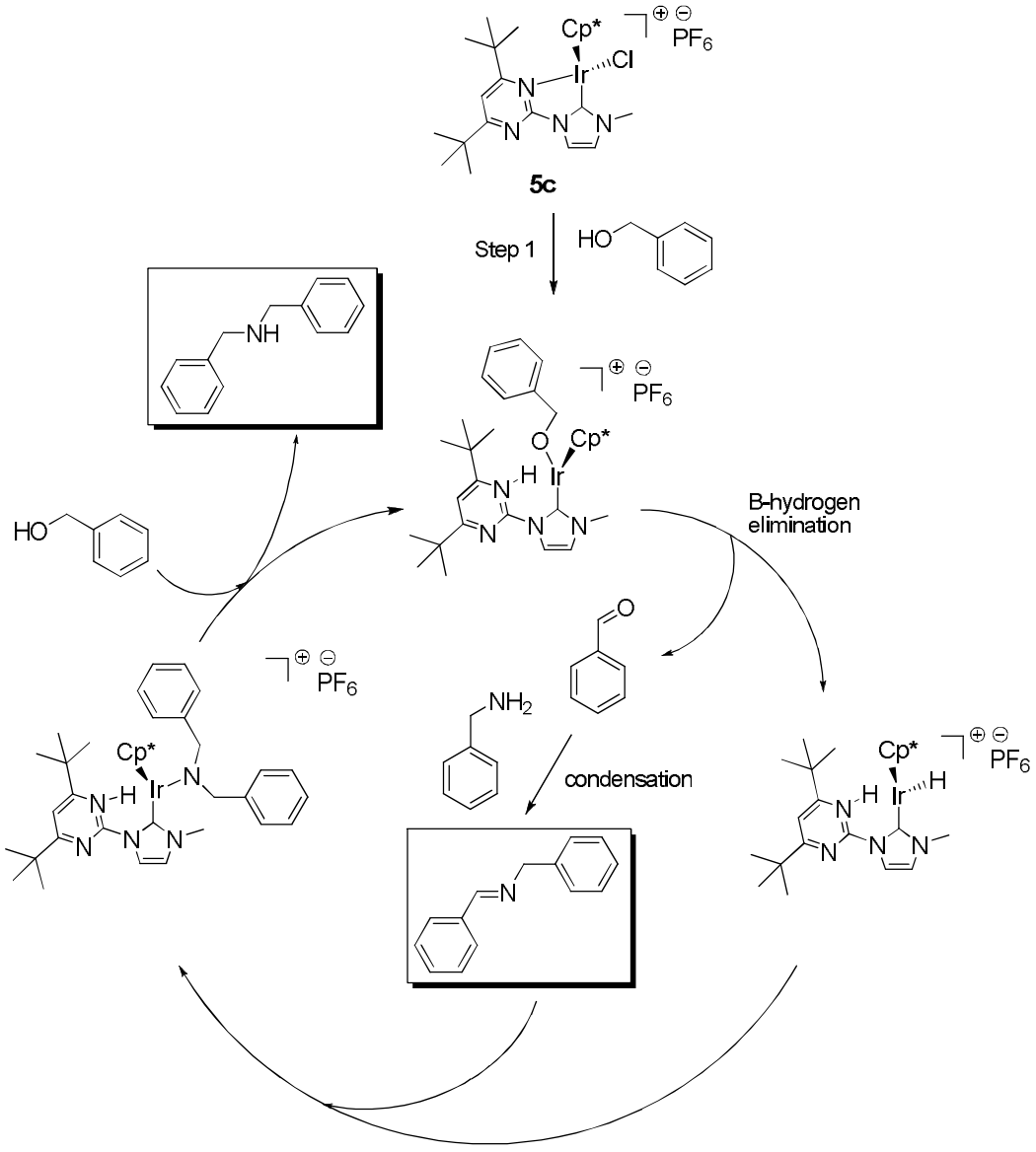

Scheme 9. Proposed mechanism for N-alkylation of amines with alcohols.

SECTION 2.6.4 Cyclization of a Primary Aminoalkene

Catalyzed cyclization of **26** to give **27** in figure 18, was chosen as a test reaction because of ongoing and intense synthetic and mechanistic interest in alkene hydroamination.[148-164] Table 8 shows that **5c** is the most active of (heteroaryl)NHC catalysts examined, with **6** as the second most active. Looking

at results from primary amine **26**, among (pyrimidyl)NHC derivatives, increase in conversion of **26** occurs on going from **5a-Bu**[88], which is virtually inactive, to **5b**, which is about as active as $[Cp^*Ir(\mu\text{-}Cl)Cl]_2$, to **5c**, which is much more active. Intriguingly, **5c-Rh** gives isomerization exclusively as quickly as **5c** performs selective hydroamination, showing a dramatic role for the central metal in the course of the cyclization, which are differences consistent with results from other known rhodium and iridium based catalysts.[149, 156]. Although our preliminary results have not resulted in a hydroamination catalyst significantly more active than recent impressive improvements in the state-of-the-art,[148-152, 164] nonetheless the fact that a completely inactive NHC-based system like **5a-Bu**[88] can be turned into a synthetically useful one constitutes a significant proof of concept.

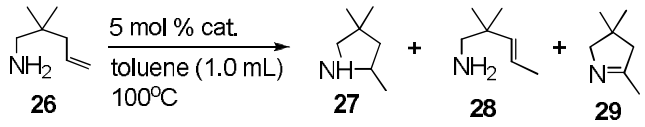

Figure 18. Products from reaction of **26**: cyclization **27**, alkene isomerization **28**, and cyclization followed by dehydrogenation **29**.

Table 8. Results for the cyclization of primary amine.[a]

Catalyst	24 h				72 h			
	26	**27**	**28**	**29**	**26**	**27**	**28**	**29**
$[Cp^*Ir(\mu\text{-}Cl)Cl]_2$	100	0	0	0	72	0	26	0
5a-Bu	100	0	0	0	99	0	1.5	0
5b	87	0	9.0	0	69	10	18	0
5c	4.0	68	9.0	?	0	72	5.0	?
5c-Rh	9.0	0	82	0	3.0	0	94	0
6	65	27	0	?	36	55	3.0	?

[a] **26** (0.25 mmol) and catalyst (5 mol %; 2.5 mol% in the case of $[Cp^*Ir(\mu\text{-}Cl)Cl]_2$ in toluene (1.0 mL) at 100 ^oC. Yields shown are based ^1H NMR spectroscopy, averaging results from two separate runs, except for $[Cp^*Ir(\mu\text{-}Cl)Cl]_2$, using 1,3,5-trimethoxybenzene as an internal standard.

The proposed mechanism for this reaction was based on the mechanism proposed by Stradiotto.[149] In the study by Stradiotto the iridium compound was $[Ir(COD)Cl]_2$ and focused on a combination of kinetic experiment, isotopic labeling, and computational work to study how aminoalkene compounds cyclize. The data showed that of the two most likely routs, one starting with the binding of the amine to the iridium and the other with the alkene first coordinating, the later was more likely to occur energetically. Because of this, it is proposed that the mechanism for the cyclizing of primary or secondary amines to their respective alkene functional groups with the first step in the cyclization occurring as the iridium binds to the alkene group. However, the binding of the primary amine to

the iridium is also likely to occur and may help explain why secondary amines cyclize so much faster than primary amines.

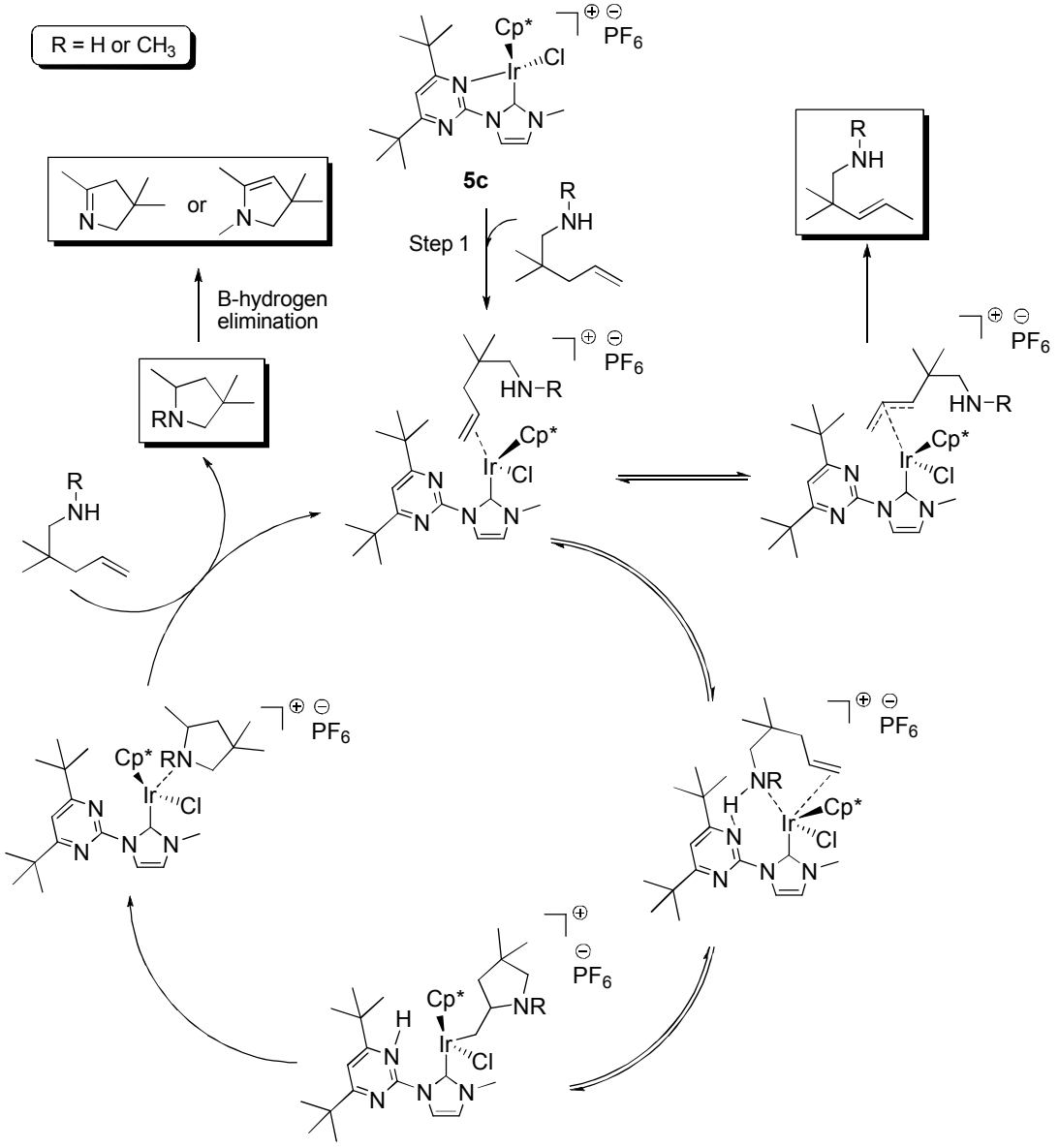

Scheme 10. Proposed mechanism for the cyclization of primary and secondary amines.

SECTION 2.6.5 Cyclization of a Secondary Aminoalkene

Catalyzed cyclization of **30** to give **31** in figure 19, was chosen as a test reaction in order to highlight the binding difference between primary and secondary amines with regards to iridium based catalysts. Due to the difficulty in determining the actual structure of what byproduct **33** may be, what is judged to be the most stable dehydrogenation product is shown. Figure 20 outlines the five most likely dehydrogenated ring structures that could be produced from **31**. Using the Hartree-Fock method with a 3-21G data set the energies for the structures was calculated and the most stable structure was found to be 1,3,3,5-tetramethyl-2,3-dihydro-1H-pyrrole, with -228459.492067 Kcal/Mol. This uncertainty, due to overlapping ^{1}H NMR peaks, in the structure also gives rise to an uncertainty in how much of **32** may be produced in this reaction.

Only the two iridium catalysts that showed the best results with the primary aminoalkene were chosen because of the small amount of **30** that was available for testing at the time. The results of the catalytic experiments are listed in table 8. It should also be noted that the consumption of the secondary amine substrate **30** is at least 20 times faster than that of the primary amine, affording cyclized product in higher yield (89%) using **5c** in only 1 h.

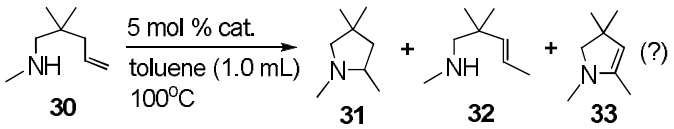

Figure19. Products from reaction of **30**: cyclization **31**, alkene isomerization **32**, and cyclization followed by dehydrogenation **33**.

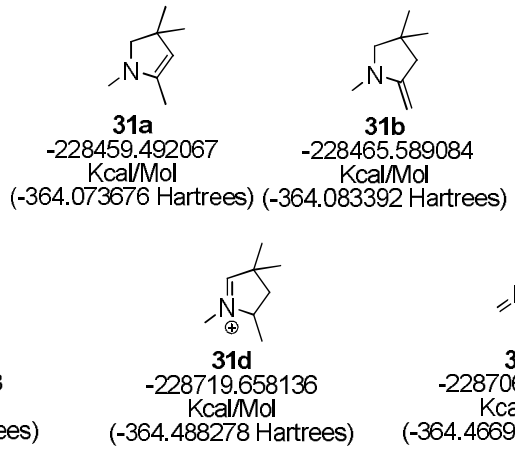

Figure 20. Five of the most likely dehydrogenated ring structures that could be produced from **31** are listed, with figure **31a** having the lowest energy calculated using Hartree-Fock method with a 3-21G data set.

Table 9. Results for the cyclization of secondary amine.[a]

Catalyst	1 hour				24 hours			
	30	**31**	**32**	**33**	**30**	**31**	**32**	**33**
5c	2.9	89	2.0	?	3.0	89	2.0	?
6	37	62	3.9	?	3.8	86	4.4	?

[a] **30** (0.25 mmol) and in toluene (1.0 mL) at 100 ^{o}C. Yields shown are based ^{1}H NMR spectroscopy, averaging results from two separate runs, using 1,3,5-trimethoxybenzene as an internal standard.

SECTION 2.7 Conclusions

In conclusion, increasing the steric bulk around the pendant nitrogen atom resulted in dramatic lengthening of the Ir-N bond as revealed by X-ray crystallography. This lengthening of the Ir-N bond also correlated to a shortening of the Ir-C for the NHC ligand. The lengthening of the Ir-N bond as the steric bulk increased was theorized to lower chelate bond strength, which was measured

using dynamic NMR behaviour and shown to decrease by 17.1 kcal mol^{-1} on going from **5a** to **5c**. In terms of temperature, the Ir-N in **5a** was still strong at 100 °C, whereas the free rotation around the imidazole-pyrimidine ring only began to slow down significantly began at -50 °C for **5c**.

The chelate in **5a** remained unbroken in the face of benzylamine, whereas **5c** reacted completely, forming a species (**5c-BA**) with a hydrogen bond interaction between the one protons on the incoming amine group and one of the nitrogens of the unchelated pyrimidyl substituent. This interaction suggests the possibility of the unchelated pyrimidyl substituent as acting as a pendant base during catalytic reactions involving proton transfer. Several different types of coupling reactions were shown to work with compound **5a**-**5c**, with the reaction rates generally increasing as the energy of activation required to break the Ir-N bond was lowered. In particular, the intramolecular cyclization reactions for primary and secondary alkeneamines showed good results. Of additional interest is the ability of compound **5c** to also carry out dehydrogenation reactions on the cyclized compounds.

SECTION 2.8 Experimental

General Methods

Reactions were performed under dry nitrogen, using a combination of Schlenk line and glovebox techniques. $CDCl_3$ was distilled from CaH_2 prior to use. NMR tube reactions were performed in resealable NMR tubes (J. Young). Unless otherwise specified, ^{1}H and ^{13}C data were measured at 30 °C on a 400-

MHz Varian NMR-S spectrometer (399.8 MHz for ^{1}H and 100.5 MHz for ^{13}C) and ^{15}N data on a 600 MHz Varian spectrometer. ^{1}H and ^{13}C NMR chemical shifts are reported in ppm downfield from tetramethylsilane and referenced to solvent resonances (^{1}H NMR: δ 2.05 for $(CD_3)(CHD_2)CO$, δ 7.27 for $CHCl_3$, 5.32 for $CHDCl_2$ and ^{13}C NMR: δ 206.68 for $(CD_3)_2CO$, δ 77.23 for $CDCl_3$, 54.00 for CD_2Cl_2). ^{1}H NMR signals are given followed by multiplicity, coupling constants *J* in Hertz, integration in parentheses. For complex coupling patterns, the first coupling constant listed corresponds to the first splitting listed, e.g. for (dt, *J* = 3.2, 7.9, 1 H) the doublet exhibits the 3.2-Hz coupling constant. $^{31}P\{^{1}H\}$ NMR chemical shifts are referenced to an external 85% H_3PO_4 (aq) capillary placed in the solvent.

IR spectra at ambient temperatures were obtained on a ThermoNicolet Nexus 670 FT-IR spectrometer. Raman samples were measured using a Thermo Scientific DXR Raman Microscope with an excitation laser set at 532 nm. Samples were examined in CD_2Cl_2 solutions in CaF_2 cells. Elemental analyses were performed at NuMega Laboratories in San Diego, CA.

All crystallographic data were collected on Bruker diffractometers equipped with APEX CCD detectors. All structures were solved by direct methods and refined with anisotropic thermal parameters and idealized hydrogen atoms. All software is contained in the SMART, SAINT and SHEXTL libraries distributed by Bruker-AXS (Madison, WI). Complete disclosures about the crystallographic work for CCDC-806197 (**5b**), 806200 (**5c**), 806201 (**5c-Rh**) and 806198 (**6**) may be found in the deposited CIF files.

Synthesis of 5b-Cl

In the glovebox, solid $(Cp^*Ir(\mu\text{-}Cl)Cl)_2$ (0.0440 g, 0.055 mmol) was then added to **8-Ph-AgCl** (0.0508 g, 0.112 mmol) in methylene chloride (10 mL) under nitrogen and the resulting mixture was allowed to stir for 18 h. The orange-red solution was then filtered through Celite in order to remove solids (presumed silver chloride) using rinses of dichloromethane. The filter cake was then washed with pentane and ethyl ether. The residue after concentration could not be successfully recrystallized, so it was purified by dissolving it in methylene chloride and precipitating with either. **5b-Cl** appeared as a yellow-red solid (0.0604 g, 0.083 mmol, 76.2 % yield). Elemental analysis was not performed.

Synthesis of 5b

In the glovebox, solid $(Cp^*Ir(\mu\text{-}Cl)Cl)_2$ (0.1750 g, 0.220 mmol) was added to **8-Ph** (0.2000 g, 0.439 mmol) and potassium hexafluorophosphate (0.1702 g, 0.925 mmol) in methylene chloride (10 mL, 0.04 M) under nitrogen and the resulting mixture was stirred for 18 h. The orange-red mixture was filtered through Celite in order to remove the silver chloride; the filter cake was rinsed with dichloromethane (5 mL total) in several portions. The residue after concentration could not be successfully recrystallized, so it was purified by dissolving it in methylene chloride and precipitating with ether. The product **5b** appeared as a yellow-red solid (0.3580 g, 0.437 mmol, 99.7 % yield). FT-IR (CD_2Cl_2 in CaF_2 cell, cm^{-1}) 3151.2, 3066.7, 2921.8, 2313.8, 1596.6, 1573.1, 1524.3, 1484.2, 1451.1, 1370.6, 1312.7, 1224.2 Anal. Calcd for $C_{30}H_{31}ClF_6IrN_4P$ (820.23 g/mol): C, 43.93; H, 3.81; N, 6.83. Found: C, 43.78; H, 3.81; N, 7.00.

Synthesis of 5c

In the glovebox, a scintillation vial was charged with **8-tBu-PF_6** (0.1688 g, 0.212 mmol) and (Cp*Ir(μ-Cl)Cl)$_2$ (0.1686 mg, 0.106 mmol), followed by acetone (10 mL, 0.04 M). To this mixture was added potassium hexafluorophosphate (176 mg, 0.956 mmol) while stirring. The reaction mixture was stirred for 14 h, after which time the solution turned a cloudy orange color. The solvent was then removed under vacuum and the residue was extracted using dichloromethane. After filtration through a Celite plug, the filtrate was concentrated under vacuum, leaving the desired product as a yellow solid, which crystallized during slow evaporation from acetone (0.3448 g, 0.442 mmol, 99.0 % yield). FT-IR (CD_2Cl_2 in CaF_2 cell, cm^{-1}) 3179.2, 3150.1, 2972.2 28.72.0, 1598.5, 1513.0, 1482.5, 1462.0, 1451.5, 1425.9, 1377.6. Anal. Calcd for $C_{26}H_{39}ClF_6IrN_4P$ (780.25 g/mol): C, 40.02; H, 5.04; N, 7.18. Found: C, 40.04; H, 5.05; N, 7.57.

Synthesis of 9-H-Ir-Cl

In a glove box, **9-H** (0.3000 g, 0.875 mmol) and silver oxide (0.1016 g, 0.4375 mmol) were placed in a vial along with a magnetic stir bar. Methylene chloride (0.5 mL, 1.75 M) was added. The vial was covered in foil to keep the reaction in the dark. The reaction was stirred for 1 h at room temperature. Solid (Cp*Ir(μ-Cl)Cl)$_2$ (0.3486 mg, 0.438 mmol) was added to the reaction and the mixture was stirred at room temperature for 8 d. The green solution was then passed through a Celite pad using acetone to rinse. The residue remaining after concentration was purified by column chromatography using a gradiant of acetone to 1:9 methanol in acetone solution. The green colored residue remaining after

concentration was then further purified by mixing the sample with ethyl acetate and passing the wash through a Celite pad. Acetone was used to rinse the Celite and product was crystallized using ethyl acetate as the anti-solvent. Product **9-H-Ir-Cl** appeared as a powder (0.2114 g, 0.2991 mmol, 34.2 % yield). Anal. Calcd for $C_{29}H_{37}Cl_2IrN_4$ (704.75 g/mol): C, 49.42; H, 5.29; N, 7.95. Found: C, 46.24; H, 4.93; N, 7.43. With 0.5 mol of chloroform-*d* from NMR sample, Anal. Calcd: C, 46.35; H, 4.94; N, 7.33.

Synthesis of 9-H-Ir

A scintillation vial was charged with **9-H-Ir-Cl** (0.0535 g, 0.076 mmol) and acetone (3 mL, 25 mM). Potassium hexafluorophosphate (0.0293 g, 0.159 mmol) was added and the mixture was stirred for 18 h at room temperature. The mixture was passed through a Celite pad and the solvent was removed from the filtrate under vacuum. In order to remove any remaining potassium hexafluorophosphate, the residue was washed with water (5 mL, 15 mM) leaving behind a yellow powder which was dried under vacuum for 2 d to leave **9-H-Ir** (0.0537 g, 0.0659 mmol, 86.9 % yield). Anal. Calcd for $C_{29}H_{38}ClF_6IrN_4P$: C, 42.78; H, 4.58; N, 6.88. Found: C, 43.15; H, 4.80; N, 6.81.

Synthesis of 10

An oven dried and nitrogen-filled round bottom flask (250 mL) was charged with sodium hydride (60% in oil, 0.4513 g, 11.3 mmol) and N-methylpyrrolidone (10 mL, 0.11 M). The flask set in an ice bath and solid imidazole (0.7681 g, 11.3 mmol) was added slowly under a positive pressure of nitrogen. After the foaming subsided **7-Ph** (2.63 g, 9.86 mmol; made according to reference[130]) was added

and the flask was heated in a 140 ºC oil bath for 16 h. The mixture was allowed to cool and N-methylpyrrolidone was removed using a silica column (3 cm wide, 15 cm high) using dichloromethane to elute. After concentrating product-containing fractions, **10** appeared as an off white solid (2.53 g, 8.49 mmol, 86.0 % yield). Anal. Calcd for $C_{19}H_{14}N_4$ (298.34): C, 76.49; H, 4.73; N, 18.78. Found: C, 76.16; H, 5.1; N, 18.54.

Synthesis of 12

A dry Schlenk flask (250 mL), while in the glovebox, was charged with imidazole (1.20 g, 17.7 mmol) and N-methylpyrrolidone (15 mL, making a 1.2 M solution). The flask was then set in an ice bath and the contents allowed to stir for 5 min. Sodium hydride (50% in oil, 0.825 g, 17.5 mmol) was added in portions over 1 h, during which time the mixture foamed from gas evolution. Compound **7-tBu** (3.06 g, 13.5 mmol, made according to reference[131]) was added slowly to the solution while stirring. The solution was set to stir in an oil bath at 140 °C under nitrogen for 24 h. After cooling, the mixture was diluted with methylene chloride (50 mL) and washed with water (300 mL, followed by 3 X 50 mL). The yellow organic layer was then dried over magnesium sulfate, filtered, and the solvent was removed from the filtrate by rotary evaporation. The yellow residue was purified using column chromatography (10 cm wide, 20 cm high) with a 6:1 ratio of pentane to ethyl acetate (product R_f = 0.4). Product **12** appeared as light yellow crystals (2.81 g, 10.9 mmol, 80.0 % yield). Anal. Calcd for $C_{15}H_{22}N_4$ (258.36): C, 69.73; H, 8.58; N, 21.69. Found: C, 69.37; H, 8.81; N, 21.54.

Synthesis of 11-Ph-I

An oven dried round bottom flask (250 mL) maintained under nitrogen was charged with **10** (1.01 g, 3.38 mmol) to which was added iodomethane (4.94 g, 34.8 mmol) and the resulting mixture was stirred under nitrogen for 24 h. The excess iodomethane was then removed under vacuum using rotary evaporation, with some inadvertent loss of product during transfer. **11-Ph-I** appeared as an off white solid (1.22 g, 2.76 mmol, 81.7 % yield). Anal. Calcd for $C_{20}H_{17}N_4I$ (440.28): C, 54.56; H, 3.89; N, 12.73. Found: C, 54.95; H, 4.11; N, 12.72.

Synthesis of 8-Ph

This procedure resembles one in reference.[87] **7-Ph** (2.5037 g, 11.04 mmol) and 1-methylimidazole (0.75 mL) were heated in a 110 ºC oil bath. The mixture was stirred for 17 h. NMR analysis of an aliquot indicated that the reaction was incomplete, so an additional portion of 1-methylimidazole (0.75 mL) was added and heating was continued for 28.5 h. After cooling, acetone was added and the mixture was filtered. The solid was washed with cold acetone and dried, leaving colorless solid **8-Ph** (2.9512 g, 7.167 mmol if the formula includes 3.5 equiv of water, 80.3 % yield). Anal. Calcd for $C_{20}H_{17}ClN_4$ (348.83): C, 68.86; H, 4.91; N, 16.06. Found: C, 57.99; H, 5.78; N, 13.51. Anal. Calcd for $C_{20}H_{17}ClN_4$ + 7/2 H_2O: C, 58.32; H, 5.87; N, 13.60.

Synthesis of 13-tBu-I

A round bottom flask (200 mL), while in the glovebox, was charged with **12** (1.46 g, 5.64 mmol), iodomethane (4.36 g, 30.8 mmol), and dichloromethane (30 mL, 1.2 M). The reaction was then left to stir under nitrogen for 24 h. Solvent and excess iodomethane was then removed by rotary evaporation and the residue

stored under oil pump vacuum. Product **13-tBu-I** (2.26 g, 5.63 mmol, 99.8 % yield) appeared as an off white solid. Anal. Calcd for $C_{16}H_{25}N_4I$ (400.30): C, 48.01; H, 6.29; N, 14.00. Found: C, 48.19; H, 6.16; N, 13.92

Synthesis of 13-tBu-PF_6

A round bottom flask (250 mL), while under nitrogen, was charged with **13-tBu-I** (7.65 g, 19.1 mmol) and acetone (60 mL, 0.32 M). To this potassium hexafluorophosphate (10.6 g, 57.4 mmol) was added while stirring. The reaction was left to stir for 24 h at room temperature before water (200 mL) was added, leading to formation of yellow solid. The solid was vacuum filtered, rinsed with benzene, and left to dry under oil pump vacuum for 24 h. Product **13-tBu-PF_6** appeared as a pale yellow solid (4.08 g, 9.75 mmol, 72.2 % yield). Anal. Calcd for $C_{16}H_{25}F_6N_4P$ (418.36): C, 45.93; H, 6.02; N, 13.39. Found: C, 47.55; H, 5.88; N, 12.94. Anal. Calcd for $C_{16}H_{25}F_6N_4P$ + 1/6 C_6H_6: C, 47.28; H, 6.07; N, 13.00.

Synthesis of 9-Ph

In a glove box, 1-(2,6 diisopropyl) imidazole (0.5136 g, 2.2495 mmol) and **7-Ph** (0.6001 g, 2.2495 mmol) were added to a vial containing a magnetic stir bar. N-methylpyrrolidone (0.5 mL, making a 5.2 M solution) was added to the sample in order to dissolve the solids. The sample was heated at 160°C for 40 h in an oil bath. The reaction was checked using H-NMR. The sample was heated under high vacuum in order to distill off the N-methylpyrrolidone. The residue was purified by column chromatography (10 cm wide, 15 cm high) using a gradient of methylene chloride to ethanol. **9-Ph** appeared as a statically charged powder (0.9800 g, 1.9796 mmol, 88.0 % yield).

Synthesis of 8-Ph-AgCl

In the glovebox, solid **8-Ph** (0.3064 g, 0.878 mmol) was added to a magnetically stirred suspension of silver(I) oxide (0.103.6 g, 0.447 mmol) in methylene chloride (3 mL) in a 10 mL vial. The vial was wrapped in aluminum foil in order to keep the reaction in the dark and the reaction mixture was stirred for 16 h. The reaction mixture was filtered and the solvent removed from the filtrate, leaving **8-Ph-AgCl** as a grayish solid (0.3560 g, 0.799 mmol, 88.9 % yield). Anal. Calcd for $C_{20}H_{17}AgClN_4$ (456.70): C, 52.60; H, 3.75; N, 12.27. Found: C, 52.86; H, 3.50; N, 12.34.

Synthesis of 13-tBu-Ag

In a scintillation vial which was covered in aluminum foil to keep light out of the reaction, to **13-tBu-PF_6** (0.3020 m, 0.722 mmol) and sodium hydroxide (2.0 mL, 1N) was added dichloromethane (4.0 mL). Silver(I) oxide (0.0830 g, 0.360 mmol) was added to the vial and the resulting reaction mixture was stirred for 2 d at room temperature. Aliquots were periodically removed, diluted with $CDCl_3$ and analyzed by proton NMR. The reaction mixture was then filtered through Celite and the Celite was washed with dichloromethane (3 x 10 mL). The combined filtrates were dried using magnesium sulfate, filtered, and the filtrate concentrated under vacuum, leaving **13-tBu-Ag** as a pale yellow solid (0.4240 g, 0.532 mmol, 73.8 % yield). Anal. Calcd for $C_{32}H_{48}AgF_6N_8P$ (797.61): C, 48.19; H, 6.07; N, 14.05. Found: C, 48.20; H, 5.77; N, 14.01.

Synthesis of 9-Ph-AgCl

The **9-Ph** (108.7 mg, 0.219 mmol) was added to a solution of silver oxide (0.0354 g, 0.153 mmol) dissolved in methylene chloride (20 mL, 7.65 mM) inside a 50 mL flask with a magnetic stir bar under nitrogen. The flask was wrapped in aluminum foil in order to keep the reaction in the dark and the mixture was left to stir for 16 h. The reaction was filtered through Celite and concentrated to 2 mL of solvent. **9-Ph-AgCl** was precipitated using petroleum ether (25 mL) as a sticky brown solid (0.1055 g, 0.1753 mmol, 79.9 % yield). Elemental Analysis was not in agreement with theoretical values.

Synthesis of 5c-BA

In the glovebox, a scintillation vial was charged with **5c** (0.0111 g, 0.014 mmol) and ^{15}N labeled benzylamine (0.0015 g, 0.014 mmol), followed by CD_2Cl_2 (0.5 mL, 0.03 M). The resulting solution was a slightly yellow color, which was characterized using FT-IR and NMR techniques. FT-IR (CD_2Cl_2 in CaF_2 cell, cm^{-1}): 3288.5, 3198.8, 3134.4, 3091.7, 3067.5, 3032.6, 2971.0, 2932.6, 2870.2, 1710.6, 1600.4, 1580.1, 1518.0, 1444.8, 1282.4.

CHAPTER 3 – Iridium Complexes with NHC Featuring Pyridine Pendant Groups

Chapter 2 discussed pyrimidyl NHC complexes which were the focus of much of my work, along with related data on imidazolyl NHC complexes by Hai Tran. Differences between the two systems might be due the basicity of the pendant nitrogen, or the geometry of the chelate. In order to vary basicity without changing chelate geometry, pyridyl NHCs were attractive targets. While planning the types of pyridine complexes that were to be targeted it was discovered that **5w**, in figure 21, had already be published by Jin in 2008, albeit with a chloride anion rather than a hexafluorophosphate anion.[165] The other three proposed iridium complexes were still novel, so initially the synthesis began at about the same time as the work on the pyrimidine complexes. However, due to some unique difficulties in synthesizing complexes with pyridine rings, **5z** was not created until all of the work with the pyrimidine based compounds was finished.

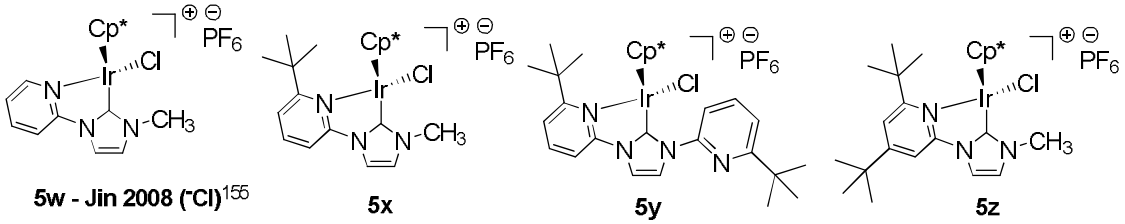

Figure 21. Targeted (pyridyl)NHC iridium complexes.

SECTION 3.1 NHC Ligands with Pyridine Substituents

Similar to the NHC ligands with pyrimidine rings that were discussed in chapter 2, chapter 3 will focus on NHC ligands with pyridine substituents. Here the goal will also be to design ligands that have chelating nitrogen atoms which may be labile enough to also act as pendant bases under catalytic conditions.

Thus, this is another method for altering the nitrogen-iridium bond strength by switching the pyrimidine ring out for a pyridine ring. By comparing the basicities of pyrimidine and pyridine (pK_a of protonated forms 1.3[124] and 5.2,[125] respectively) the related pendant bases could be expected to have different coordination and catalytic properties.

SECTION 3.2 Synthesis of Precursors for (Pyridyl)NHC Ligands

In order to make the requisite pyridyl imidazolium salts the mono-*tert*-butyl pyridine starting materials were prepared from literature,[16] while a new synthetic method had to be developed for the di-*tert*-butyl pyridyl analog. For both compounds **16-PF_6** and **17** the synthesis followed a similar methodology to that used for the pyrimidine based imidazolium salts (paths B and A respectively, Scheme 2.). The yield of **16-I** from **15** was excellent whereas that of **17** from **15** and **14-Br** was not, perhaps due to the high temperature which caused a breakdown in the pyridine ring. We did not attempt significant optimization of the latter reaction because of discovering subsequent undesired ring metalation chemistry, as described below.

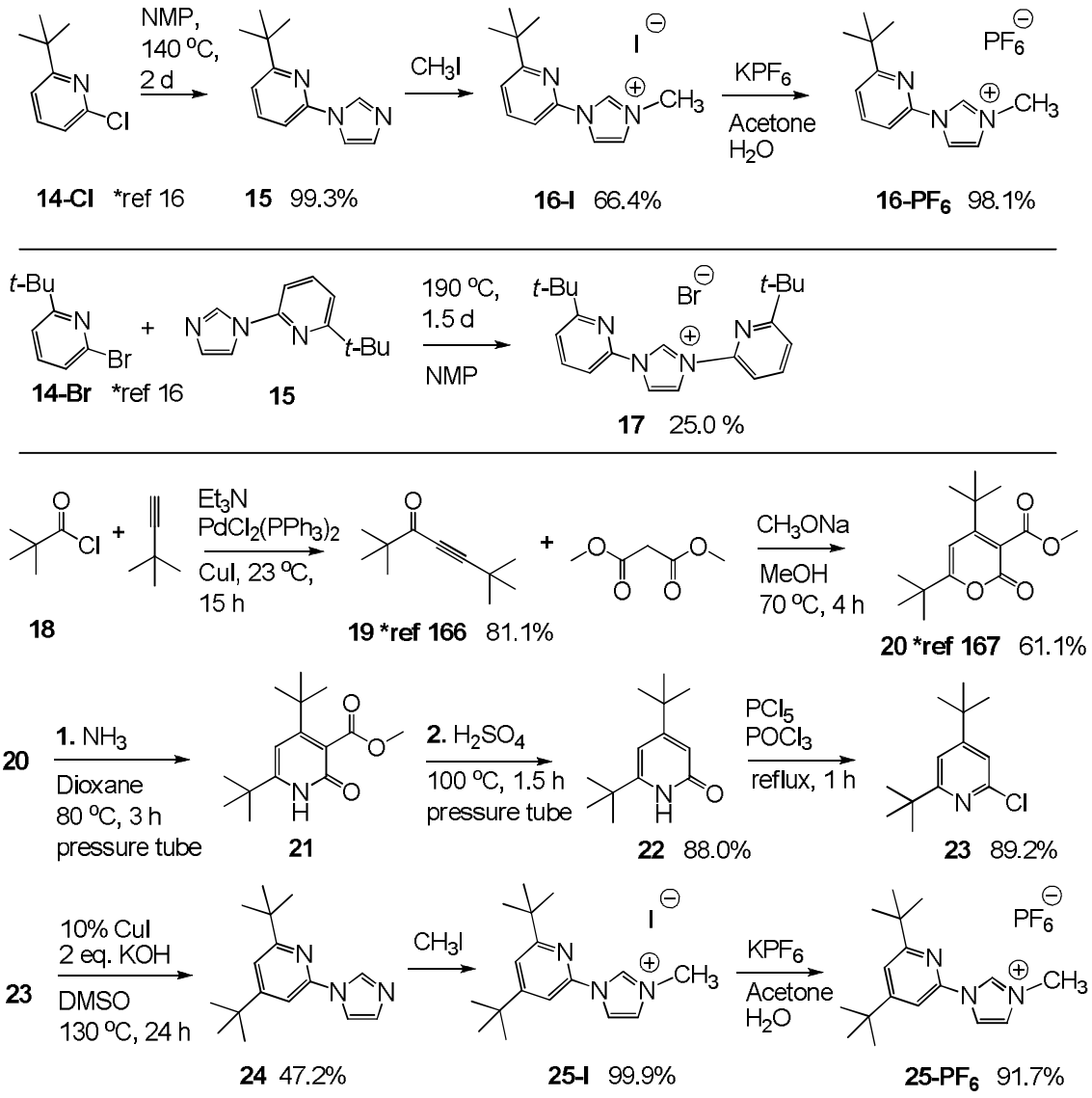

Scheme 11. Synthetic routes to precursors for (pyridyl)NHC complexes **5x**, **5y**, and **5z**.

In order to create the di-*tert*-butyl pyridyl imidazolium salt **25-PF$_6$**, first the alkynyl ketone **19** (2,2,6,6-tetramethylhept-4-yn-3-one) was created using a method published by Grotjahn *et al.* in 2002.[166] Streitwieser's 1981 published method was used to create pyrancarboxylate **20**.[167] The oxygen in the ring was

then exchanged for a nitrogen atom using ammonia and then the methyl ester group was removed using strong acid to give **22**. Phosphorus pentachloride was then used to form **23** with a good yield after which an Ullmann type copper catalyzed reaction was used to form **24**. The final steps of precursor synthesis followed the previously listed methods for methylation and anion exchange, converting **24** into **25-I** and then **25-PF_6**. The salts were characterized by elemental analysis and NMR spectroscopy, where the ^{1}H NMR spectra showed a very low field resonance in the range δ 9-11 ppm characteristic of the NC*H*N imidazolium proton.

SECTION 3.3 Synthesis of (Pyridyl)NHC Silver Complexes and Ir(III) Derivatives

Following the same methodology as in chapter 1, section 1.3, silver oxide was used to create NHC silver carbene intermediates that could then be used for transmetallation to the target iridium species. The yield for compound **25-Ag** was low, possibly due to the insolubility of the compound because of bridging between silver complexes.

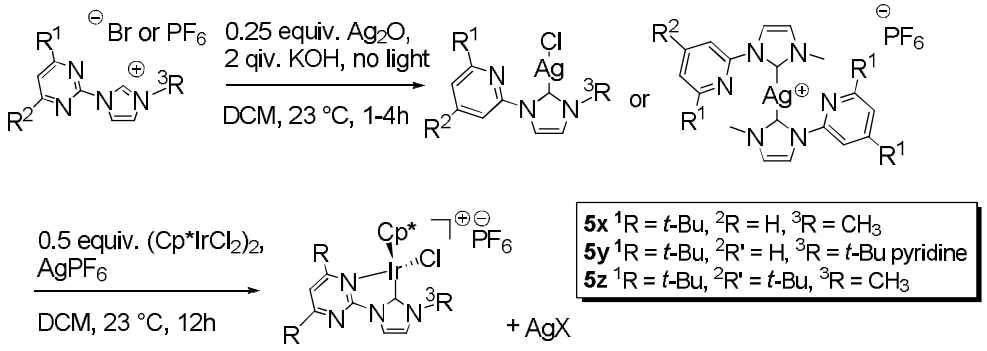

Figure 22. Synthetic route for silver and iridium (pyridyl)NHC complexes.

Table 10. Formation of Silver and Iridium (Pyridyl)NHC Complexes.[a]

Imidazolium salt	Ag complex	% Yield	Iridium Complex	% Yield
16-PF_6	**16-Ag**	66.0	**5x**	50.9
17[b]	**-**	-	**5y**	96.0
25-PF_6	**25-Ag**	42.1	**5z**	76.6

[a] For compounds **16-PF_6** and **17**, 0.5 equivalents of silver oxide was used and no KOH was added. For **25-PF_6** 0.25 equivalents of silver oxide was used and 2 equivalents of KOH was added. [b] Compound **17** was made without first isolating the silver complex.

SECTION 3.4 Crystallographic Studies of the (Pyridyl)NHC Iridium complexes

The crystal structures for all of the (pyridyl)NHC iridium complexes were obtained; bond distances and torsion angles of interest are listed in table 2. The actual crystal structures are shown in figures 23-25. Interestingly, when the mono-*tert*-butyl pyridine ring was used, the pyridyl ring metallated at the C2 carbon, rather than coordinating at the nitrogen. This is most likely due to sterics since **5z**, which had the di-*tert*-butyl pyridine ring was uncoordinated to the metal in the crystalline phase. The iridium to carbene carbon distance for **5z** was within the expected range.

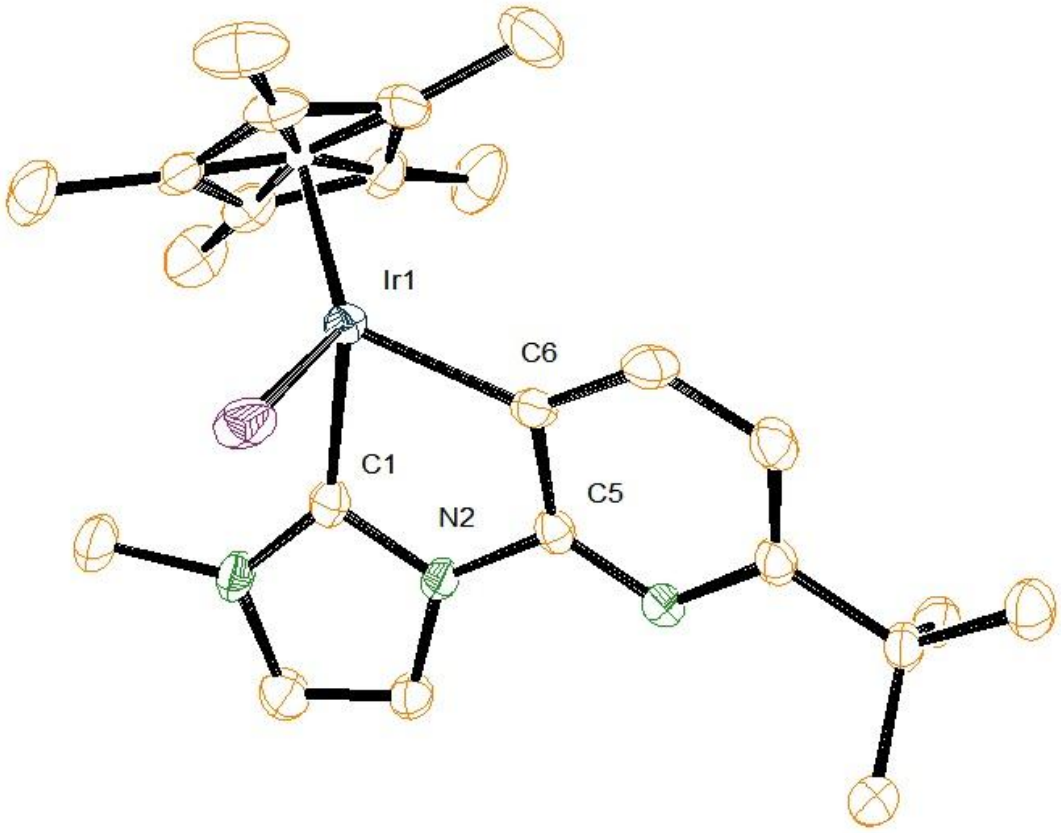

Figure 23. The (pyridyl)NHC iridium(III) compound **5x** formed from **16-Ag** with a the [(6-*tert*-butyl)pyridyl]imidazolidene ligand. The pyridine ring is bound to Ir at carbon. The crystal system was rhombohedral with the space group R-3.

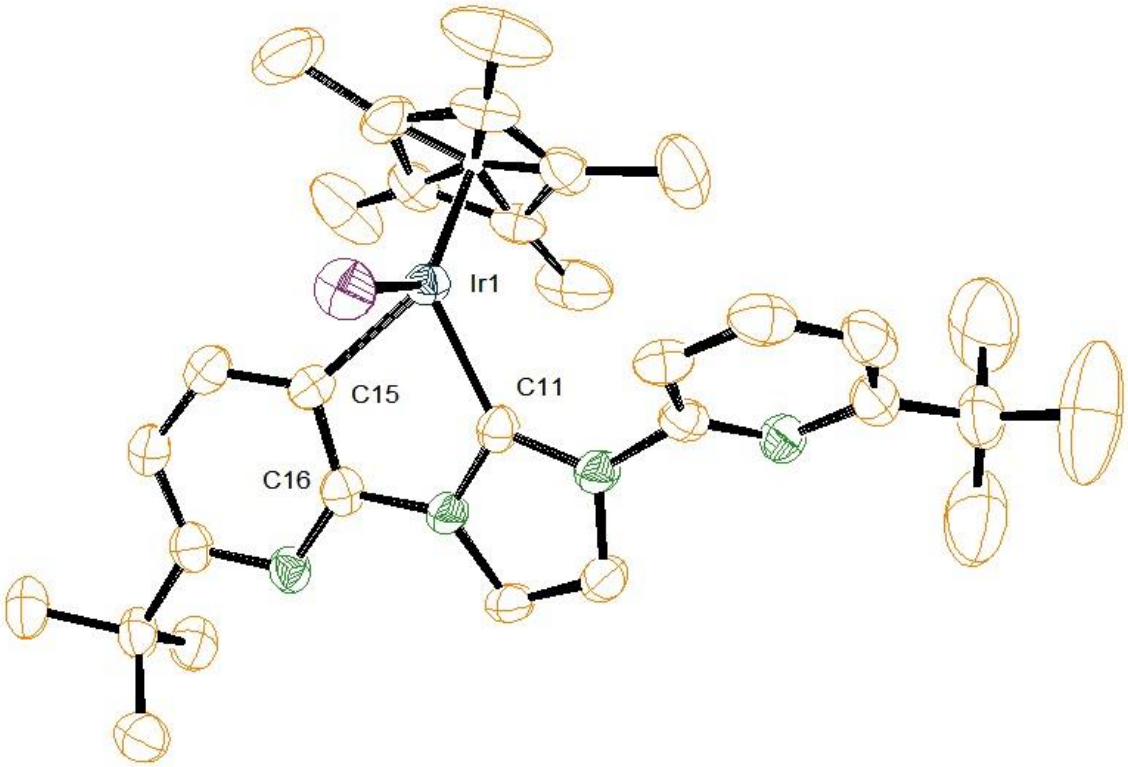

Figure 24. The (pyridyl)NHC iridium(III) compound **5y** formed from imidazolium salt **17**, with one (6-*tert*-butyl)pyridyl substituent at each nitrogen. One of the pyridine rings is bound to Ir at carbon, whereas the other is unmetallated. The crystal system was orthorhombic with the space group Pbca.

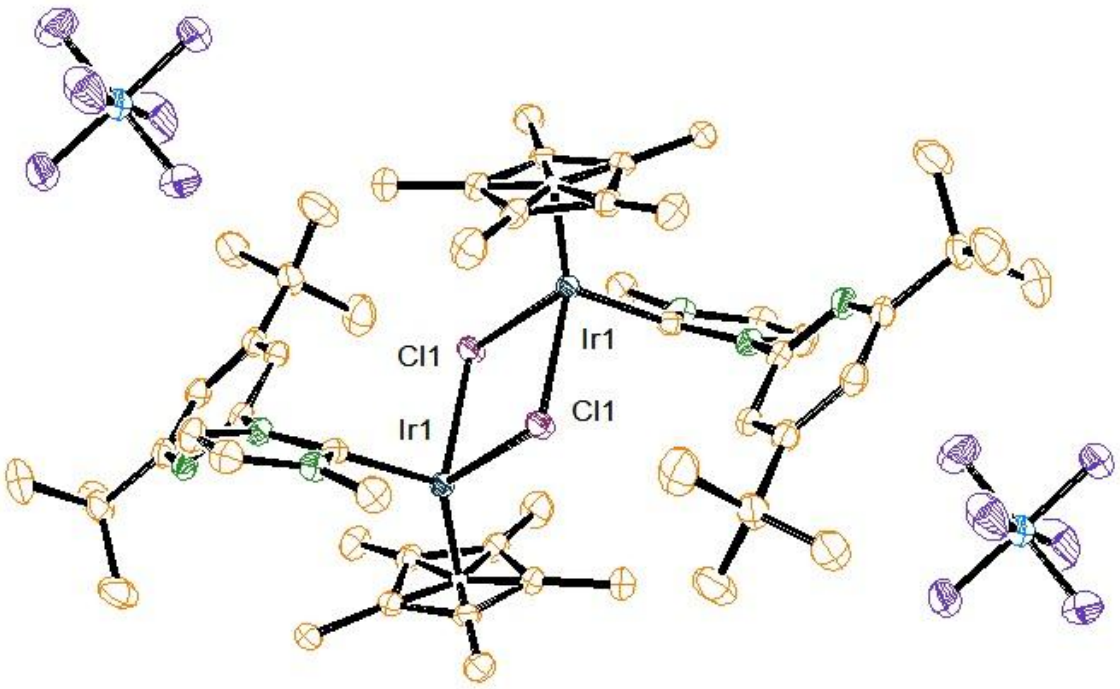

Figure 25. The (pyridyl)NHC iridium(III) compound **5z** with an intact [(di-*tert*-butyl)pyridyl]imidazolidene ligand, formed from **25-Ag**. The crystal system was triclinic with the space group P-1. In the solid state, 5z crystallized as a dimer. Solution-phase studies are consistent with a monomer and chelation of the pyridyl substituent at N3.

Table 11. X-ray crystallographic data of (pyridyl)NHC iridium complexes.

Iridium Compound	Ir-Carbene Distance (Å)	Ir-N Distance (Å)	Carbene-M-N Angle (°)	C1-N1-C4-N3 Torsion Angle (°)
5w[50]	2.004(7)	2.120(6)	76.0(3)	4.85
5x[a]	2.005(6)	2.069(6)	77.6(2)	0.6
5y[a]	2.002(5)	2.045(5)	77.2(2)	2.4
5z[b]	2.065(3)	(4.489)	-	31.82

[a] Compounds **5x** and **5y** were bound at a carbon, not nitrogen, on the pyridine ring. [b] The pyridine ring was turned away from the iridium, with too great a distance for there to be a bond present.

SECTION 3.5 Solution-phase Studies of the Structure of **5z**, its Reactivity and Catalytic Studies

The x-ray crystallography data for **5z** revealed that in the crystalline state the compound is a dimer, forming through a bridging chloride rather than form an Ir-N bond. In order to study how **5z** behaves in solution ^{15}N NMR data was gathered for compounds **25-PF$_6$**, **5z**, and **5z-BA**. The ^{15}N shifts showed that as an imidazolium salt with no coordination to the pyridine ring the shift is -104.5 ppm. The ^{15}N pyridine peak for **5z** shifts up field to -181.4 ppm, indicating some coordination to the iridium metal.[122] Finally, when another amine group is bound to the iridium metal, as with **5z-BA**, the now free pyridine nitrogen has a peak shift downfield to -96.2 ppm. This shift in the ^{15}N NMR data is clear evidence of interaction in solution between the pyridine ring and iridium metal in **5z**.

In order to compare the potential of the iridium (pyridyl)NHC complexes that were developed to have chelating nitrogen groups with those of the NHC pyrimidine complexes an NMR study was designed using ^{15}N labeled benzyl amine. Approximately 0.04 mmol of **5z** was combined with an equimolar amount of labeled benzyl amine, with 0.6 mL of CD_2Cl_2 as solvent. The NMR data are shown in scheme 12, with comparisons to the compounds studied in chapter 1. The results for all of the ^{15}N labeled benzyl amine experiments along with the ^{15}N NMR data for the relevant compounds is summarized in table 12.

Table 12. ^{15}N NMR chemical shift data for complexes and model compounds.

Compound	Solvent	Temp (^{o} C)	Heteroaryl N free	Heteroaryl N interacting	Imidazolium or imidazolylidene N1 (N-Me)	Imidazolium or imidazolylidene N-3 (with heteroaryl)	Coord. $PhCH_2NH_2$
13-tBu-PF_6	CD_2Cl_2	30	-125.7	----	-204.1	-182.3	---
13-tBu-Ag	CD_2Cl_2	30	-125.4	----	-195.4	-171.2	---
5c	Acetone-d_6	-18	-128.6	-191.2 (coord)	-201.8	-177.7	---
5c-BA	CD_2Cl_2	-90	-100.6	-118.0 (H-bond)	-192.4	-170.0	-388.4[a]
PF_6-imidazolium salt of 6	Acetone-d_6	30	-152.6, -251.4	----	-178.7	-177.9	----
6-Ag-PF_6	Acetone-d_6	30	-125.3, -230.1	----	-204.0	-204.8	---
6	Acetone-d_6	30	-179.7	-189.0 (coord)	-143.6	-158.3	---
6-BA	CD_2Cl_2	-90	-226.8	-135.3 (H-bond)	-189.8	-195.9	-385.2
25-PF_6	$CDCl_3$	30	----	-104.5	-205.9	-183.2	----
5z	CD_2Cl_2	30	----	-181.4 (coord)	-204.0	-178.8	----
5z-BA	CD_2Cl_2	-60	----	-96.2 (H-bond)	-191.5	-170.4	-385.0

[a] Data for compound made with 15N-labeled benzylamine, probe temperature 30 °C

For the pyridyl system of **5z-BA** at -60 ^{o}C, the pyridyl N in the ^{1}H-^{15}N gHMBC spectrum is at -96.2 ppm was seen. In contrast, the pyridyl N for **5z** is at -181.4 ppm, clearly showing an upfield shift of 85.2 ppm which is strong evidence[122, 137] for coordination of the nitrogen to iridium. Distinctive features of **5z-BA** include a four-spin system for the $–CH_2NH_2$ unit, with the two NH protons resonating at 6.65 and 4.01 ppm.

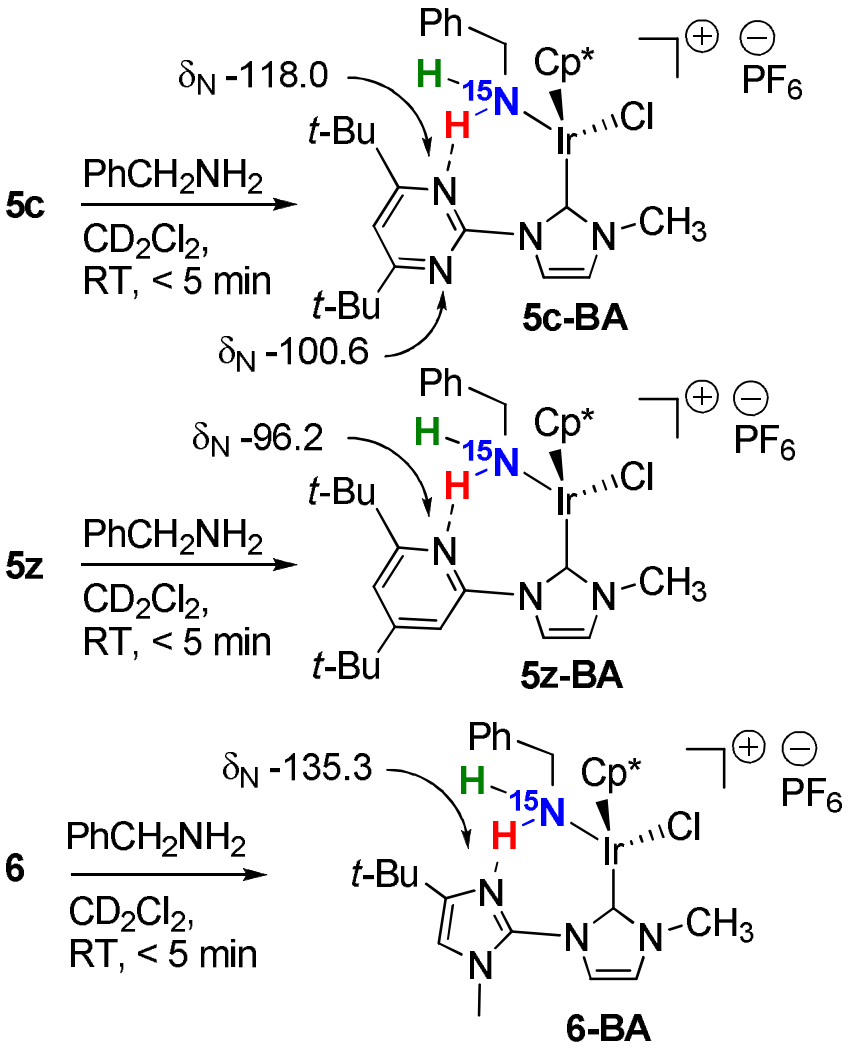

Scheme 12. NMR data derived from ^{1}H-^{15}N gHMBC spectrum, taken of samples **5c**, **5z**, and **6** complexed with ^{15}N labeled benzyl amine, shows clear interaction between the proton on the benzyl amine and the unchelated nitrogen atom.

SECTION 3.5.1 Cyclization of a Primary Aminoalkene

Catalyzed cyclization of primary amine **26** in figure 26, to give **27** in figure 21, was performed in order to compare the (pyridyl)NHC based catalysts to the pyrimidyl analogs made in chapter 2. The solvent was changed to *d*-THF in order

to get better solubility of the iridium complexes. The reactions were also performed in sealed J. Young NMR tubes in order to eliminate any loss of reactant material or accidental introduction of contamination that might be introduced because of sampling. Table 13 shows that **5a** is still the most active of (heteroaryl)NHC catalysts examined, with **5z** as the second most active. Looking at results from primary amine **26**, among (pyridyl)NHC derivatives, increase in conversion occurs on going from **5w**, which is virtually inactive, to $[Cp^*Ir(\mu\text{-}Cl)Cl]_2$, and finally to **5z** and **5c**, which are the most active. For the primary amine reaction, the production of **29**, can also be observed for **5z** and **5c,** with **5z** producing more than 50**.**

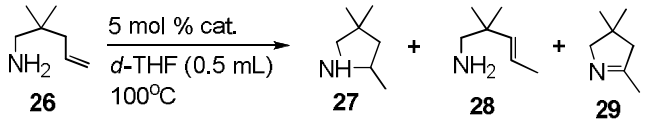

Figure 26. Products from reaction of **26**: cyclization **27**, alkene isomerization **28**, and cyclization followed by dehydrogenation **29**.

Table 13. Results for the cyclization of primary amine **26**.[a]

Catalyst	1 hour				24 hours				72 hours			
	26	**27**	**28**	**29**	**26**	**27**	**28**	**29**	**26**	**27**	**28**	**29**
[Cp*Ir(μ-Cl)Cl]$_2$	69	0	17	0	61	1.6	26	0	51	3.6	31	0
5w	96	0	2.1	0	92	0	5.6	0	78	0.5	5.6	0
5z	68	22	1.1	7.8	0	78	2.0	17	0	72	0.5	26
5c	60	31	4.1	9.1	0	78	3.3	21	0	64	0.4	33

[a] **26** (0.125 mmol) and catalyst (5 mol %; 2.5 mol% in the case of [IrCp*Cl$_2$)$_2$] in *d*-THF (0.5 mL) at 100 ^{o}C. Yields shown are based ^{1}H NMR spectroscopy, averaging results from two separate runs, except for **5c**, using 1,3,5-trimethoxybenzene as an internal standard.

SECTION 3.5.2 Cyclization of a Secondary Amine

Catalyzed cyclization of secondary amine **30 to** give **31 in** figure 27, was chosen so that the (pyridyl)NHC complexes could be compared to the pyrimidine analogs studied in chapter 2. Just as in figure 26, the solvent was changed to *d*-THF in order to get better soluablity of the iridium complexes. The catalysts **5c**, **5z**, and **6** all cyclized the secondary amine very quickly, with **5c** working slightly faster than **5z**, which was in turn slightly faster than **6**. This relative rate of reactivity suggests that there may be an inverse correlation between the basicity of the chelating nitrogen group and the reactivity of the catalyst for interacting with incoming proton donors. Due to the difficulty in determining the actual structure of what **33** may be, the most likely product of a redox reaction is shown, where the enamine double bond is located in the most substituted position

possible. This uncertainty in the structure also gives rise to an uncertainty in how much of **32** may be produced in this reaction due to peak overlap.

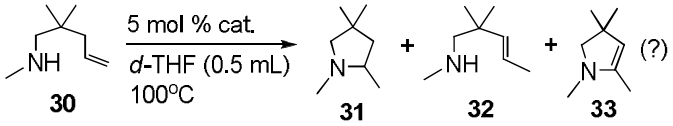

Figure 27. Products from reaction of **30**: cyclization **31**, alkene isomerization **32**, and cyclization followed by dehydrogenation **33**.

Table 14. Results for the cyclization of secondary amine.[a]

Cat.	1 hour				24 hours				72 hours			
	30	**31**	**32**	**33**	**30**	**31**	**32**	**33**	**30**	**31**	**32**	**33**
5w	99	0	0	0	95	1.3	1.0	0	85	2.6	1.0	0
5z	16	83	0	0	0	84	0	0	0	79	0	0
5c	2.9	89	2.0	0	3.0	89	2.0	0	-	-	-	-
6	37	62	3.9	0	3.8	86	4.4	0	-	-	-	-

[a] **30** (0.125 mmol) and catalyst in *d*-THF (0.5 mL) at 100 °C. Yields shown are based ^{1}H NMR spectroscopy, averaging results from two separate runs, except for **5c** and **6**, using 1,3,5-trimethoxybenzene as an internal standard.

SECTION 3.6 Conclusions

The development of the (pyridyl)NHC ligands allowed for a series of comparisons to be draw for both the steric effects and electronic tuning of the ligands relative to the iridium metal center. One of the most revealing findings was that a single *tert*-butyl substituent on the pendant pyridine adjacent to the nitrogen atom did completely prevent Ir-N bond formation, but surprisingly lead to formation of a carbon-metal bond on the other side of the pyridine ring, shown in crystallography of **5w**, figure 18. Inclusion of a second *tert*-butyl substituent on

the pyridine ring, as in **5z**, did block cyclometallation. The 2D NMR evidence points to coordination between the pyridine ring and iridium in solution. The Ir-N chelation can be broken by a coordinating amine (as in the pyrimidyl case), but also on crystallization, forming a chloride-bridged dication with no Ir-N interaction in the solid. Although we have no direct way of measuring Ir-N bond strength as we did in the case of the fluxional (pyrimidyl)NHC systems, it seems like in the case of di-*tert*-butylpyridyl species there is also a weakened interaction between the nitrogen and iridium, as desired

When compounds **5w** and **5z** were tested as catalysts for cyclizing primary and secondary amines the results clearly showed that the strongly chelated **5w** had little reactivity while **5z** completely consumed starting material within 24 hours for both kinds of alkeneamines. However, when examining the data primary amine reactions it appears that **5c** is very slightly faster that **5z**. In the case of cyclizing secondary amines the order of reactivity may be related to the basicity of the chelating nitrogen atom, with what is most likely has the least basic nitrogen, **5c**, being the fastest while **6** may have the most basic nitrogen and appears to be the slowest catalyst, but we note that the rate differences are small (less than a factor of two). It is possible that metal-ligand bond strength (lability), hydrogen bonding strength, or a combination of these factors may enter into play in what is certainly a multistep catalytic process.

SECTION 3.7 Experimental

Synthesis of 5x

Compound **16-I** (0.2504 g, 0.7296 mmol) was added to a stirred suspension of silver oxide (0.0876 g, 0.378 mmol) in dichloromethane (3 mL) in a 10 mL vial under nitrogen. The vial was wrapped in aluminum foil in order to keep the reaction in the dark and left to stir for 2 h. The solution was a shiny silver color. Solid $(Cp^*Ir(\mu\text{-}Cl)Cl)_2$ (0.2939 g, 0.3689 mmol) was added under nitrogen and the reaction mixture was allowed to stir for 24 h. The orange-red solution was filtered through cotton in order to remove the silver chloride, using rinses of dichloromethane to dissolve the sample. After concentration, the residue was recrystallized from cold dichloromethane as a mixture of iodine and chloride bound atoms to the iridium metal center, based on ^1H NMR spectra that showed two species were present because of two separate sets of peaks observed between 8.00 and 6.50 ppm. In order to replace the iodine with chloride the sample was dissolved in methanol (3 mL) along with an excess of potassium chloride (20:1 ratio). The mixture was set to stir at 65 ºC for 3 d. Water was then added to the reaction and the sample precipitated out. The solid was set to dry under vacuum for 3 d, leaving **5x,** a yellow-red solid (0.2278 g, 0.3799 mmol, 50.9% yield). Anal. Calcd for $C_{23}H_{33}Cl_2IrN_3$ (614.65 g/mol): C, 44.94; H, 5.41; N, 6.84. Found:C, 45.13; H, 5.01; N, 6.76.

Synthesis of 5y

Compound **17** (0.0504 g, 0.1213 mmol) was added to a stirred suspension of silver oxide (0.0140 g, 0.0060 mmol) in dichloromethane (4 mL) in a 50 mL flask

while under nitrogen. The flask was wrapped in aluminum foil in order to keep the reaction in the dark and left to stir for 2.5 h. The solution was a brown color. Solid $(Cp^*Ir(\mu\text{-}Cl)Cl)_2$ (0.0397 g, 49.83 μmol) was added under nitrogen and the reaction mixture was allowed to stir for 24 h. The caramel colored solution was purified through column chromatography on silica gel, eluting with a solution of acetone and methylene chloride (1:1 ratio). The brown solvent was removed using a rotary evaporator and then the solid dried under vacuum for 1 day, leaving **5y**, a brown foam (0.0692 g, 95.96 μmol, 96.0% yield). Brown crystals were then grown using vapor diffusion of methanol into pentane for x-ray analysis. The x-ray analysis revealed that the compound was neutral and the halogen bound the iridium metal had a ratio of 22% bromide and 78% chloride, giving the sample an effective molecular weight of 721.16 g/mol. Elemental analysis was not performed on the sample.

Synthesis of 5z

In a 20 mL screw cap vial, solid $(Cp^*Ir(\mu\text{-}Cl)Cl)_2$ (0.3309 g, 0.4183 mmol) was added to **25-PF_6** (0.3304 g, 0.4153 mmol) and silver hexafluorophosphate (0.1077 g, 0.4260 mmol) in methylene chloride (1 mL) under nitrogen. The resulting mixture was stirred for 18 h. The orange-red mixture was filtered through Celite in order to remove the silver chloride; the filter cake was rinsed with dichloromethane (5 mL total) in several portions. The orange/red colored solution was purified through column chromatography on silica gel in a solution of ethyl acetate. The red solvent was remove using a rotary evaporator and then the solid was set to dry under vacuum for 1 day, leaving **5z,** a red foam (0.4956

g, 0.6360 mmol, 76.6% yield). Red crystals were then grown using vapor diffusion of ether into ethyl acetate for x-ray analysis. The x-ray analysis revealed that the compound was a dimer when in the solid state. Anal. Calcd for $C_{27}H_{40}ClF_6IrN_3P$ (779.26 g/mol): C, 41.61; H, 5.17; N, 5.39. Found: C, 41.45; H, 5.30; N, 5.39.

Synthesis of 15

In a glovebox, a 250 mL Schlenk flask with a stir bar was charged with NaH (1.658 g, 61.1 wt % in oil, 42.2 mmol) and NMP (30 mL). Outside the glovebox, the flask was placed in an ice bath. Under positive nitrogen flow was added imidazole (2.93 g, 43.0 mmol) in portions over 5 min, producing foaming, and the flask was capped with a septum once more. After 5 min, the ice bath was removed. After 50 min, under positive nitrogen flow was added 6-*tert*-butyl-2-chloropyridine (5.71 g, 33.7 mmol). The flask was capped with a septum once more, and the flask was placed in a 140 ^{o}C oil bath for 44 h. To the cooled mixture was added water (150 mL), and the resulting mixture was extracted with CH_2Cl_2 (5 x 50 mL). Analysis by TLC showed that most product was in extracts 1 and 2, with a trace in 4. Extracts 1 and 2 were combined as were 3 and 4, and each portion was washed with water (3 x 125 mL). The combined aqueous washes were back-extracted with CH_2Cl_2 extract 5. After drying, filtration, and concentration, crude product (14.5 g) was purified by flash chromatography over silica, eluting with ethyl acetate / petroleum ether (1 : 4) containing some aqueous ammonia. Product-containing fractions were concentrated and the residue (6.66 g) was recrystallized from CH_2Cl_2 and hexane and pentane. **15** was

afforded as colorless crystals (5.81 g, 97%). Anal. Calcd for $C_{12}H_{15}N_3$ (201.27 g/mol): C, 71.61; H, 7.51; N, 20.88. Found: C, 71.71; H, 7.17; N, 21.00.

Synthesis of 16-I

Compound **15** (0.1356 g, 0.673 mmol) and iodomethane (2.1970 g, 15.478 mmol) were added to round bottom flask with a magnetic stir bar under nitrogen. The reaction was then left to stir under nitrogen for 24 h. Excess iodomethane was then removed under vacuum. The **16-I** appeared as an off white solid (0.1534 g, 0.447 mmol, 66.4% yield, low yield due to spillage). Anal. Calcd for $C_{13}H_{18}N_3I$ (343.21 g/mol): C, 45.49; H, 5.29; N, 12.24. Found: C, 45.12; H, 5.01; N, 12.06.

Synthesis of 16-PF_6

Solid **16-I** (0.3004 g, 0.875 mmol) was added to a 20 mL vial, followed by acetone (10 mL) as the solvent. To the resulting suspension, potassium hexafluorophosphate (0.1620 g, 0.880 mmol) dissolved in acetone (5 mL) was added while stirring. The reaction turned a pale yellow color and was then left to stir for 2 h at room temperature. The mixture was filtered through Celite, the filter cake was rinsed with acetone (5 mL) and the combined filtrates concentrated by rotary evaporation. In order to ensure that the ion exchange fully took place more potassium hexafluorophosphate (0.1674 g, 0.909 mmol) dissolved in methanol (5 mL) was added while stirring. After 2 h water was added to precipitate the product as a solid, and the solvent was decanted off.

The **16-PF_6** appeared as an pale yellow solid (0.1496 g, 0.4141 mmol, 47.4% yield). Anal. Calcd for $C_{13}H_{18}F_6N_3P$ (361.27 g/mol): C, 43.22; H, 5.02; N, 11.63. Found: C, 43.60; H, 4.66; N, 11.90.

Synthesis of 16-AgI

Solid **16-I** (0.1495 g, 0.436 mmol) was added to a suspension of silver oxide (0.053 g, 0.2287 mmol) in methylene chloride (4 mL) in a 20 mL vial containing a magnetic stir bar under nitrogen. The vial was wrapped in aluminum foil in order to keep the reaction in the dark. The reaction was set to stir for 16 hours. Afterwards, the reaction was filtered through Celite and the solvent removed from the filtrate. The residual **16-AgI** appeared as a gray/silver colored solid (0.1297 g, 0.288 mmol, 66.2% yield). Anal. Calcd for $C_{13}H_{18}IN_3$ (343.21 g/mol): C, 45.49; H, 5.29; N, 12.24. Found: C, 45.12; H, 5.01; N, 12.06.

Conversion of 20 to 21

Two thick-walled pressure reaction tubes (48 mL volume each) were charged with half of a sample of **20** (containing ca. 15% of unknown impurity from its reported synthesis) (2.833 g, 10.6 mmol assuming 100% purity). To each tube was added 1,4-dioxane (6 mL) followed by concentrated ammonium hydroxide (12 mL to each). Each tube was sealed with a threaded Teflon stopper and the tubes were heated for 2.8 h in an oil bath held at 80 ^{o}C, behind a safety shield, as the contents were stirred. Initially, within about 20 min the solids mostly dissolved, giving a cloudy mixture. After an additional 15 min and thereafter, reappearance of solids was noted. After a total of 2.8 h, the tubes were allowed to cool before the contents were transferred to a round-bottom flask. Methanol

was used in portions for quantitative transfer. The mixture was concentrated to dryness by rotary evaporation, followed by storage under oil pump vacuum overnight, leaving white solid (2.23 g). Analysis by ^{1}H, $^{13}C\{^{1}H\}$, HSQC and HMBC NMR spectroscopy was consistent with the presence of a mixture of compounds with a methyl ester group verses a carbocyclic group (molar ratio 1 to 10) on the ring. For **21** in the mixture: ^{1}H ($CDCl_3$, 499.94 MHz) δ 10.94 (br s, 1H), 6.36 (d, *J* = XX, 1H), 6.13 (d, *J* = XX, 1H), 1.36 (s, 9H), 1.25 ppm (s, 9H). $^{13}C\{^{1}H\}$ ($CDCl_3$, 125.72 MHz) δ 165.53, 165.37, 112.8, 100.5, 35.50, 35.09, 30.2, 29.3 ppm.

For the intermediate in the mixture: ^{1}H ($CDCl_3$, 499.94 MHz) δ 12.00 (br s, 1H), 6.18 (s, 1H), 3.87 (s, 3H), 1.32 (s, 9H); second tBu singlet obscured by large singlet for carbocyclic group at 1.36 ppm. $^{13}C\{^{1}H\}$ ($CDCl_3$, 125.72 MHz) δ 169.6, 163.5, 160.2, 156.0, 100.8, 52.3, 36.8, 35.3, 30.5, 29.2 ppm.

To the solid was added concentrated sulfuric acid (12 mL) and the resulting syrup was stirred as the flask was held in a 100 ^{o}C oil bath for 2 h. The flask was cooled in ice, and ice chips (ca. 50 cc) were added, followed by portions of KOH (20.0 g) in water (15 mL). The mixture was still acidic (pH = 1) but by adding portionwise most of a mixture of K_2CO_3 (20.3 g) and water (20 mL) until no more foaming was evident, the pH was raised to 9. The resulting heterogeneous mixture was diluted with water (200 mL) and extracted with DCM (1 x 100 mL, 3 x 50 mL) in a 250 mL separatory funnel. The first three organic extracts were combined and washed with water (2 x 100 mL). The two water washes were

combined and back-extracted with the fourth DCM extract. Organic extracts were dried over $MgSO_4$, filtered, and the filtrate concentrated. The white solid was stored under oil pump vacuum for 1 d, leaving **21** (1.94 g, 9.35 mmol, 88% overall yield from **20**). Anal. Calcd. for $C_{13}H_{21}NO$ (207.32 g/mol): C, 75.32; H, 10.21; N, 6.76. Found: C, 76.31; H, 10.91; N, 7.14.

Synthesis of 23

The **22** (2.47 g, 11.915 mmol) was added to a dry 100 mL Schlenk flask containing phosphorus oxychloride (2.1 mL) as the solvent. The solution was then bubbled with nitrogen gas for 5 min and the flask was placed in a 100°C oil bath. Phosphorus pentachloride (2.853 g, 13.702 mmol) was then added to the reaction slowly, with fizzing seen while stirring, while kept under a nitrogen atmosphere. A condenser was then attached to the flask and the oil bath was heated to 165 °C. After 1 h the reflux was stopped and the volatiles were removed under reduced pressure (20 mm Hg) at 120°C. The residue was a white solid with a yellow colored oil. To this, water (24 mL) was added and the reaction was set in an ice bath. Potassium hydroxide (3.8966 g, 68.509 mmol) was slowly added to the flask to adjust the pH. The yellow colored solution was then worked up using water (5 mL) and diethyl ether (50 mL) in a 250 mL separatory funnel. The aqueous layer was then extracted four times with diethyl ether (4 x 25 mL). The organic layers were then combined and washed with two portions of saturated potassium carbonate solution (2 X 40 mL) and once with water (40 mL). The organic layer was dried over magnesium sulfate and most of the yellow

colorant was removed on a plug of silica, using diethyl ether as the solvent. The solvent was removed under vacuum to give the final product.

23 appeared as an pale yellow oil (2.3458 g, 10.391 mmol, 89.2% yield). Anal. Calcd for $C_{13}H_{20}ClN$ (225.76 g/mol): C, 69.16; H, 8.93; N, 6.20. Found: C, 68.90; H, 9.32; N, 6.47.

Synthesis of 24

On the balance, **23** (0.148 g, 0.656 mmol) was added to a dry 25 mL flask, then dimethyl sulfoxide (1.3 mL) was added as the solvent. Imidazole (0.067 g, 0.984 mmol), copper (I) iodide (0.0273 g, 0.0656 mmol), and potassium hydroxide (0.0773 g, 1.3776 mmol) were then added to the reaction flask in that order. The solution, green in color, was then bubbled with nitrogen gas for 5 min and the flask placed in a 150°C oil bath for 48 h. After 1 h of heating the reaction solution turned a dark red color. The reaction was checked periodically by analyzing aliquots by ^{1}H NMR spectroscopy until all of the peaks for the starting material were gone. The red liquid was then worked up with 10 mL of 10% ammonium hydroxide and 30 mL of methylene chloride in a 150 mL separatory funnel. The brown colored aqueous phase was then extracted with three portions of methylene chloride (3 x 20 mL). The organic layers were then combined and washed with 10 mL of saturated ammonium chloride solution. The organic layer, a brown color, was dried over sodium sulfate and most of the brown colorant was removed by passing the mixture through a plug of silica, using methylene chloride as the eluant. After concentration, the residue was further purified

through recrystallization using the diffusion of pentane into a diethyl ether solution while the sample was kept in the freezer.

The **24** appeared as white crystalline solid (0.797 g, 0.380 mmol, 47.2% yield). Anal. Calcd for $C_{16}H_{23}N_3$ (257.37 g/mol) C, 74.67; H, 9.01; N, 16.33. Found: C, 74.47; H, 8.95; N, 16.09.

Synthesis of 25-I

Solid **24** (0.093 g, 0.363 mmol) and iodomethane (0.515 g, 3.629 mmol) were added to a 20 mL vial with a magnetic stir bar. The reaction was then left to stir under nitrogen for 2 h. Excess iodomethane was then removed under vacuum. The **25-I** appeared as white solid (0.136 g, 0.341 mmol, 93.9% yield). Anal. Calcd for $C_{17}H_{26}IN_3$ (399.31 g/mol): C, 51.13; H, 6.56; N, 10.52. Found: C, 50.90; H, 6.39; N, 10.66.

Synthesis of 25-PF_6

The **25-I** (0.1266 g, 0.317 mmol) was added to a 20 mL vial with acetone (2 mL) as the solvent. To this potassium hexafluorophosphate (0.061 g, 0.333 mmol) dissolved in water (2 mL) was added while stirring. The reaction turned a pale yellow color and was then left to stir for 1 h at room temperature. The acetone was then removed under vacuum and a white solid precipitated out of the solution. An aqueous workup was done using 5 mL of water and 5 mL of methylene chloride in a 60 mL separatory funnel. The aqueous phase was then extracted with three portions of methylene chloride (3 x 5 mL). The organic layers were then combined and the methylene chloride was removed under vacuum.

The **25-PF_6** appeared as white solid (0.114 g, 0.273 mmol, 86.2% yield). Anal. Calcd for $C_{17}H_{26}F_6N_3P$ (417.37 g/mol): C, 48.92; H, 6.28; N, 10.07. Found: C, 49.20; H, 6.06; N, 10.33.

Synthesis of 25-Ag

Solid **25-PF_6** (0.048 g, 0.114 mmol) was added to a 20 mL vial, wrapped in foil to keep light out, followed by methylene chloride (2 mL) as the solvent. To the resulting solution was added sodium hydroxide (0.1 mL, 1 M) followed by silver oxide (0.0091 g, 0.038 mmol). The mixture was set to stir under nitrogen for 10 h. The resulting mixture was a tan color solution. An aqueous workup was done using 5 mL of water and 5 mL of methylene chloride in a 60 mL separatory funnel. The aqueous phase was then extracted with three portions of methylene chloride (3 X 5 mL). The organic layers were then combined and the methylene chloride was removed under vacuum.

The **25-Ag** appeared as tan foam (0.044 g, 0.055 mmol, 97.3% yield). Anal. Calcd for $C_{34}H_{50}AgF_6N_6P$ (795.63 g/mol): C, 51.33; H, 6.33; N, 10.56. Found: C, 51.60; H, 6.23; N, 10.66.

CHAPTER 4 – Future Work Designing Catalytic Systems

As part of my time in graduate school I have been able to work with several talented undergraduate students. Two of them in particular, Khoi Le and Ariana Pérez, have agreed to work with me on two completely new projects for the Grotjahn lab. Khoi will work on developing novel NHC metal complexes with the goal of being able to synthesize commercially interesting chemicals from glycerol. This research will be funded for three months by a grant from the California State University Program for Education and Research in Biotechnology (CSUPERB). Ariana has been working on developing metal-free catalysts for the processing of vegetable oil into methyl ester compounds for biodiesel. I have included in chapter 4 the research proposals that I developed for the two projects since these projects are, in a sense, the future work for my particular branch of research.

SECTION 4.1 Developing Catalysts for Renewable Materials

Recently there has been a renewed interest in developing fuels and materials from renewable feed stocks, aimed at weaning the world economy of petroleum and its derivatives.[168-170] One of the many possible bio-renewable feed stocks for this industrial renaissance is glycerol, which has become cheap and abundant due to the rise in bio-diesel production from triglycerides that forms glycerol as a side product.[171] Several groups have already begun to explore the possible fine chemicals that can be derived from glycerol, typically with the goal

of selectively removing one or two of the alcohol groups.[172] The goal of this research project will be to develop a catalyst that can transform glycerol into a more industrially useful compound, shown in figure 28.

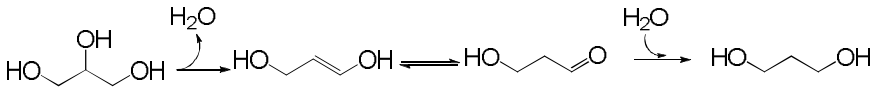

Figure 28. One possible reaction mechanism 1,3-propanediol formation via dehydration hydrogenation, taken from Hanefeld (2011).[171]

Of all the derivatives of glycerol, 1,3-propanediol is commercially the most interesting. It is used in resins, engine coolants, dry-set mortars, water based inks, but most of it is used in the production of polypropylene teraphthalate (PPT), which is a polyester synthesized from 1,3-propanediol and teraphtalic acid.[168, 171] 1,3-propanediol is marketed by DuPont as Sorona™ and Shell sells it under the trade name Corterra™.[173] With all of the uses that 1,3-propanediol has it is not surprising that there have already been several different methods developed for manufacturing it. Shell's process for the production of 1,3-propanediol involves hydroformylation of ethylene oxide to the intermediate 3-hydroxypropanal, followed by *in situ* hydrogenation to 1,3-propanediol using a homogeneous Co/Ru-based catalyst system.[174] The DuPont-Degussa process consists of the hydration of acrolein, which is apparently is easily accessible via selective air oxidation of propene, to 3-hydroxypropanal followed by *in situ* hydrogenation to 1,3-propanediol.[175] A joint venture by DuPont and Tate & Lyle uses a fermentation process based on glycerol, with the goal of selectively removing one or two of the glucose alcohol groups.[176]

In order to improve upon the existing industrial synthetic methods there have been several studies published on the conversion of glycerol to 1,3-propanediol. Most of the recent work focused on using heterogeneous catalyst such as tungsten oxide or with either rhodium, ruthenium, or palladium co-catalysts.[172, 177-180] Of the work that focused on the development of homogenous catalysts, Bullock was able to develop a ruthenium based catalyst that showed some deoxygenation of glycerol in sulfolane at 110^{o}C, though the yield was poor.[181] Schlaf was able to improve upon this with the development of several different ruthenium aqua complexes which showed the potential to be good deoxygenation catalysts at tempatures above 175 ^{o}C, although there was still poor selectivity for 1,3-propanediol production.[182]

Our goal is to attempt developing a catalyst based on iron for glycerol transformation was based on several factors, among them relative abundance of raw materials, low cost, and minimal environmental impact. Iron is attractive because of its relative abundance (it is the fourth most abundant element on earth), and its chemical similarity to ruthenium. This, in turn, makes iron a much more cost effective metal to use and has the added bonus of being an easy metal to work with due to its very low toxicity compared to other metals. The proposed design of the iron complexes is based on strongly chelating nitrogen containing N-heterocyclic carbene ligands, as shown in figure 29. These types of carbene ligands have been shown to have excellent electron donating properties, which should help in developing stable, yet reactive catalysts.[183] These

complexes will then be tested using similar methods listed in references listed in references 177-180.

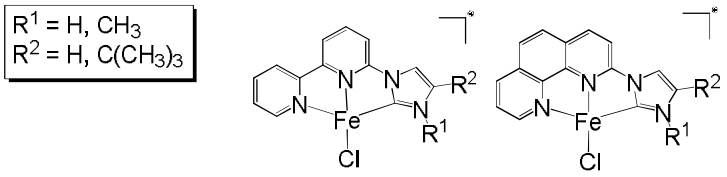

Figure 29. The proposed ligand-iron complexes for glycerol reduction catalyst.

SECTION 4.2

With the estimated oil reserves left in the world nearing their predicted peak[184] there has been a renewed interest at the governmental[185], economic[186], and social levels[187] for developing alternative forms of energy. The focus of this project is to develop an effective, metal-free, catalyst for the production of bio-diesel fuels. The current methods for processing bio-fuels involve strong bases and high temperatures in reactions that can take several hours to complete; depending on the scale of the reaction.[188-189] The general method used in industry is out lined in scheme 13. The goal is to develop a safe, efficient catalyst that can operate at low temperatures. The catalyst development will be based on using nitrogen containing compounds that can react with the triglycerides harvested from various plant sources, allowing for processing of oils into biodiesel.

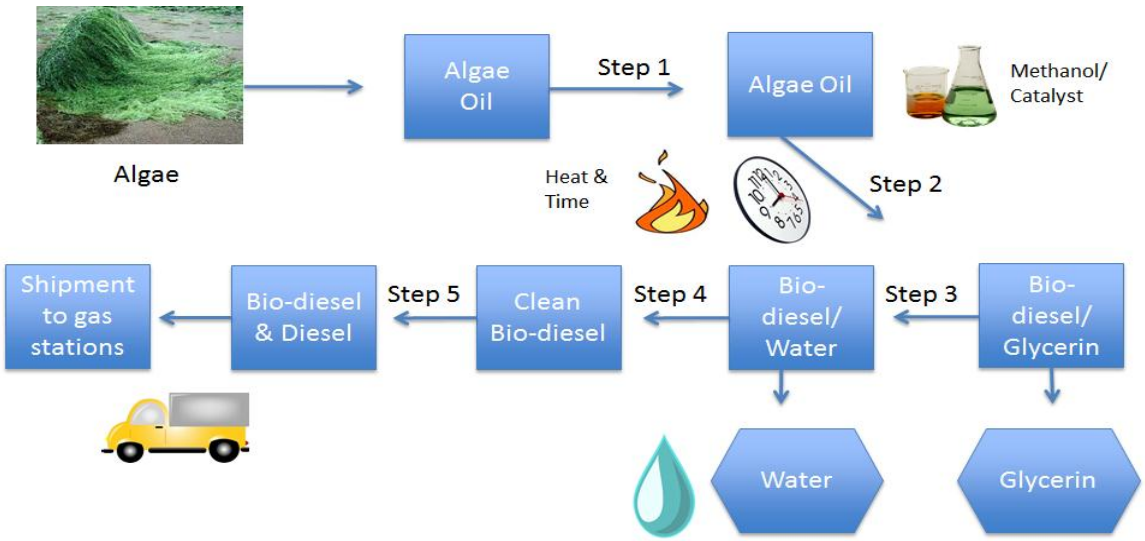

Scheme 13. General method for large scale production of biodiesel.

In order to accomplish this goal, we will be breaking the project down into two parts. First the potential catalysts will need to be screened for reactivity using published methodology for similar transesterification reactions.[190] The catalytic reaction, out lined in figure 30, would be based on a simplified analog of triglycerides, such as isopropyl stearate as a model, and the substituting alcohol group would be methanol. The reactions would be monitored using several different instruments, including nuclear magnetic resonance (NMR) and gas chromatography coupled to mass spectrometry (GCMS). These catalysts will be based on 4-dimethylaminopyridine (DMAP), a cheap, relatively available compound that has been shown to work well for esterification and transesterification reactions.[191]

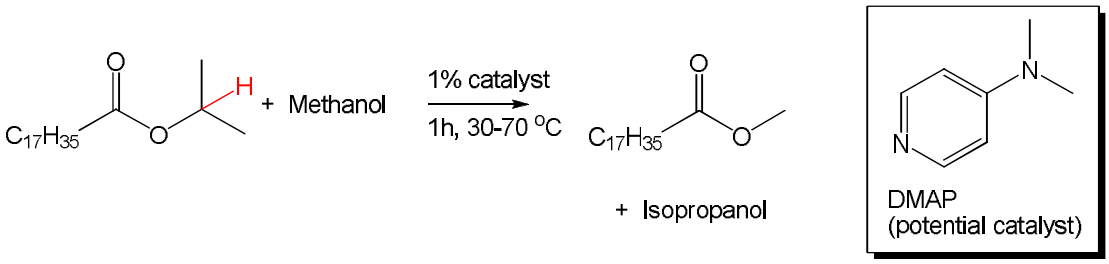

Figure 30. Proposed catalytic testing and experiment set-up.

Once a potential catalyst(s) has been found, the catalyst's ability to process oil derived from vegetable or algae sources will be explored. This process will be optimized for maximum yield and the method developed will be compared to conventional methods used in industry. The conversion of starting material to product and isopropanol can be monitored by ^{1}H NMR spectroscopy through the peak shift of the hydrogen, labeled red, of isopropyl stearate. It is possible that the time needed for reactivity will be lower due to the non-ionic nature of the catalyst. Once the testing has been completed the project could be used as a springboard for further catalytic development or the compound could be patented and pushed to market.

CHAPTER 5 – UCSD Socrates Fellow

During the 2010-2011 academic year I was funded by the National Science Foundation as a GK-12 fellow at UCSD, a program that awarded 12-month fellowships to eligible UCSD PhD students and stipends for eligible San Diego-area teachers to work together to enhance the science classroom. The UCSD program, called the Socrates program, focused on education at the high school level. Graduate students and high school teachers worked together in order to develop and implement compelling, inquiry-based science lessons for high school students. I was partnered with Duke Raley, at East Lake High School, and also worked as an ACS science coach[192], helping to start a chemistry club at East Lake. During that time I also conducted outreach programs with local elementary schools through the East Lake chemistry club and helped to create a booth at the San Diego science festival.

One of the projects that I helped to develop was an interactive exercise designed to teach students about electron orbital shapes. The students carry out several different exercises in dropping marbles onto folded paper that has sheets of carbon paper underneath it. This is then used to show how patterns of electron density have be organized into different shapes based on the number of nodes, or blank spaces, around the nucleus that is drawn at the center of the paper. The exercise concludes with exploratory questioning on orbital shapes by explaining how the patterns may appear in 3-D. This project has been submitted to the Journal of Chemical Education for publication.[193]

SECTION 5.1 Overview of the Electron Orbital Exercise

As part of the current high school chemistry standards in America, students are expected to know that electrons orbit the nucleus of an atom and that these orbits form certain patterns that are labeled *s, p, d,* or *f.*[194] However, the connection between the orbital labels, shapes, and location around can be a difficult one to make since students do not see this in their everyday experiences.[195] In order to help the students learn about the probability of finding an electron around an atom, the students must learn the meaning of electron density. By mapping out an area around a center point, representing a nucleus of an atom, the student will begin to see a pattern emerge. The shape of this pattern will change as folds are made in the paper, representing nodes, which give rise to regions around a nucleus where the electrons are not likely to be found. This method of generating an approximation of electron density around an atom is similar to the idea behind computer models that calculate the electron density of molecules.[196-197]

Once the students have a conceptualization about why the orbitals have a particular shape it is important to make the connection to an orbital's designated letter (i.e. *s, p, d* and *f*), derived from the characteristics of their spectroscopic emission lines: sharp, principal, diffuse, and fundamental.[198] By creating a model of the orbital themselves, the students gain a greater understanding of concept based on their involvement in the exercise.[199-200] Finally, the idea of these electron orbitals forming layers around a nucleus is key to setting the foundation for later topics in chemical reactivity; such as learning about valence electrons in

bonding, how atoms can absorb and transmit energy and light, and why atomic bonds have certain geometries based on the Pauli exclusion principle and Valence Electron Shell Pair Repulsion theory.[201-202]

SECTION 5.2 Implementation Guide

It is very unlikely that students will know much about electron density around an atom or the patterns that the electron orbitals form at the beginning of the exercise. However, it is still important to ask the students about their prior knowledge of electron density. This will help to both establish a common ground for the class's level of knowledge as well as lead to questioning why they would be interested in knowing about atomic orbitals and electron density. The next question for the class should be about something to which they can relate, such as how LCD screens, photovoltaic panels, or LASERs work. All of these devices could not have been developed without knowing how electrons interact with the nucleus of an atom. Finally, it is important to define electron density as the probability to find an electron in a certain area around a nucleus.

When showing the students how to carry out the lab it will be very helpful to first walk the students through how to fold the paper and collect data. The first step is to have the students divided into groups of four, with each student numbered one through four. All of the students need to see that the carbon paper has an active (black) side and a glossy, inactive side. The first template, labeled number 1 in the student packet and listed in the appendix under figure 69 and shown here in figure 31, is for the *s* orbital and does not need to be folded. The

only thing that needs to be done is to lay the paper on top of the carbon paper, which should have the dark black side up.

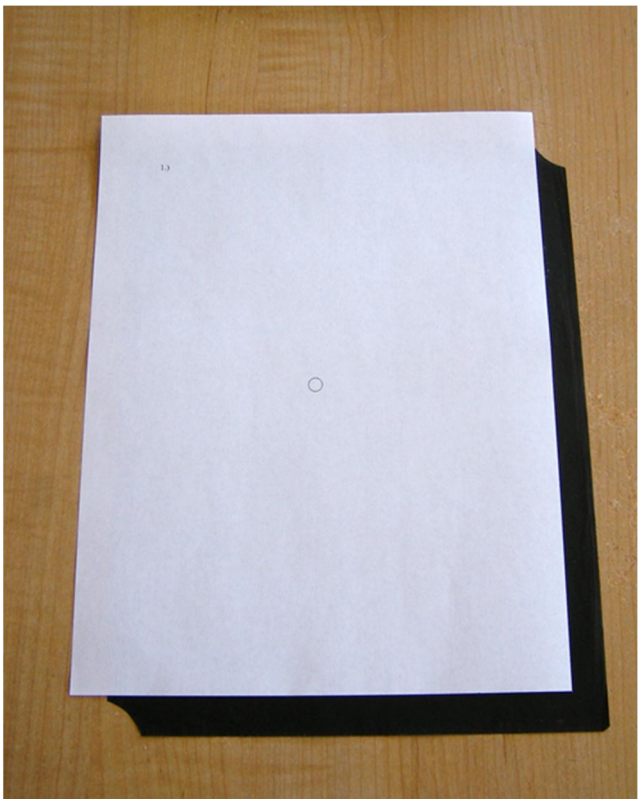

Figure 31. Carbon paper under the template for the *s* orbital is used so that the areas where the marbles are dropped will be marked.

The second paper needs to be folded along the dotted lines. The fold is held in place by a paperclip as shown in figure 32**.** The paper is placed on top of the carbon paper, with the black side up, so that the ridge will remain while the marbles are being dropped onto the paper.

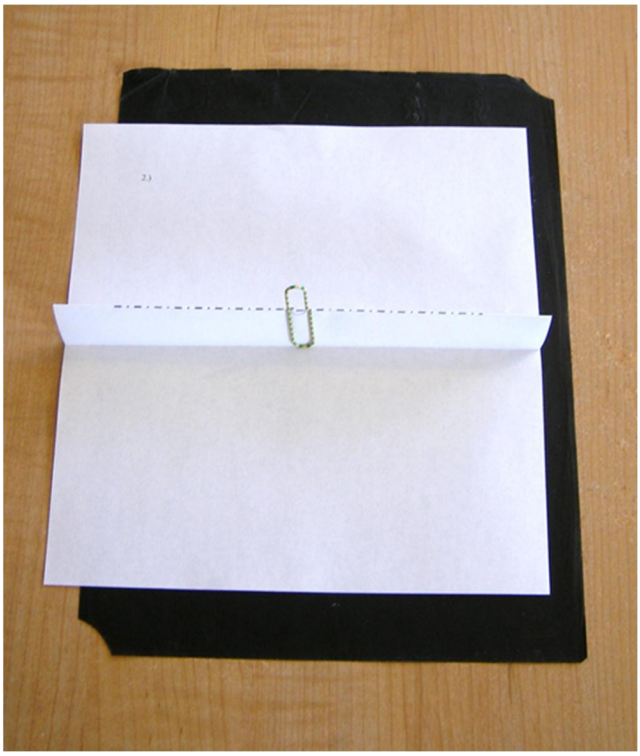

Figure 32. A paperclip is used in the template for the *p* orbital in order to keep the paper from flattening out.

The third piece of paper is also folded along the dotted lines, on both sides. The red “I” shape is there so that the students can cut that part of the paper along the red lines. This will then allow of the paper to neatly fold into itself as shown in figure 33. The fold is held in place by a paperclip and the paper is placed on top of the carbon paper, with the black side up. The paper targets are now ready to have marbles drops on it and the spots analyzed, as shown in figure 34.

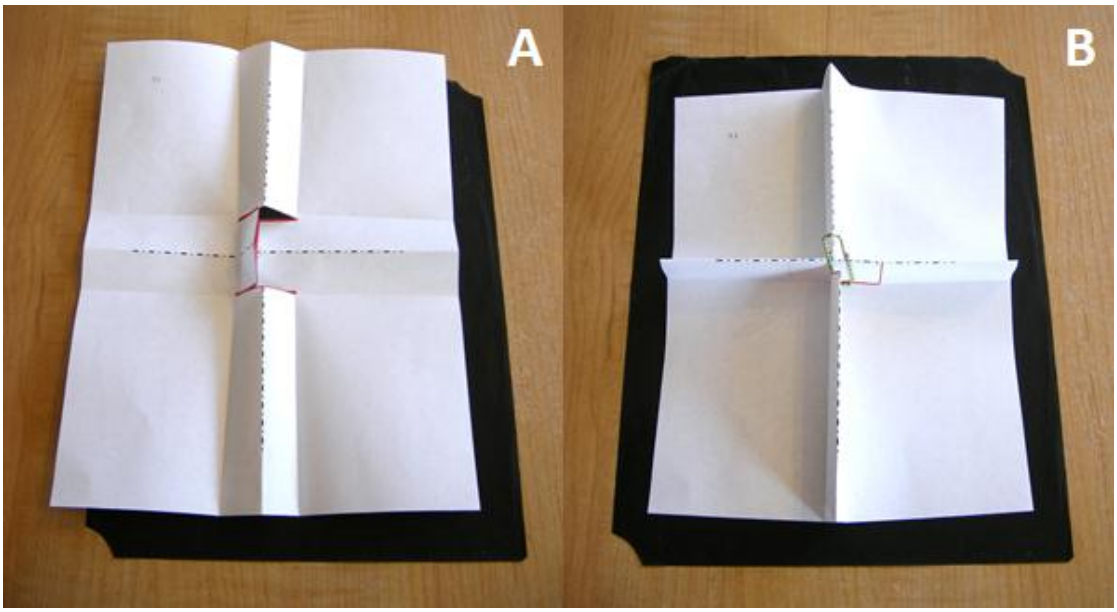

Figure 33. First fold the paper along all the dotted lines, as shown in part A, then cut along the red lines. This will allow the paper to be folded into itself, shown in part B. A paperclip can be used to maintain the ridges while marbles are dropped on the paper.

Figure 34 Student dropping marbles on to the folded paper target for the *d* orbital.

SECTION 5.3 Understanding the Results

The results of the experiment can now be analyzed by the students as they look for the patterns that begin to emerge on the back side of the paper targets. Figure 35 shows a student examining the paper target designed to give a *d* type orbital. There is a student worksheet that should be handed out at this point although it can be given to the students earlier in the class. The answer key is listed in the appendix section as figure 67. Filling out the worksheet individually and then going over it together as a will help the students to fill in the questions that they may have been confused about as well as drawing the correct conclusions from the general patterns that they found during the experiment.

Figure 35. A student analyzing the data she gathered from dropping marbles on to the folded paper target for the *d* orbital.

The key points in the explanation of the exercise are that the random patterns on folded paper can be used to illustrate the probability of finding an electron in a certain energy level around a nucleus, which can then be used to map the electron density around the nucleus, which we can then say is forming a

particular pattern. These patterns can also be defined by the areas where there is no electron density, which are called nodes. To illustrate the increasing number of nodes as the atomic orbitals go from *s,* to *p,* and then to *d* the clown balloon can be tied into a circle and then twisted into a figure eight, and then into a four leaf clover. As the balloon is twisted the area representing electron density becomes more confined since each new twist is adding a node. In order to avoid confusion it may also help to start by explaining that an s orbital would actually look more like a traditional round balloon, rather than simply a long skinny balloon with the ends tied together.

SECTION 5.4 Implementation Strategies

Students should work in groups of four, with each student being assigned one of four numbers prior to handing out the paper shapes. Then explain that group members three and four will work together, which will let students know beforehand on which part of the demonstration on paper folding they need to concentrate most closely. Make sure to point out during the explanation of results how the folded areas of the paper represented the nodes because they do not have any spots correlating to electron density.

Where electrons can be found around an atom and the connection to the orbital shapes are fundamental concepts in both chemistry and physics. Having this knowledge can then help the students to predict the geometric shapes that are found using VESPR.[203] It should be noted though that VESPR theory is not without flaws and may be replaced in advanced chemistry courses.[204]

Understanding the general bonding angles will in turn be useful for understanding molecular shapes and how biological structures often require chemicals to have a certain chirality for them to be reactive. By developing a method for the students to be able to recreate the shape of the *s, p,* and *d* orbitals this lab exercise provides a tangible link between using probability (dropping the marble) to map the electron density around an atoms nucleolus (using carbon paper to keep track of the accumulating hits).

Appendix

General comments: Throughout this section, the assignment of imidazolylidene or imidazolyl H as being proximal or distal to the N-CH_3 substituent is based on analogy with assignments for **5b** and **9b-Cl**, which was made with the use of ROESY or NOE data, respectively. Data which appear to support this assignment: we note that in all cases, there appears to be a gHMBC crosspeak between the N-CH_3 protons and the imidazolylidene carbon attached with the upfield proton NMR peak (for example, in **5b**, there is a HMBC cross peak between H 4.10 and C 126.6 ppm, moreover there is an HSQC crosspeak between H 7.41 and C 126.6). For **5b**, ROESY data showed the proximity of the proton resonating at 7.41 ppm to the N-CH_3 protons. Furthermore, ROESY data on **5b** helped assign which resonances belonged to the Ph nearest the metal: irradiation of the Cp* methyl proton peak caused enhancement of the doublet at 8.46 ppm but not the one at 8.27 ppm, and irradiation of the doublet at 8.27 caused no enhancement of the Cp* Me singlet whereas irradiation at 8.46 did lead to enhancement. For *t*-Bu species **5c** at low temperature therefore the downfield *t*-Bu proton peaks were assigned to the *t*-Bu nearest the metal, in analogy with assignements for **5b**. Subsequent ROESY data was also gathered for **5z** in order to elucidate the exact assignment of the proton peaks as well as verifying the position of the ^{15}N peaks.

Table 15. Crystal data and structure refinement for **9-Ph**.

Identification code	ZS075 B2 p4	
Empirical formula	C32 H32 Cl4 N4	
Formula weight	614.42	
Temperature	150(2) K	
Wavelength	0.71073 Å	
Crystal system	Triclinic	
Space group	P-1	
Unit cell dimensions	a = 8.8369(7) Å	α = 97.1100(10)°.
	b = 10.8166(9) Å	β = 94.6140(10)°.
	c = 16.2952(13) Å	γ = 92.0740(10)°.
Volume	1538.9(2) $Å^3$	
Z	2	
Density (calculated)	1.326 Mg/m^3	
Absorption coefficient	0.413 mm^{-1}	
F(000)	640	
Crystal size	0.26 x 0.17 x 0.12 mm^3	
Crystal color, habit	Colorless Block	
Theta range for data collection	1.26 to 27.56°.	
Index ranges	-11<=h<=11, -13<=k<=13, -21<=l<=20	
Reflections collected	19452	
Independent reflections	6853 [R(int) = 0.0384]	
Completeness to theta = 25.00°	99.7 %	
Absorption correction	Multi-scan	
Max. and min. transmission	0.9521 and 0.9002	
Refinement method	Full-matrix least-squares on F^2	
Data / restraints / parameters	6853 / 0 / 365	
Goodness-of-fit on F^2	1.043	
Final R indices [I>2sigma(I)]	R1 = 0.0413, wR2 = 0.1006	
R indices (all data)	R1 = 0.0545, wR2 = 0.1089	
Largest diff. peak and hole	0.558 and -0.358 $e.Å^{-3}$	

Table 16. Crystal data and structure refinement for **9-H-Ir**.

Identification code	grot300	
Empirical formula	C29 H37 Cl F6 Ir N4 P	
Formula weight	814.25	
Temperature	153(2) K	
Wavelength	0.71073 Å	
Crystal system	Monoclinic	
Space group	P2(1)/n	
Unit cell dimensions	a = 13.760(2) Å	α = 90°
	b = 12.731(2) Å	β = 91.763(2)°
	c = 17.622(3) Å	γ = 90°
Volume	3085.6(8) $Å^3$	
Z	4	
Density (calculated)	1.753 g/cm^3	
Absorption coefficient	4.528 mm^{-1}	
F(000)	1608	
Crystal size	0.30 x 0.24 x 0.18 mm^3	
Theta range for data collection	1.85 to 25.57°	
Index ranges	-16<=h<=15, -15<=k<=15, -12<=l<=21	
Reflections collected	22399	
Independent reflections	5735 [R(int) = 0.0357]	
Completeness to theta = 25.00°	99.7 %	
Absorption correction	Multi-scan	
Max. and min. transmission	0.4962 and 0.3436	
Refinement method	Full-matrix least-squares on F^2	
Data / restraints / parameters	5735 / 0 / 388	
Goodness-of-fit on F^2	1.086	
Final R indices [I>2sigma(I)]	R1 = 0.0216, wR2 = 0.0499	
R indices (all data)	R1 = 0.0262, wR2 = 0.0521	
Largest diff. peak and hole	1.157 and -0.903 e $Å^{-3}$	

Table 17. Crystal data and structure refinement for **5b**.

Identification code	grot269	
Empirical formula	C30 H31 Cl F6 Ir N4 P	
Formula weight	820.21	
Temperature	123(2) K	
Wavelength	0.71073 Å	
Crystal system	Monoclinic	
Space group	P2(1)/c	
Unit cell dimensions	a = 9.5810(4) Å	α = 90°
	b = 20.6584(8) Å	β = 93.9620(10)°
	c = 15.0288(6) Å	γ = 90°
Volume	2967.5(2) $Å^3$	
Z	4	
Density (calculated)	1.836 g/cm^3	
Absorption coefficient	4.710 mm^{-1}	
F(000)	1608	
Crystal size	0.36 x 0.30 x 0.10 mm^3	
Crystal color, habit	Orange plate	
Theta range for data collection	1.68 to 25.49°	
Index ranges	-11<=h<=11, -24<=k<=24, -18<=l<=18	
Reflections collected	40565	
Independent reflections	5509 [R(int) = 0.0244]	
Completeness to theta = 25.00°	100.0 %	
Absorption correction	Multi-scan	
Max. and min. transmission	0.6502 and 0.2819	
Refinement method	Full-matrix least-squares on F^2	
Data / restraints / parameters	5509 / 0 / 383	
Goodness-of-fit on F^2	1.036	
Final R indices [I>2sigma(I)]	R1 = 0.0188, wR2 = 0.0455	
R indices (all data)	R1 = 0.0202, wR2 = 0.0461	
Largest diff. peak and hole	2.639 and -0.472 e $Å^{-3}$	

Table 18. Crystal data and structure refinement for **5c**.

Identification code	grot288a	
Empirical formula	C29 H45 Cl F6 Ir N4 O P	
Formula weight	838.31	
Temperature	100(2) K	
Wavelength	1.54184 Å	
Crystal system	Monoclinic	
Space group	P2(1)/n	
Unit cell dimensions	a = 8.4499(7) Å	α = 90°.
	b = 12.6418(9) Å	β = 94.287(3)°.
	c = 30.747(2) Å	γ = 90°.
Volume	3275.2(4) $Å^3$	
Z	4	
Density (calculated)	1.700 Mg/m^3	
Absorption coefficient	9.665 mm^{-1}	
F(000)	1672	
Crystal size	0.35 x 0.30 x 0.15 mm^3	
Crystal color, habit	Orange Block	
Theta range for data collection	4.53 to 66.23°.	
Index ranges	-9<=h<=9, 0<=k<=14, 0<=l<=36	
Reflections collected	5463	
Independent reflections	5468 [R(int) = 0.0824]	
Completeness to theta = 65.00°	97.4 %	
Absorption correction	Multi-scan	
Max. and min. transmission	0.3250 and 0.1330	
Refinement method	Full-matrix least-squares on F^2	
Data / restraints / parameters	5468 / 0 / 391	
Goodness-of-fit on F^2	1.010	
Final R indices [I>2sigma(I)]	R1 = 0.0498, wR2 = 0.1434	
R indices (all data)	R1 = 0.0508, wR2 = 0.1444	
Largest diff. peak and hole	2.381 and -1.818 $e.Å^{-3}$	

Table 19. Crystal data and structure refinement for **5x**.

Identification code	grot251
Empirical formula	C23 H31 Cl Ir N3 O0.33
Formula weight	582.49
Temperature	100(2) K
Wavelength	0.71073 Å
Crystal system	Rhombohedral
Space group	R-3
Unit cell dimensions	a = 21.6752(19) Å α = 90°
	b = 21.6752(19) Å β = 90°
	c = 26.287(2) Å ɣ = 120°
Volume	10695.3(16) $Å^3$
Z	18
Density (calculated)	1.628 g/cm^3
Absorption coefficient	5.744 mm^{-1}
F(000)	5160
Crystal size	0.39 x 0.33 x 0.22 mm^3
Crystal color, habit	Orange block
Theta range for data collection	1.33 to 25.48°
Index ranges	-24<=h<=22, -26<=k<=22, -30<=l<=31
Reflections collected	15752
Independent reflections	4398 [R(int) = 0.0533]
Completeness to theta = 25.00°	99.9 %
Absorption correction	Analytical
Max. and min. transmission	0.3673 and 0.2140
Refinement method	Full-matrix least-squares on F^2
Data / restraints / parameters	4398 / 0 / 265
Goodness-of-fit on F^2	1.028
Final R indices [I>2sigma(I)]	R1 = 0.0362, wR2 = 0.0933
R indices (all data)	R1 = 0.0415, wR2 = 0.0958
Largest diff. peak and hole	2.122 and -0.856 e $Å^{-3}$

Table 20. Crystal data and structure refinement for **5y**.

X-ray ID	grot220
Sample/notebook ID	ZS013
Empirical formula	C31 H40 Br0.22 Cl0.78 Ir N4
Formula weight	706.25
Temperature	198(2) K
Wavelength	0.71073 Å
Crystal system	Orthorhombic
Space group	Pbca
Unit cell dimensions	a = 16.2808(10) Å α = 90°.
	b = 13.7890(8) Å β = 90°.
	c = 26.6395(16) Å γ = 90°.
Volume	5980.5(6) $Å^3$
Z	8
Density (calculated)	1.569 Mg/m^3
Absorption coefficient	4.858 mm^{-1}
F(000)	2816.1
Crystal size	0.10 x 0.08 x 0.06 mm^3
Crystal color/habit	yellow plate
Theta range for data collection	1.53 to 28.28°.
Index ranges	-16<=h<=21, -10<=k<=18, -32<=l<=34
Reflections collected	23295
Independent reflections	7098 [R(int) = 0.0494]
Completeness to theta = 25.00°	100.0 %
Absorption correction	Semi-empirical from equivalents
Max. and min. transmission	0.7479 and 0.6305
Refinement method	Full-matrix least-squares on F^2
Data / restraints / parameters	7098 / 0 / 346
Goodness-of-fit on F^2	1.020
Final R indices [I>2sigma(I)]	R1 = 0.0457, wR2 = 0.1051
R indices (all data)	R1 = 0.0663, wR2 = 0.1188
Largest diff. peak and hole	2.193 and -2.080 $e.Å^{-3}$

Table 21. Crystal data and structure refinement for **5z**.

Identification code	ZS-302 #8	
Empirical formula	C58 H88 Cl2 F12 Ir2 N6 O2 P2	
Formula weight	1646.62	
Temperature	90(2) K	
Wavelength	0.71073 Å	
Crystal system	Triclinic	
Space group	P-1	
Unit cell dimensions	a = 12.0360(7) Å	α = 80.127(2)°.
	b = 12.5925(8) Å	β = 63.055(2)°.
	c = 13.0880(8) Å	γ = 68.254(2)°.
Volume	1642.46(17) $Å^3$	
Z	1	
Density (calculated)	1.665 Mg/m^3	
Absorption coefficient	4.256 mm^{-1}	
F(000)	820	
Crystal size	0.21 x 0.15 x 0.05 mm^3	
Crystal color, habit	Orange Block	
Theta range for data collection	2.46 to 26.44°.	
Index ranges	-15<=h<=15, -15<=k<=15, -16<=l<=16	
Reflections collected	26417	
Independent reflections	6700 [R(int) = 0.0442]	
Completeness to theta = 25.00°	99.5 %	
Absorption correction	Semi-empirical from equivalents	
Max. and min. transmission	0.8154 and 0.4685	
Refinement method	Full-matrix least-squares on F^2	
Data / restraints / parameters	6700 / 0 / 406	
Goodness-of-fit on F^2	1.038	
Final R indices [I>2sigma(I)]	R1 = 0.0222, wR2 = 0.0538	
R indices (all data)	R1 = 0.0248, wR2 = 0.0553	
Extinction coefficient	not measured	
Largest diff. peak and hole	1.176 and -0.508 e.$Å^{-3}$	

X = I, Cl, or PF_6
R^1 = H, Ag, or Cp*Ir Cl
R^2 = Empty, CH_3, or DIPPY
R^3 = N or CH
R^4 = H, Phenyl, or *t*-Butyl
R^5 = H, Phenyl, or *t*-Butyl

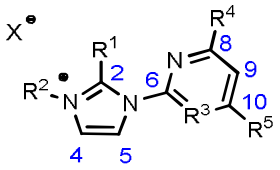

Figure 36. Diagram for interpreting the ^{1}H and ^{13}C NMR tables 19 and 20.

Table 22. Table listing all of the ^{1}H NMR data for the compounds synthesized in this dissertation.

		^{1}H (chemical shifts in ppm, coupling constants in Hz)							
	Solvent	R^1 Cp* or H	Im-H4 (1H)	Im-H5 (1H)	R^2	H9 (1H)	R^3	R^4	R^5
9-H-Ir-Cl[a]	$CDCl_3$	1.60 (s, 15H)	7.13 (d, *J* = 2.0)	8.16 (d, *J* = 2.2)	---[a]	8.17 (t, *J* = 5.7)		9.50 (d, *J* = 5.7)	8.94 dd, *J* = 1.8, 4.6)
9-H-Ir[b]	CD_2Cl_2	1.50 (s, 15H)	7.22 (d, *J* = 2.0)	8.17 (d, *J* = 2.2)	---[a]	7.71 (dd, *J* = 5.8)		8.97 (dd, *J* = 2.1, 4.8)	8.85 dd, *J* = 2.3, 5.8)
5b	$CDCl_3$	1.41 (s, 15H)	7.41 (d, *J* = 2.0)	8.05 (d, *J* = 2.0)	4.10 (s, 3H)	7.89 (s)		3.46 (broad, C2 + C6, 2H) 7.70-7.57 (m, C3-C5, 3H)	3.27 (d, *J* = 8.5, C2 + C6, 2H) 7.70-7.57 (m, C3-C5, 3H)
5c	$CDCl_3$	1.57 (s, 15H)	7.40 (d, *J* = 2.3)	7.83 (d, *J* = 2.3)	4.06 (s, 3H)	7.56 (s)		1.51 (s, 18H)	
5c	Acetone-d_6 (-80 °C)	1.64 (s, 15H)	7.78 (s)	8.29 (s)	4.09 (s, 3H)	7.90 (s)		1.40 (s, 18H)	
5c	Acetone-d_6	1.63 (s, 15H)	7.68 (d, *J* = 1.6)	8.12 (d, *J* = 1.2)	4.13 (s, 3H)	7.87 (s)		1.54 (s, 18H)	
5x	$CDCl_3$	1.80 (s, 15H)	6.97 (d, *J* = 2.2)	7.63 (s)	3.95 (s, 3H)	6.90 (d, *J* = 7.6)		7.89 (d, *J* = 7.8)	1.30 (s, 9H)
5z	CD_2Cl_2	1.48 (s, 15H)	7.33 (d, *J* = 2.1)	7.73 (s)	4.01 (s, 3H)	7.64 (s)	7.47 (s)	1.52 (s, 9H)	1.41 (s, 9H)
10	$CDCl_3$	8.66 (s, 1 H)	7.15 (s)	7.95 (s)	---	7.18 (s)		1.39 (s, 18H)	
8-Ph	$CDCl_3$	11.52 (s, 1H)	7.71 (s)	8.25 (s)	4.43 (s, 3H)	8.11 (s)		8.25 (d, *J* = 7.9, C2+C6, 4H) 7.60-7.54 (m, C3-C5, 6H)	
I3-tBu-I	$CDCl_3$	10.52 (s, 1H)	7.86 (s)	8.21 (s)	4.43 (s, 3H)	7.41 (s)		1.42 (s, 18H)	
16-I	$CDCl_3$	10.99 (s, 1H)	7.71 (d, *J* = 1.8)	8.26 (d, *J* = 1.8)	4.31 (s, 3H)	8.07 (d, *J* = 7.9)	7.46 d, *J* = 7.9)	7.92 (dd, *J* = 7.9, 8.2)	1.36 (s, 9H)
21	$CDCl_3$					6.18 (s)	3.87 (s, methyl ester)	1.32 (s, 9H)	1.36 (s, 9H)
22	$CDCl_3$					6.13 (s)	6.36 (s)	1.36 (s, 9H)	1.25 (s, 9H)
23	$CDCl_3$					7.21 (s)	7.10 (s)	1.36 (s, 9H)	1.31 (s, 9H)

Table 22. Continued

		^{1}H (chemical shifts in ppm, coupling constants in Hz)							
	Solvent	R^1 Cp* or H	Im-H4 (1H)	Im-H5 (1H)	R^2	H9 (1H)	R^3	R^4	R^5
24	$CDCl_3$	8.38 (s, 1H)	7.11 (d, *J* = 1.6)	7.26 (d, *J* = 1.6)		7.68 (s)	7.19 (s)	1.39 (s, 9H)	1.37 (s, 9H)
25-PF$_6$	$CDCl_3$	9.35 (s, 1H)	7.50 (d, *J* = 1.8)	8.17 (d, *J* = 1.8)	4.10 (s, 3H)	7.45 (s)	7.57 (s)	1.37 (s, 9H)	1.36 (s, 9H)
8-Ph-AgCl	$CDCl_3$	---	7.16 (d, *J* = 1.8)	8.38 (d, *J* = 1.8)	3.76 (s, 3H)	8.16 (s)		8.35 (d, *J* = 6.5, C2+C6, 2H) 7.64-7.58 (m, C3-C5, 3H)	
13-tBu-Ag	$CDCl_3$	---	7.35 (dd, *J* = 2, 1.3, 2H)	8.23 dd, *J* = 2, 1.3, 2H)	4.02 (s, 3H)	7.25 (s, 2H)		1.26 (s, 36H)	
16-Ag-I	$CDCl_3$	---	7.11 (d, *J* = 2.95, 2H)	7.87 (d, *J* = 2.96, 2H)	4.01 (s, 3H)	7.99 (d, *J* = 8.1)	7.37 d, *J* = 7.8)	7.76 (t, *J* = 7.8)	1.39 (s, 9H)
5c-BA[c]	CD_2Cl_2	1.44 (s, 15H)	7.27 (d, *J* = 2.1)	7.39 (d, *J* = 2.1)	4.16 (s, 3H)	7.58 (s)		1.35 (s, 18H)	
5c-BA[d]	CD_2Cl_2 (-90 °C)	1.35 (s, 15H)	7.28 (s)	7.34[d]	4.04 (s, 3H)	7.45 (s)		1.27 (br, 18H)	
6-BA[e]	$CDCl_3$	1.54 (s, 15H)	7.35 (s)	7.21 (s)	4.12(s, 3H)	6.82 (s)		1.26 (s, 9H)	3.52 (s, 3H)
6-BA[f]	CD_2Cl_2	1.54 (s, 15H)	7.21 (d, 2.1)	7.34 (d, 2.1)	4.10 (s, 3H)	6.82 (s)		1.26 (s, 9H)	3.52 (s, 3H)
5z-BA[g]	CD_2Cl_2	1.37 (s, 15H)	7.16 (s)	7.30 (s)	4.04 (s, 3H)	7.51 (s)	7.02 (s)	1.29 (s, 9H)	1.25 (s, 9H)

[a] Peaks for DIPPY group: On the ring: 7.58 (t, *J* = 7.9 1H), 7.42 (d, *J* = 7.9 2H), on the isopropyl groups: 3.27 (q, *J* = 6.6 1H), 2.74 (q, *J* = 6.6 1H), 1.43 (d, *J* = 6.6 3H), 1.28 (d, *J* = 6.6 3H), 1.25 (d, *J* = 6.6 3H), 0.92 (d, *J* = 6.6 3H). [b] Peaks for DIPPY group: On the ring: 7.61 (t, *J* = 7.9 1H), 7.45 (d, *J* = 8.3 2H), on the isopropyl groups: 3.24 (q, *J* = 6.8 1H), 2.71 (q, *J* = 6.8 1H), 1.42 (d, *J* = 6.8 3H), 1.26 (d, *J* = 6.8 3H), 1.23 (d, *J* = 6.8 3H), 0.91 (d, *J* = 6.8 3H). [c] Peaks for coordinated $PhCH_2NH_2$: 7.30-7.41 (m, 5H), 4.33 (t, *J* = 11.9, 1H), 3.88 (dt, *J* = 4.4, 12.9, 1H,), 4.17 (t, , *J* ≈ 12 partially hidden by 3H singlet of methyl peak, 1H for NH), 6.63 (br t, *J* ≈ 12, 1H for NH). [d] Peak for second imidazolylidene CH overlapping with those for Ph of amine, but its chemical shift of 7.34 ppm was suggested by appearance of a crosspeak in ^{1}H-^{15}N gHMBC. Peaks for coordinated $PhCH_2NH_2$: 7.28-7.41 (m, 5H), 7.06 (br app t, *J* ≈ 10, 1H, NH), 4.25 (t, *J* = 12), ca. 4.02 (m partially hidden by 3H singlet at 4.04 ppm for N-CH_3), 3.97 (sl br t, *J* ≈ 12, 1H). [e] Peaks for coordinated $PhCH_2NH_2$: 7.31-7.39 (m, 5H), 4.05 (t, *J* = 11.6, 1H), 3.91 (dt, *J* = 3.2, 12.4, 1H,), 3.95 (t, *J* ≈ 12 partially hidden by 3H singlet of methyl peak, 1H for NH), 7.67 (br t, *J* ≈ 12, 1H for NH).

Table 22. Continued

[f] Peaks for coordinated $PhCH_2NH_2$: 7.60 (br, 1H), 7.37-7.39 (m, 4H), 7.31-7.35 (m, 1H?, hard to discern because of overlap with doublet at 7.34 for imidazolylidene ring H), 4.04 (d of app t, $J \approx 3, 11$) and 3.96-4.04 (br, NH) (total of the two partially overlapping signals, 2H), 3.92 (dt, $J = 4.1, 12.1$, 1H). [g] Peaks for coordinated $PhCH_2NH_2$: 7.35 (m, 5H), 6.65 (dddd, $J_{HH} = 4.7, 11.6, 11.7$ $J_{HN} = 73.1$ 1H), 4.27 (ddd, $J = 1.8, 11.7, 13.6$ 1H), 4.01 (dddd, $J_{HH} = 1.5, 10.9, 11.3$ $J_{HN} = 70.7$ 1H), 3.88 (dddd, $J_{HH} = 1.7, 4.7, 12.5, 13.1$ 1H).

Table 23. Table listing all of the ^{13}C NMR data for the compounds synthesized in this dissertation.

		^{13}C (chemical shifts in ppm, coupling constants in Hz)											
	Solvent	R^1	C2	C4	C5	R^2	C6	C8	C9	C10	R^3	R^4	R^5
9-H-Ir-Cl[a]	$CDCl_3$	93.2 (s, $C(CH_3)_5$), 10.4 (s, $C(CH_3)_5$)	165.4	128.0	117.2	---[a]	157.0	162.0	123.3	160.6			
9-H-Ir[b]	CD_2Cl_2	93.7 (s, $C(CH_3)_5$), 9.4 (s, $C(CH_3)_5$)	166.0	129.2	117.8	---[b]	158.1	161.7	122.2	160.2			
5b	$CDCl_3$	95.5 (s, $C(CH_3)_5$), 9.5 (s, $C(CH_3)_5$)	166.6	126.6	119.6	37.8	159.3	172.0	117.0	167.0		138.3 (C1), 131.5 (C2 + C6), 134.2 (C3 + C5), 130.1 (C4)	133.9 (C1), 128.7 (C2 + C6), 132.8 (C3 + C5), 129.9 (C4)
5c	$CDCl_3$	92.8 (s, $C(CH_3)_5$), 9.4 (s, $C(CH_3)_5$)	164.9	126.1	119.4	36.7	157.8	183.2	113.9	183.2		39.5 ($C(CH_3)_3$), 30.4 ($C(CH_3)_3$)	
5c	Acetone-d_6 (-80 °C)	93.0 (s, $C(CH_3)_5$), 9.1 (s, $C(CH_3)_5$)	164.2	126.4	120.2	41.4	158.4	181.0	115.6	184.7		36.8 ($C(CH_3)_3$), 28.7 ($C(CH_3)_3$)	38.3 ($C(CH_3)_3$), 31.5 ($C(CH_3)_3$)
5c	Acetone-d_6	93.6 (s, $C(CH_3)_5$), 9.6 (s, $C(CH_3)_5$)	165.7	127.0	120.6	40.3	158.9	183.9	115.6	183.9		37.2 ($C(CH_3)_3$), 30.7 ($C(CH_3)_3$)	
5x	$CDCl_3$	90.6 (s, $C(CH_3)_5$), 9.7 (s, $C(CH_3)_5$)	162.8	121.1	115.7	36.5	161.0	159.2	116.6	143.7	130.3	37.2 ($C(CH_3)_3$), 30.4 ($C(CH_3)_3$)	---
5z	CD_2Cl_2	92.9 (s, $C(CH_3)_5$), 9.7 (s, $C(CH_3)_5$)	166.3	126.1	120.0	37.2	154.4	174.9	119.8	168.0	108.8	41.1 ($C(CH_3)_3$), 32.4 ($C(CH_3)_3$)	36.3 ($C(CH_3)_3$), 30.6 ($C(CH_3)_3$)
10	$CDCl_3$	---	136.0	130.0	116.4	---	153.5	180.0	108.9	180.0		37.7 ($C(CH_3)_3$), 29.2 ($C(CH_3)_3$)	
8-Ph	$CDCl_3$	---	137.9	124.5	118.5	37.7	152.6	167.3	111.9	167.3		134.5 (C1), 127.8 (C2 + C6), 129.3 (C3 + C5), 132.5 (C4)	
13-tBu-I	$CDCl_3$	---	135.3	125.3	118.1	38.2	150.8	181.6	112.1	181.6		38.0 ($C(CH_3)_3$), 29.2 ($C(CH_3)_3$)	
16-I	$CDCl_3$	---	135.0	124.1	118.8	37.7	144.5	170.2	111.4	140.7	120.8	37.7 ($C(CH_3)_3$), 29.9 ($C(CH_3)_3$)	---

Table 23. Continued

		^{13}C (chemical shifts in ppm, coupling constants in Hz)											
	Solvent	R^1	C2	C4	C5	R^2	C6	C8	C9	C10	R^3	R^4	R^5
21	$CDCl_3$						163.5	156.0	6.18	160.2	121.4 (methyl ester 169.6, 52.3)	36.8 ($C(CH_3)_3$), ? ($C(CH_3)_3$)	35.3 ($C(CH_3)_3$), ? ($C(CH_3)_3$)
22	$CDCl_3$						165.4	155.3	100.5	165.5	112.8	35.1 ($C(CH_3)_3$), ? ($C(CH_3)_3$)	35.5 ($C(CH_3)_3$), ? ($C(CH_3)_3$)
23	$CDCl_3$						150.5	170.2	114.5	163.4	118.2	37.6 ($C(CH_3)_3$), 30.1 ($C(CH_3)_3$)	35.1 ($C(CH_3)_3$), 30.6 ($C(CH_3)_3$)
24	$CDCl_3$		135.1	106.0	114.2		148.1	169.2	116.2	163.7	130.3	37.7 ($C(CH_3)_3$), 30.1 ($C(CH_3)_3$)	35.3 ($C(CH_3)_3$), 30.7 ($C(CH_3)_3$)
25-PF_6	$CDCl_3$		133.8	124.1	119.4	36.8	145.0	170.0	117.6	166.0	108.0	37.8 ($C(CH_3)_3$), 30.4 ($C(CH_3)_3$)	35.7 ($C(CH_3)_3$), 30.0 ($C(CH_3)_3$)
8-Ph-AgCl	$CDCl_3$	---	182.9	122.5	119.9	40.1	155.7	166.6	111.2	166.6		135.2 (C1), 127.7 (C2 + C6), 129.2 (C3 + C5), 131.2 (C4)	
13-tBu-Ag	$CDCl_3$	---	183.7 (two d, $^1J_{C-^{107}Ag}$ = 187.9, $^1J_{C-^{109}Ag}$ = 216.9)	123.1 (d, J = 6.0)	119.9 (d, J = 5.2)	40.0 (d, J = 3.0)	154.7	180.5	110.6	180.5		37.9 ($C(CH_3)_3$), 29.2 ($C(CH_3)_3$)	
16-Ag-I	$CDCl_3$	---	183.3	122.4	120.5	39.8	149.8	169.7	112.5	139.6	119.2	37.9 ($C(CH_3)_3$), 30.3 ($C(CH_3)_3$)	---
5c-BA[c]	CD_2Cl_2	91.3 (s, $C(CH_3)_5$), 9.5 (s, $C(CH_3)_5$)	153.6	125.7	127.2	40.3	158.2	182.5	113.5	182.5		38.8 ($C(CH_3)_3$), 30.0 ($C(CH_3)_3$)	
5c-BA[a] (-90 °C)	CD_2Cl_2	90.0 (s, $C(CH_3)_5$), 8.8 (s, $C(CH_3)_5$)	152.2	124.6	126.0	39.4	156.9	181.8 [e] (br)	112.2	179.8 [e] (br)		37.9 ($C(CH_3)_3$), 28.8 (br, $C(CH_3)_3$)	

Table 23. Continued

		13C (chemical shifts in ppm, coupling constants in Hz)											
	Solvent	R1	C2	C4	C5	R2	C6	C8	C9	C10	R3	R4	R5
6-BA[f]	$CDCl_3$	90.6 (s, $C(CH_3)_5$), 8.9 (s, $C(CH_3)_5$)	159.2	125.4	124.7	39.7	138.1	149.6	116.6			31.7 ($C(CH_3)_3$), 29.8 ($C(CH_3)_3$)	33.3
5z-BA[g] (-60 °C)	CD_2Cl_2	91.0 (s, $C(CH_3)_5$), 9.7 (s, $C(CH_3)_5$)	155.8	126.9	129.1	40.3	152.6	170.4	118.9	166.4	119.0	38.5 ($C(CH_3)_3$), 31.1 (br, $C(CH_3)_3$)	36.1 ($C(CH_3)_3$), 30.7 (br, $C(CH_3)_3$)

[a] Peaks for DIPPY group: On the ring: 147.8, 145.9, 134.2, 131.7, 125.1, 124.5, on the isopropyl groups: 28.5, 27.8, 27.4, 25.9, 22.7, 22.3. [b] Peaks for DIPPY group: On the ring: 147.9, 146.4, 134.6, 132.3, 125.6,125.3, on the isopropyl groups: 29.1, 28.3, 27.6, 26.1, 23.0, 22.6. [c] Peaks for coordinated $PhCH_2NH_2$: 139.0, 129.6, 129.2, 129.0, 52.1. [d] Assignments of ^{13}C NMR peaks based on 2D NMR spectra acquired at 30 °C. Peaks for coordinated $PhCH_2NH_2$: 138.0, 128.7, 128.4, 128.2, 50.9. [e] Assignments could be reversed. [f] Peaks for coordinated $PhCH_2NH_2$: 139.1, 129.0, 128.3, 128.1, 51.1. [g] Peaks for coordinated $PhCH_2NH_2$ was not possible.

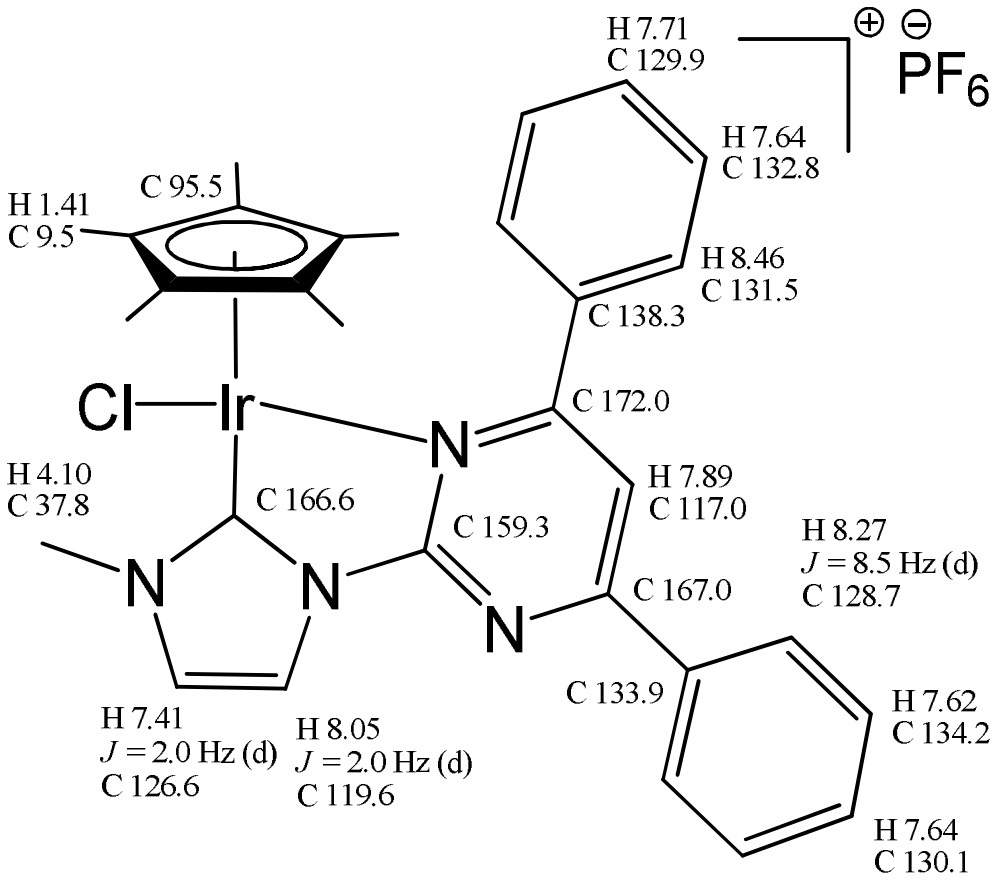

gCOSY[a]	ROESY[a]
7.41 ⇔ 8.05	1.41 ⇔ 8.46
7.70-7.57 ⇔ 8.27	1.41 ⇔ 4.10
7.70-7.57 ⇔ 8.46	4.10 ⇔ 7.41

[a] Double-headed arrow signifies crosspeak seen. For HMBC crosspeak data, integer between proton and carbon shifts indicates number of bonds between the interacting nuclei. Phenyl proton signal multiplicity or splitting (J values) could not be determined due to extensive peak overlap in ^{1}H NMR spectra,but chemical shift values could be determined from gHMBC crosspeaks.

Figure 37. Figure with corresponding data on **5b**, taken in $CDCl_3$.

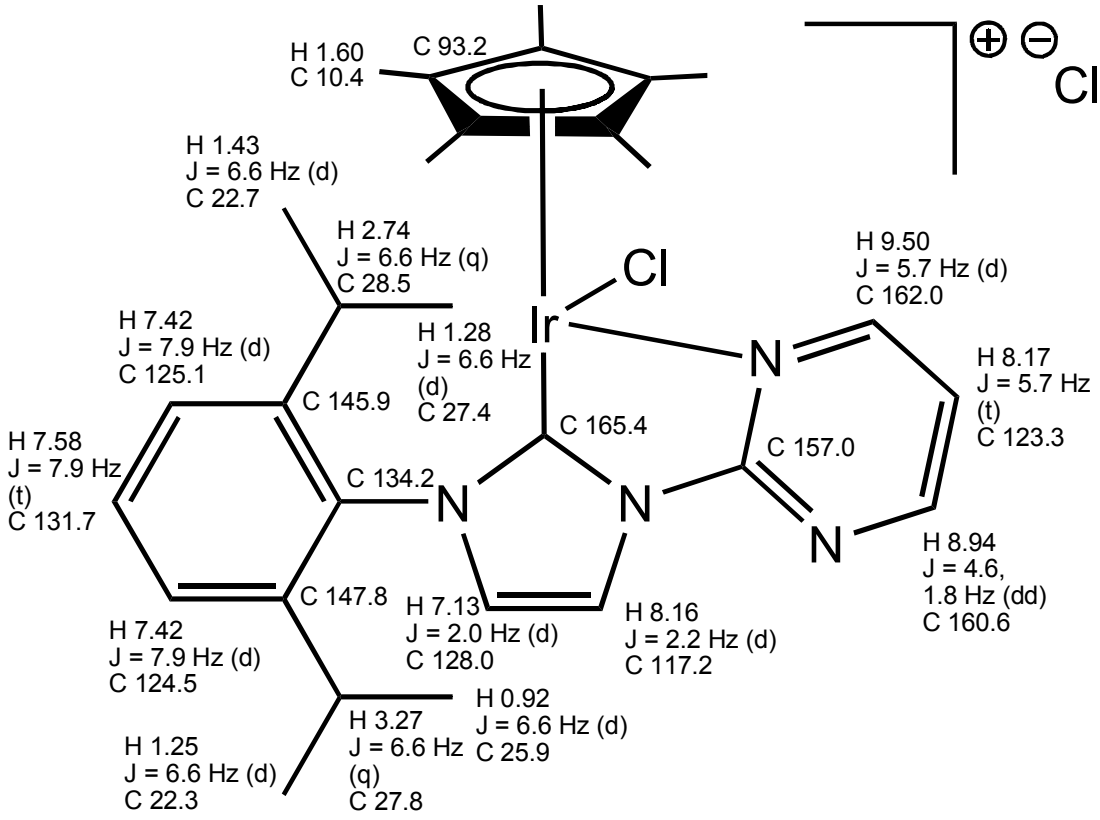

G COSY	
0.92 ⇔ 3.27	7.13 ⇔ 8.16
1.25 ⇔ 3.27	7.42 ⇔ 7.58
1.28 ⇔ 2.74	8.17 ⇔ 8.94
1.43 ⇔ 2.74	8.17 ⇔ 9.50

Figure 38. Figure with corresponding data on **9-H-Ir-Cl**, taken in $CDCl_3$.

G HMBC		
0.92 <2> 27.8	2.74 <2> 22.7	7.42 <3> 27.8
0.92 <3> 22.3	2.74 <2> 27.4	7.42 <3> 28.5
0.92 <3> 147.8	2.74 <2> 145.9	7.42 <3> 124.5
	2.74 <3> 124.5	7.42 <3> 125.1
1.25 <2> 27.8	2.74 <3> 134.2	7.42 <3> 134.2
1.25 <3> 25.9		
1.25 <3> 147.8	3.27 <2> 22.3	7.58 <3> 145.9
	3.27 <2> 25.9	7.58 <3> 147.8
1.28 <2> 28.5	3.27 <3> 125.1	
1.28 <3> 22.7	3.27 <3> 134.2	8.16 <2> 128.0
1.28 <3> 145.9	3.27 <4> 147.8	8.16 <3> 165.4
1.43 <2> 28.5	7.13 <2> 117.2	8.17 <2> 161.0
1.43 <3> 27.8	7.13 <3> 165.4	8.17 <2> 162.0
1.43 <3> 145.9		
		8.94 <2> 123.3
1.60 <2-4> 93.2		8.94 <3> 162.0
		9.50 <3> 157.0

Figure 38. Continued.

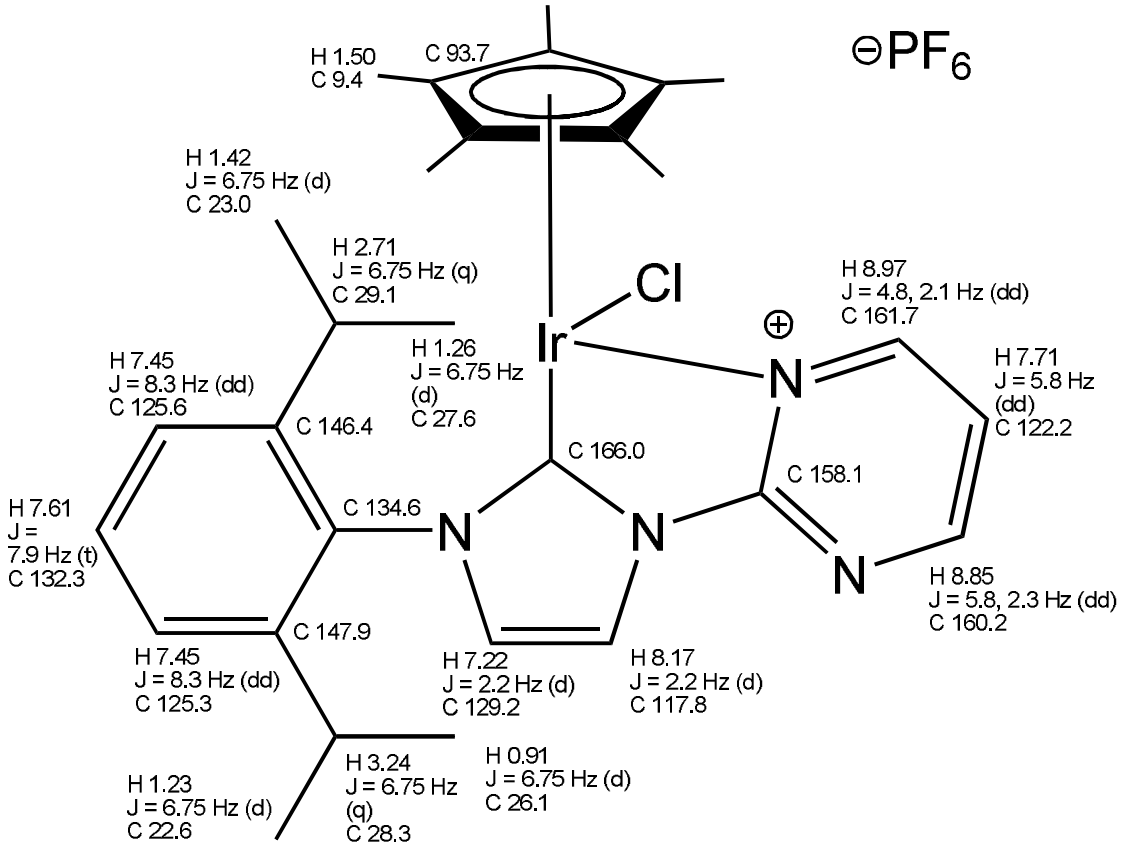

G COSY	
0.91 ⇔ 3.24	7.22 ⇔ 8.17
1.23 ⇔ 3.24	7.45 ⇔ 7.61
1.26 ⇔ 2.71	7.71 ⇔ 8.85
1.42 ⇔ 2.71	7.71 ⇔ 8.97

Figure 39. Figure with corresponding data on **9-H-Ir**, taken in CD_2Cl_2.

G HMBC		
0.91 <2> 28.3	1.50 <2-4> 93.7	7.45 <3> 28.3
0.91 <3> 22.36		7.45 <3> 29.1
0.91 <3> 147.9	2.71 <2> 23.0	7.45 <3> 125.3
	2.71 <2> 27.6	7.45 <3> 125.6
1.23 <2> 28.3	2.71 <2> 146.4	
1.23 <3> 26.1		7.61 <3> 146.4
1.23 <3> 147.9	3.24 <2> 22.6	7.61 <3> 147.9
	3.24 <2> 26.1	
1.26 <2> 29.1	3.24 <2> 147.9	8.17 <2> 129.2
1.26 <3> 23.0		
1.26 <3> 146.4	7.22 <2> 117.8	7.71 <2> 160.2
	7.22 <3> 166.0	
1.42 <2> 29.1		8.85 <2> 122.2
1.42 <3> 27.6		8.85 <3> 161.7
1.42 <3> 146.4		
		8.97 <2> 122.2
		8.97 <3> 160.2

Figure 39. Continued.

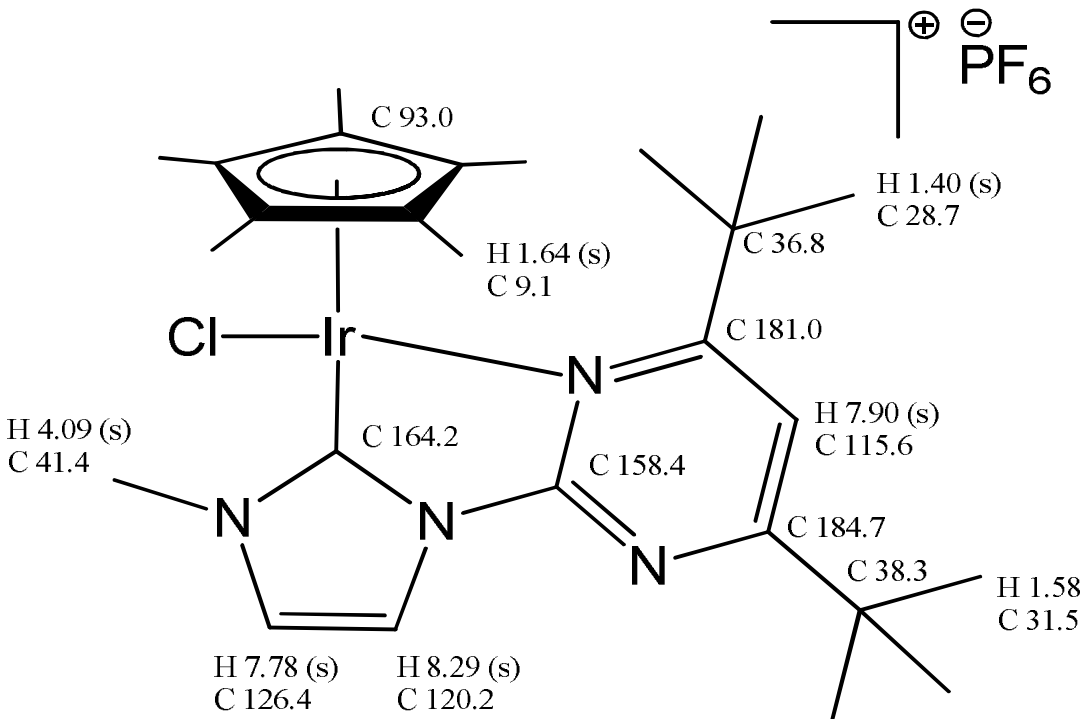

gHMBC		
1.40 <3> 181.0	4.09 <3> 164.2	1.40 <2> 36.8
7.90 <2> 181.0	1.64 <3> 164.2	1.58 <2> 38.3
1.58 <3> 184.7	8.29 <3> 164.2	7.78 <2> 120.2
7.90 <2> 184.7	7.78 <3> 164.2	8.29 <2> 126.4
1.64 <2> 93.0	4.09 <3> 126.4	

*2D NMR data allowed the assignment of ^{1}H and ^{13}C NMR resonances in each *t*-Bu group and also the pyrimidyl C to which the *t*-Bu is attached, but assignment of which *t*-Bu is proximal and which is distal to the Ir is based on analogy with data for **5b** and may be reversed.

Figure 40. Figure with corresponding data on **5c**, taken in acetone-d_6 at -80°C.

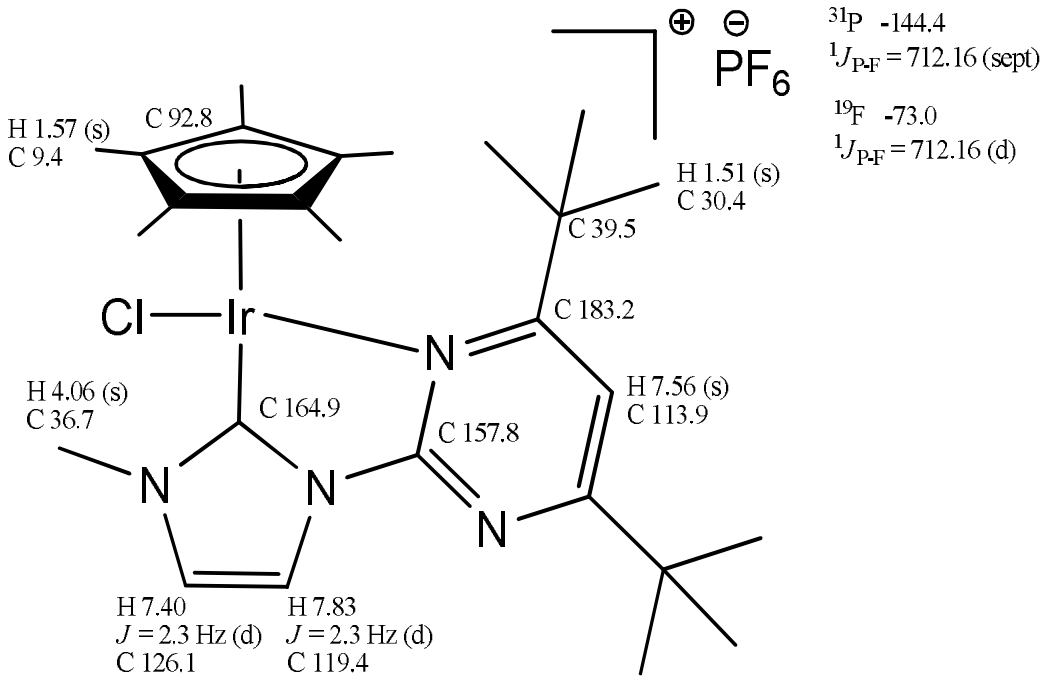

gHMBC		
1.57 <3> 164.9	7.40 <3> 164.9	7.83 <3> 164.9
1.57 <2> 92.8	7.40 <2> 119.4	7.83 <2> 126.1
4.06 <3> 164.9	7.56 <2> 183.2	
4.06 <3> 126.1	7.56 <3> 39.5	

*Data for sample at 30 °C probe temperature; values for nuclei undergoing site exchange (e.g. those in t-Bu groups) are an average

Figure 41. Figure with corresponding data on **5c**, taken in $CDCl_3$ at 30 °C.

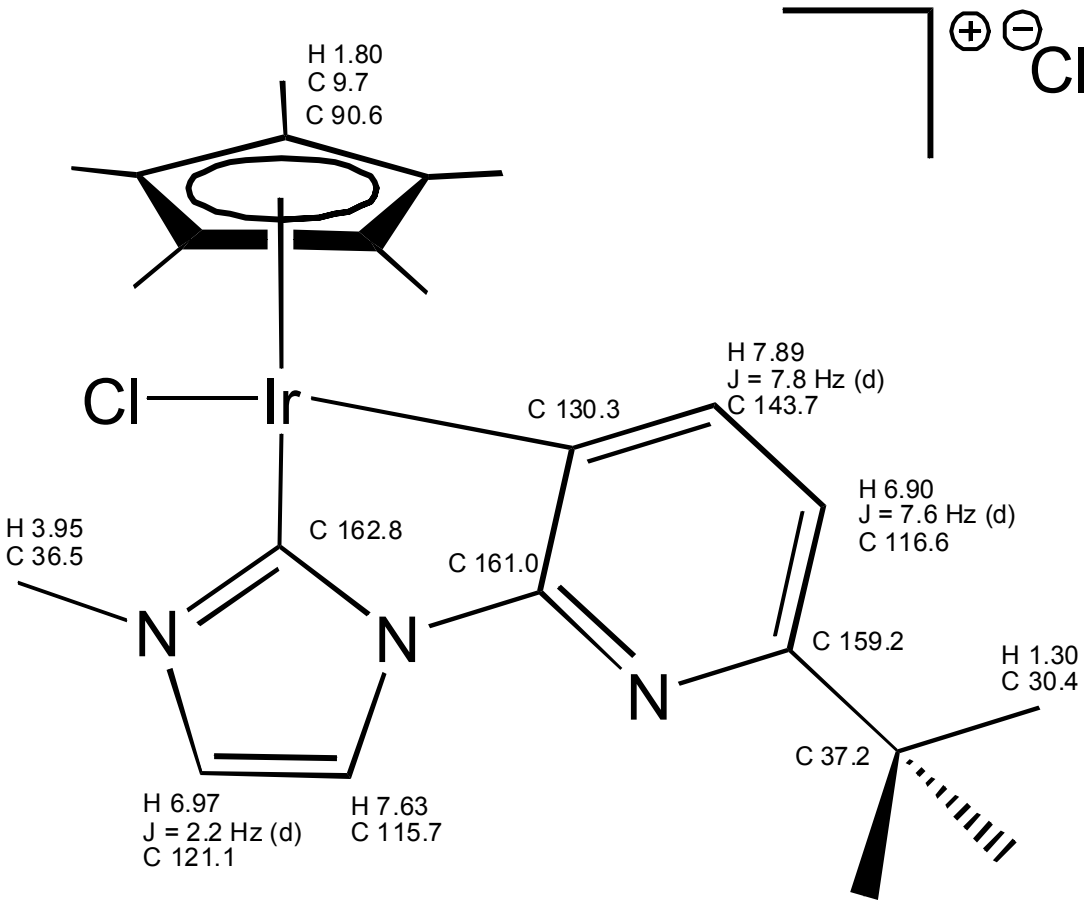

G COSY
6.90 ⇔ 7.89
6.97 ⇔ 7.63

G HMBC		
1.30 <2> 37.2	3.95 <3> 121.1	6.97 <2> 115.7
1.30 <3> 30.4	3.95 <3> 162.8	6.97 <3> 162.8
1.30 <3> 159.2		
	6.90 <3> 130.3	7.89 <3> 159.7
1.80 <2> 90.6	6.90 <4> 161.0	7.89 <3> 161.0
1.80 <4> 130.3		
1.80 <4> 162.8		

Figure 42. Figure with corresponding data on **5x**, taken in $CDCl_3$.

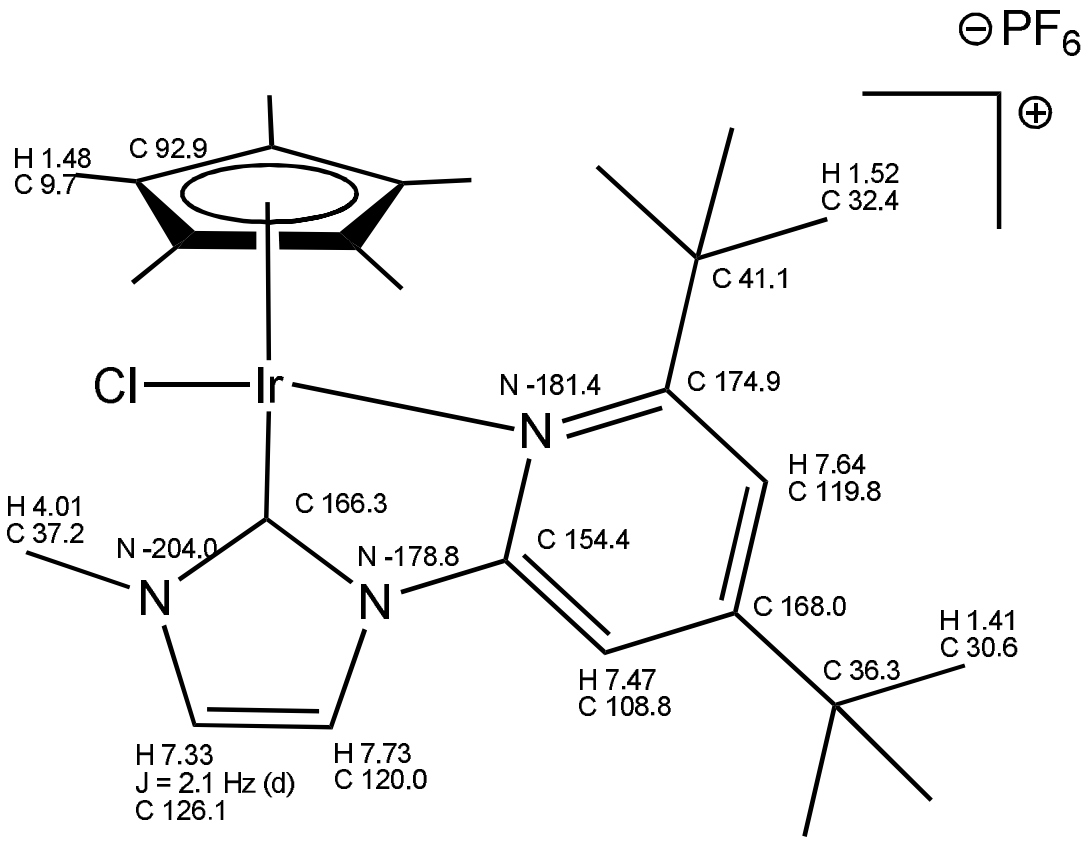

G COSY
7.33 <3> 7.73
7.47 <4> 7.64

G HSQC	
1.41 ⇔ 30.6	7.33 ⇔ 126.1
1.48 ⇔ 9.7	7.47 ⇔ 108.8
1.52 ⇔ 32.4	7.64 ⇔ 119.8
4.01 ⇔37.2	7.73 ⇔120.0

Figure 43. Figure with corresponding data on **5z**, taken in CD_2Cl_2.

G HMBC		
1.41 <1,3> 30.6	1.52 <1,3> 32.4	7.47 <3> 119.8
1.41 <2> 36.3	1.52 <2> 41.1	7.64 <2> 174.9
1.41 <3> 168.0	1.52 <3> 174.9	7.64 <3> 36.3
1.48 <1,4> 9.7	4.01 <2> 37.2	7.64 <3> 41.1
1.48 <2,3> 92.9	4.01 <3> 126.1	7.64 <3> 108.8
1.48 <3> 166.3	4.01 <3> 166.3	7.64 <3> 174.9
	7.33 <2> 120.0	7.73 <2> 126.1
	7.33 <3> 166.3	7.73 <3> 166.3

NOESY		
1.41 ==> 7.64	4.01 ==> 1.48	7.47 ==> 7.73
1.41 ==> 7.47	4.01 ==> 7.33	7.64 ==> 1.52
1.48 ==> 4.01		7.73 ==> 7.33
1.52 ==> 7.64		7.73 ==> 7.47

G HMBC ^{15}N
7.73 <2> -178.8
7.33 <3> -178.8
7.64 <3> -181.4
4.01 <2> -204.0
7.33 <2> -204.0
7.73 <3> -204.0

Figure 43. Continued.

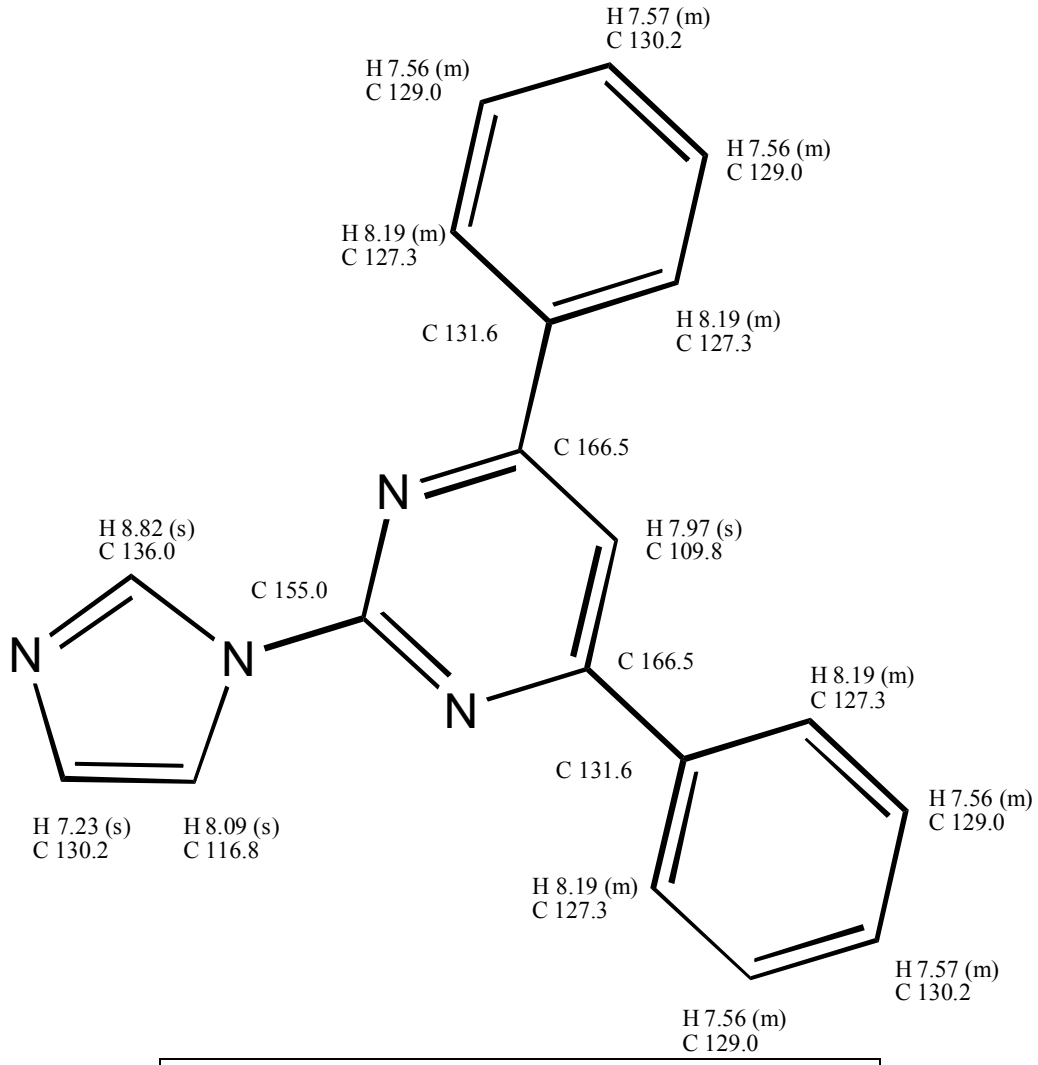

G COSY	
7.23 ⇔ 8.09 7.23 ⇔ 8.82 7.56 ⇔ 8.19	7.57 ⇔ 8.19 8.09 ⇔ 8.82

G HMBC		
8.82 <3> 130.2 8.82 <3> 116.8	8.09 <3> 136.0 8.09 <2> 130.2	7.56 <8> 136.0 7.56 <3> 129.0
8.19 <3> 166.5 8.19 <7> 136.0 8.19 <2> 131.6 8.19 <3> 127.3	7.97 <2> 166.5 7.97 <6> 136.0 7.57 <9> 136.0 7.57 <3> 127.3	7.23 <4> 155.0 7.23 <3> 136.0

Figure 44. Figure with corresponding data on **10**, taken in $CDCl_3$.

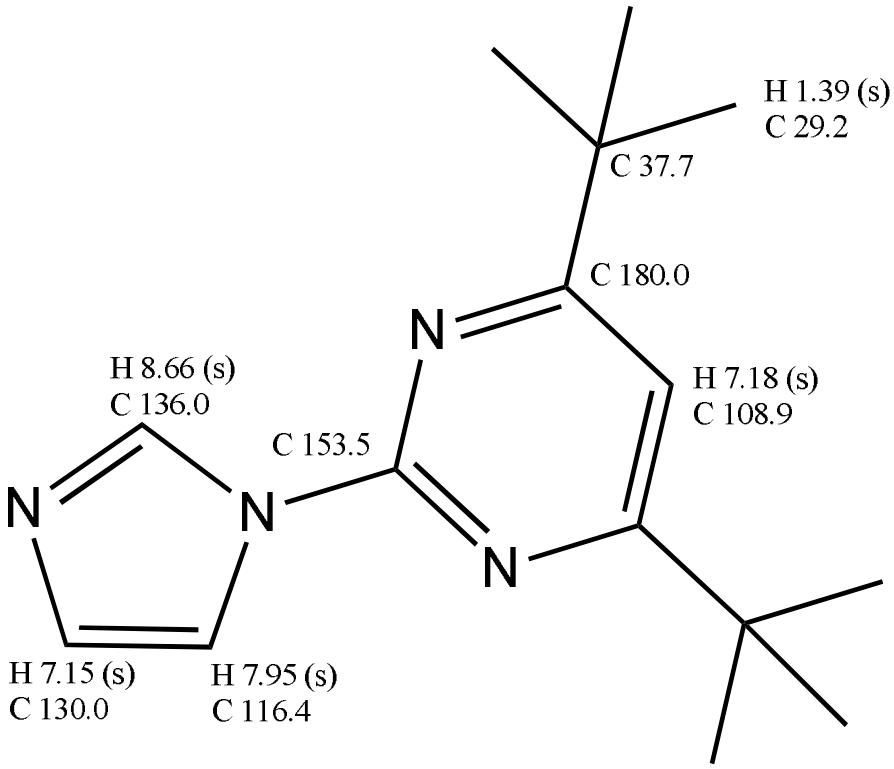

gCOSY
7.15 ⇔ 7.95
7.15 ⇔ 8.66
7.95 ⇔ 8.66

gHMBC	
180.0 <2>7.18	130.0 <2> 7.95
	130.0 <3> 8.66
37.7 <2>1.39	
	136.0 <3> 7.15
116.4 <3> 8.66	136.0 <3> 7.95

Figure 45. Figure with corresponding data on **12**, taken in $CDCl_3$.

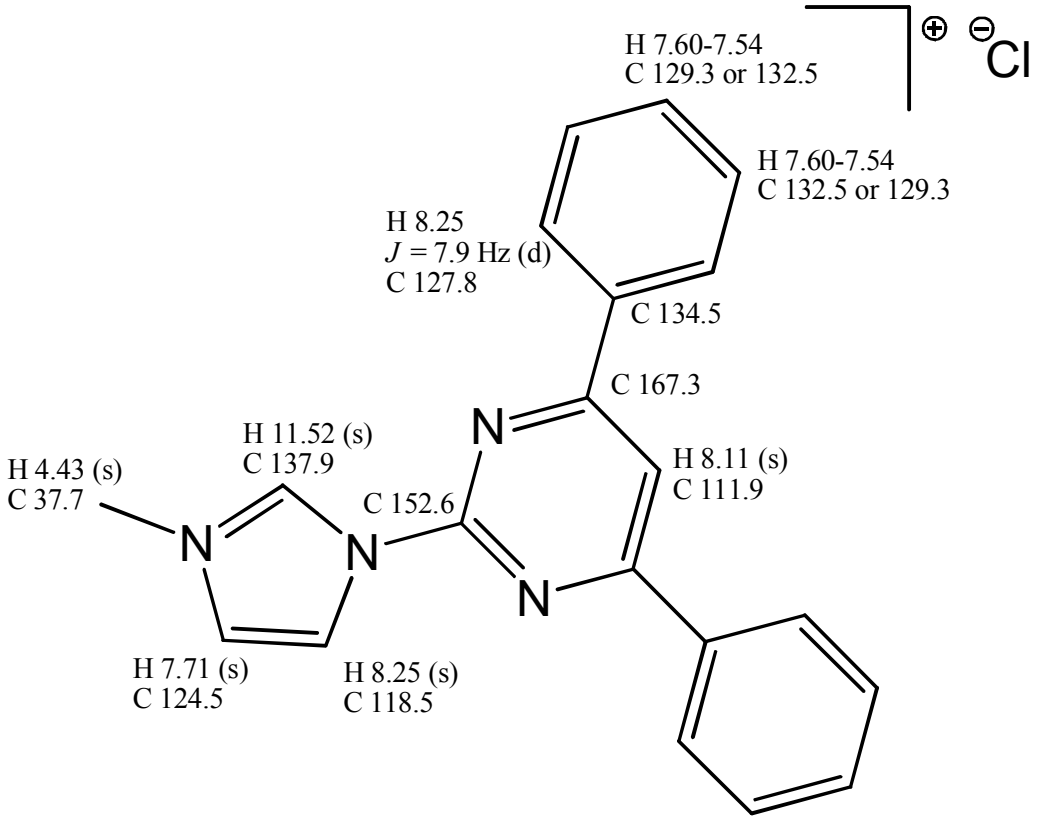

gCOSY	
7.55 ⇔ 8.25	7.71 ⇔ 11.52
7.71 ⇔ 8.25	8.25 ⇔ 11.52

gHMBC		
4.43 <3> 124.5	7.71 <3> 118.5	8.25 <2> 124.5
4.43 <3> 137.9	7.71 <3> 137.9	8.25 <3> 137.9
7.55 <2 or 3> 127.8	8.11 <2> 167.3	8.3 <2 or 3> 132.5
7.55 <2 or 3> 129.3	8.11 <3> 134.5	8.3 <3> 127.8
7.55 <3 or 4> 134.5		8.3 <3> 167.3
		11.5 <3> 118.5
		11.5 <3> 124.5

*NOE data were used to assign the proton resonating at 7.71 ppm as the one closer to the N-CH_3 substituent (chemical shift 4.43 ppm).

Figure 46. Figure with corresponding data on **9-Ph**, taken in $CDCl_3$.

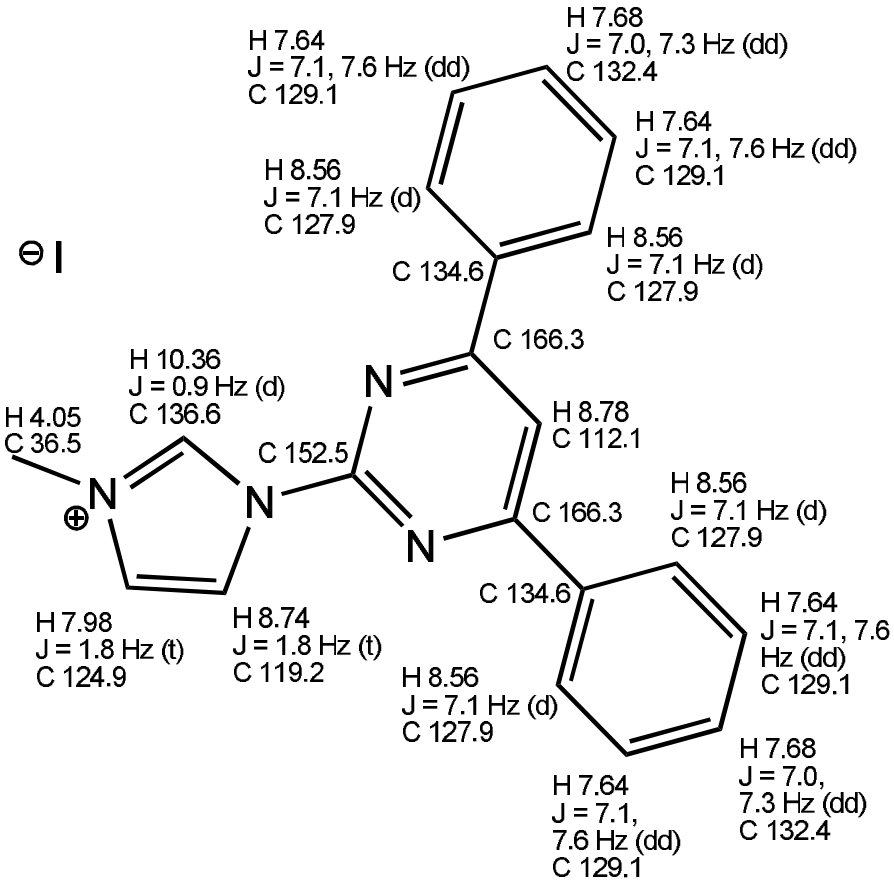

G COSY	
4.05 ⇔ 10.36 8.56 ⇔ 7.64	7.98 ⇔ 8.74 7.98 ⇔ 10.36 8.74 ⇔ 10.36

G HMBC		
4.05 <3> 124.9 4.05 <3> 136.6	7.98 <2> 119.2 7.98 <3> 136.6	8.74 <2> 124.9 8.74 <3> 136.6
7.64 <2> 127.9	8.56 <3> 127.9 8.56 <3> 132.4	8.78 <3> 134.6
7.68 <2> 129.1 7.68 <3> 127.9 7.68 <3> 134.6		10.36 <3> 119.2 10.36 <3> 124.9

*Assignment of the proton at 7.98 ppm relative to 4.05 ppm based on NOE data.

Figure 47. Figure with corresponding data on **11-Ph-I**, taken in *d*-DMSO.

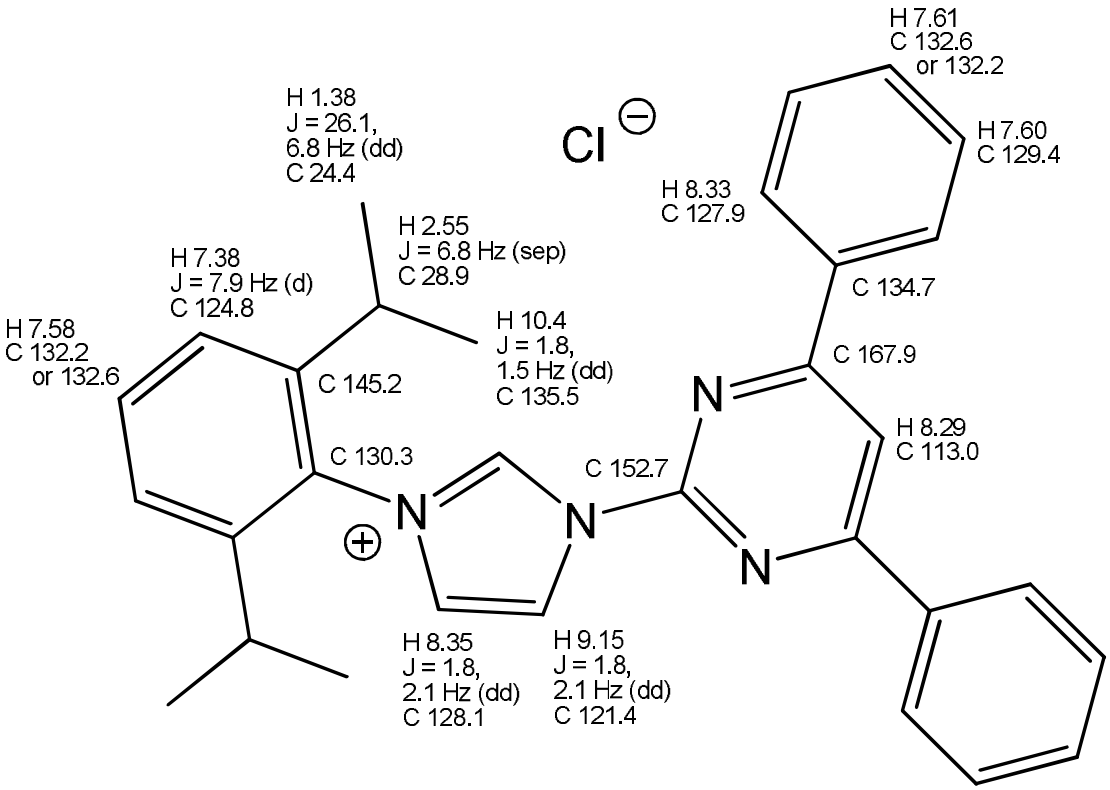

G COSY	
1.38 ⇔ 2.55	8.35 ⇔ 9.15
7.38 ⇔ 7.58	8.35 ⇔ 10.40
7.60 ⇔ 8.33	9.15 ⇔ 10.40

G HMBC		
1.38 <3> 24.4	7.35 <3> 28.9	8.34 <3> 167.9
1.38 <2> 28.9	7.35 <3> 124.8	
1.38 <3> 145.2	7.35 <3> 130.3	9.15 <2> 128.1
		9.15 <3> 135.5
2.55 <3> 124.9	7.58 <3> 134.7	
2.55 <3> 130.3	7.58 <3> 145.2	10.41 <3> 121.4
2.55 <2> 145.2		10.41 <3> 128.1
	8.29 <3> 134.7	

Figure 48. Figure with corresponding data on **9-Ph**, taken in $CDCl_3$.

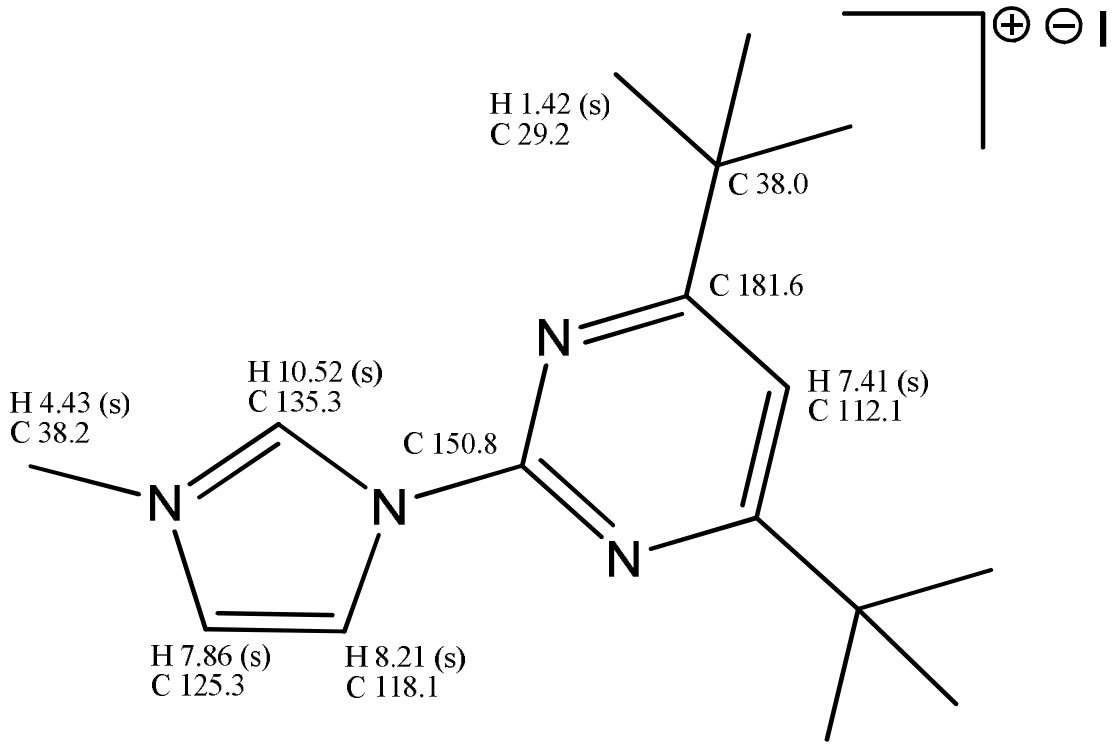

gHMBC		
7.41 <2> 181.6	7.86 <3> 135.3	10.52 <3> 125.3
		10.52 <3> 118.1
4.43 <3> 135.3	8.21 <3> 135.3	
4.43 <3> 125.3		

Figure 49. Figure with corresponding data on **13-tBu-I**, taken in $CDCl_3$.

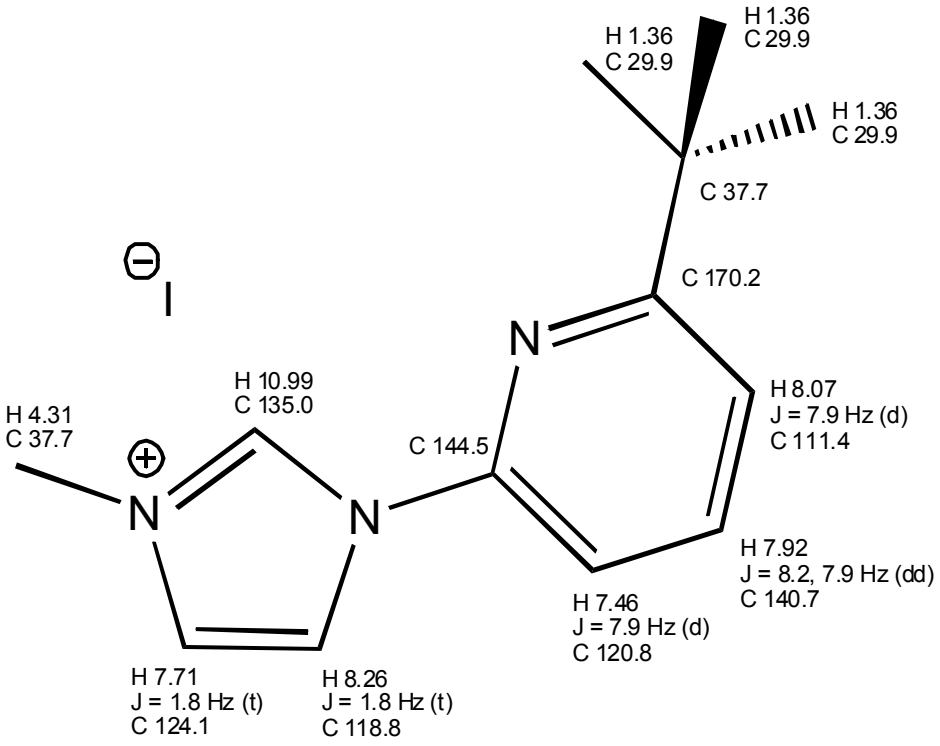

G COSY	
7.46 ⇔ 7.92 7.92 ⇔ 8.07	7.71 ⇔ 8.26 7.71 ⇔ 10.99 8.26 ⇔ 10.99

G HMBC		
1.36 <3> 29.9 1.36 <2> 37.7 1.36 <3> 170.2 4.31 <3> 124.1 4.31 <3> 135.0 7.46 <2> 170.2	7.71 <2> 118.8 7.71 <3> 135.0 7.92 <3> 170.2 7.92 <3> 144.5	8.26 <2> 124.1 8.26 <3> 135.0 10.97 <3> 124.1 10.97 <3> 118.8

Figure 50. Figure with corresponding data on **16-I**, taken in $CDCl_3$.

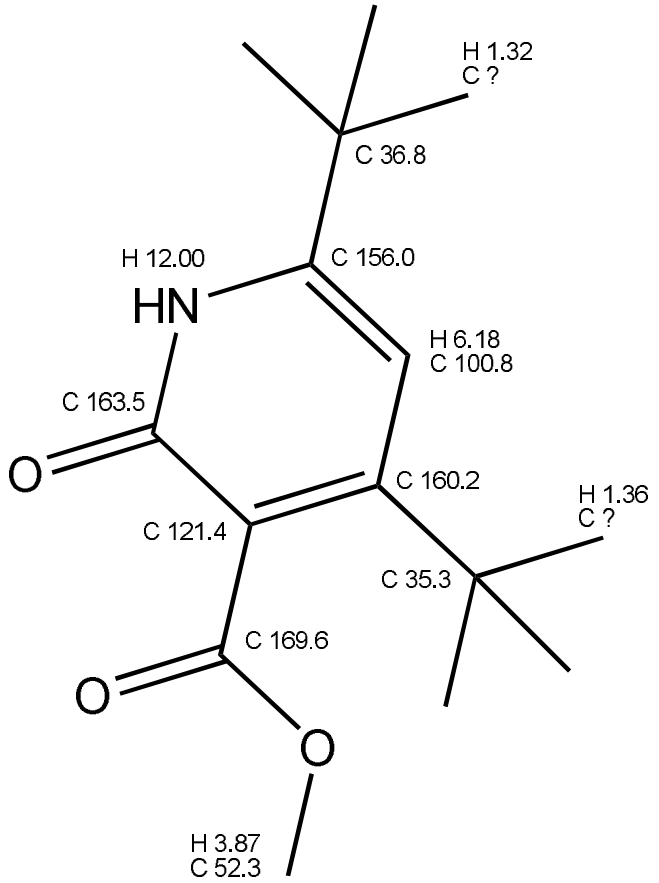

G HMBC
1.32 <2> 36.8
1.36 <3> 160.2
3.87 <3> 169.6
6.18 <3> 121.4

Figure 51. Figure with corresponding data on **21**, taken in $CDCl_3$.

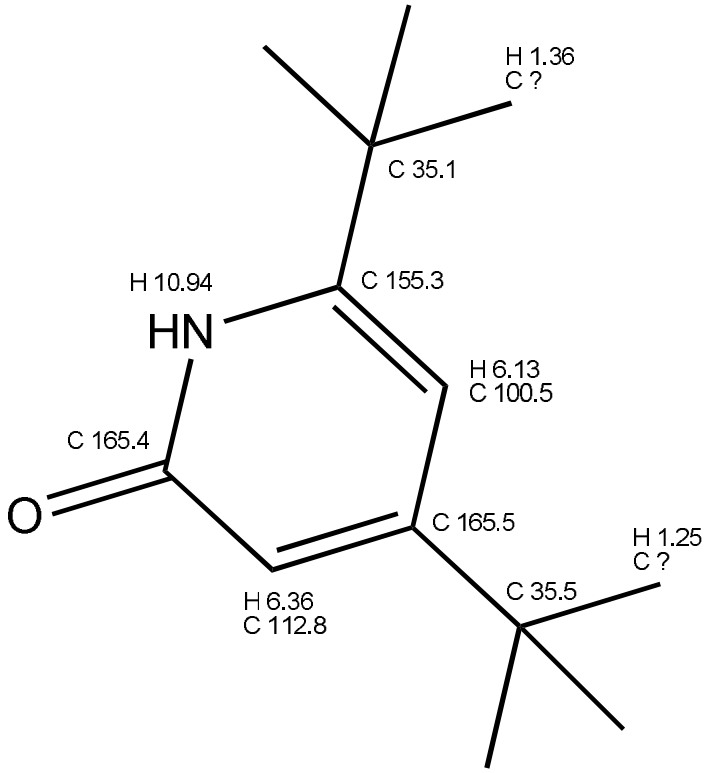

G HMBC	
1.25 <2> 35.5	6.13 <3> 35.5
1.25 <3> 165.5 or 165.4	6.13 <3> 112.8
1.36 <2> 35.1	6.36 <3> 35.5
1.36 <3> 155.3	6.36 <3> 100.5
6.13 <3> 35.1	

Figure 52. Figure with corresponding data on **22**, taken in $CDCl_3$.

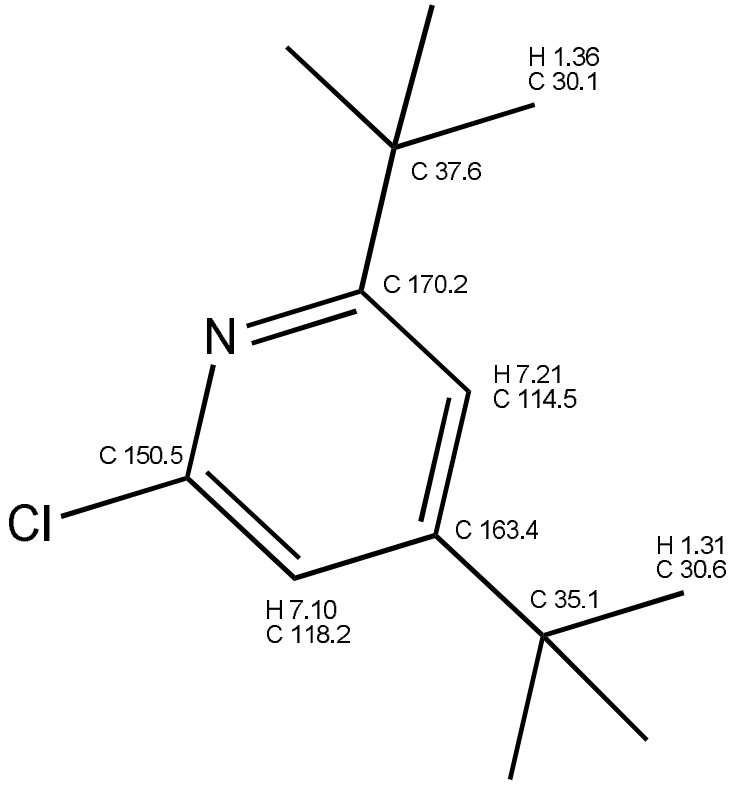

G HSQC
1.31 ⇔ 30.6 1.36 ⇔ 30.1 7.10 ⇔ 118.2 7.21 ⇔ 114.5

G HMBC		
1.31 <1,3> 30.6 1.31 <2> 35.1 1.31 <3> 163.4	1.36 <1,3> 30.6 1.36 <2> 35.1 1.36 <3> 163.4 7.10 <1> 118.2	7.10 <3> 114.5 7.21 <2> 170.2 7.21 <3> 118.2

Figure 53. Figure with corresponding data on **23**, taken in $CDCl_3$.

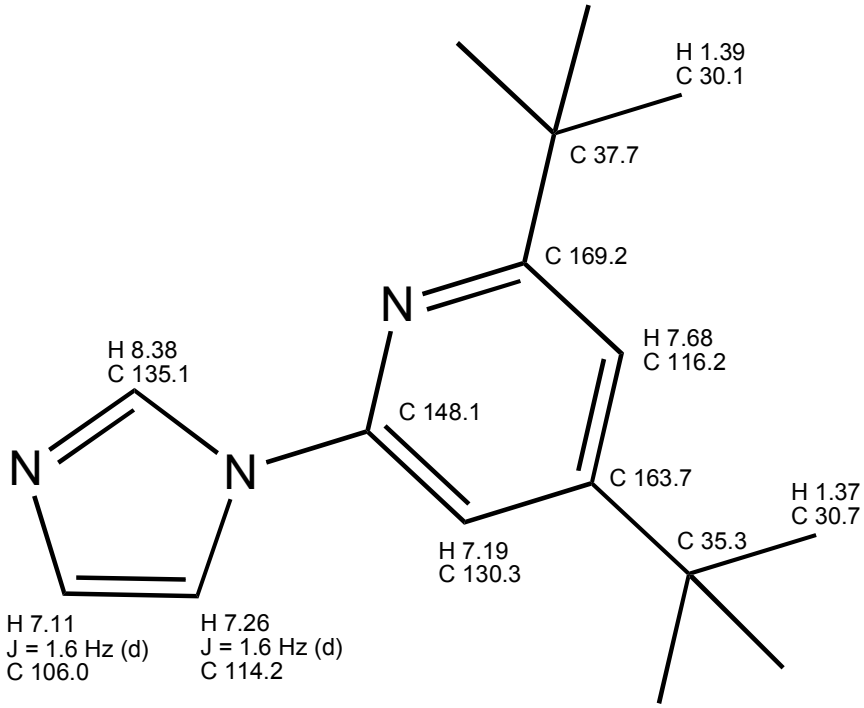

G HSQC	
1.37 ⇔ 30.7 1.39 ⇔ 30.1 7.11 ⇔ 106.0	7.19 ⇔ 130.0 7.26 ⇔ 114.2 7.68 ⇔ 116.2 8.38 ⇔135.1

G HMBC		
1.37 <1,3> 30.7	7.11 <2> 114.2	7.26 <1> 114.2
1.37 <2> 35.7	7.19 <1> 130.3	7.26 <2> 106.0
1.37 <3> 163.7	7.19 <3> 35.3	7.68 <3> 130.0
1.39 <1,3> 30.1		8.38 <1> 135.1
1.39 <2> 37.7		8.38 <3> 114.2
1.39 <3> 169.2		8.38 <4> 130.3

Figure 54. Figure with corresponding data on **24**, taken in $CDCl_3$.

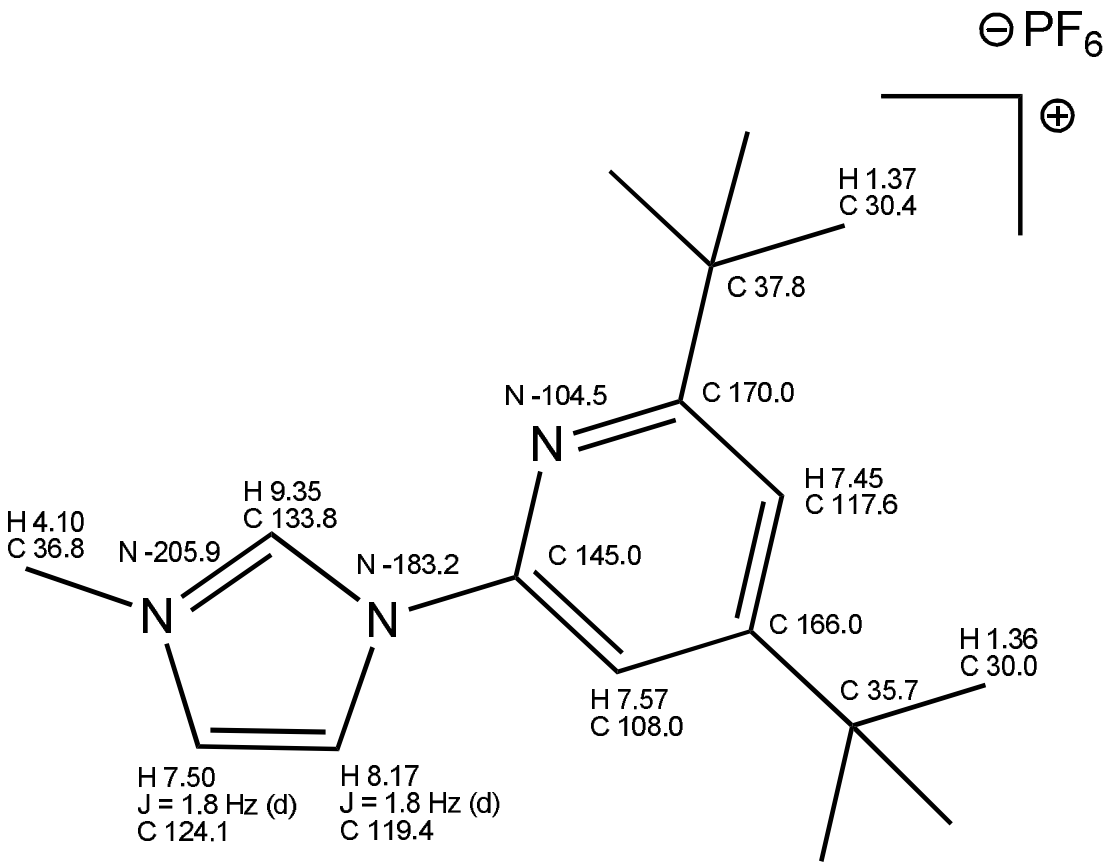

G COSY
4.10 <4> 9.35
7.45 <4> 7.57
7.50 <3> 8.17
7.50 <4> 9.35
8.17 <4> 9.35

G HSQC	
1.36 ⇔ 30.0	7.50 ⇔ 124.1
1.37 ⇔ 30.4	7.57 ⇔ 108.0
4.10 ⇔ 36.8	8.17 ⇔ 119.4
7.45 ⇔ 117.6	9.35 ⇔133.8

Figure 55. Figure with corresponding data on **25-PF_6**, taken in $CDCl_3$.

G HMBC		
1.36 <1,3> 30.4	7.45 <2> 170.0	7.57 <3> 117.6
1.36 <2> 35.7	7.45 <3> 35.7	8.17 <1> 119.4
1.36 <3> 166.0	7.45 <3> 37.8	8.17 <2> 124.1
1.37 <1,3> 30.0	7.45 <3> 108.0	8.17 <3> 133.8
1.37 <2> 37.8	7.50 <1> 124.1	9.35 <1> 133.8
1.37 <3> 170.0	7.50 <2> 119.4	9.35 <3> 36.8
4.10 <1> 36.8	7.50 <3> 36.8	9.35 <3> 119.4
4.10 <3> 124.1	7.50 <3> 133.8	9.35 <3> 124.1
4.10 <3> 133.8	7.57 <2> 166.0	9.35 <3> 145.0
	7.57 <3> 35.7	

G HMBC (N-H)	
4.10 <2> -205.9	8.17 <2> -183.2
7.45 <3> -104.5	8.17 <3> -205.9
7.50 <2> -205.9	9.35 <2> -183.2
7.50 <3> -183.2	9.35 <2> -205.9

Figure 55. Continued.

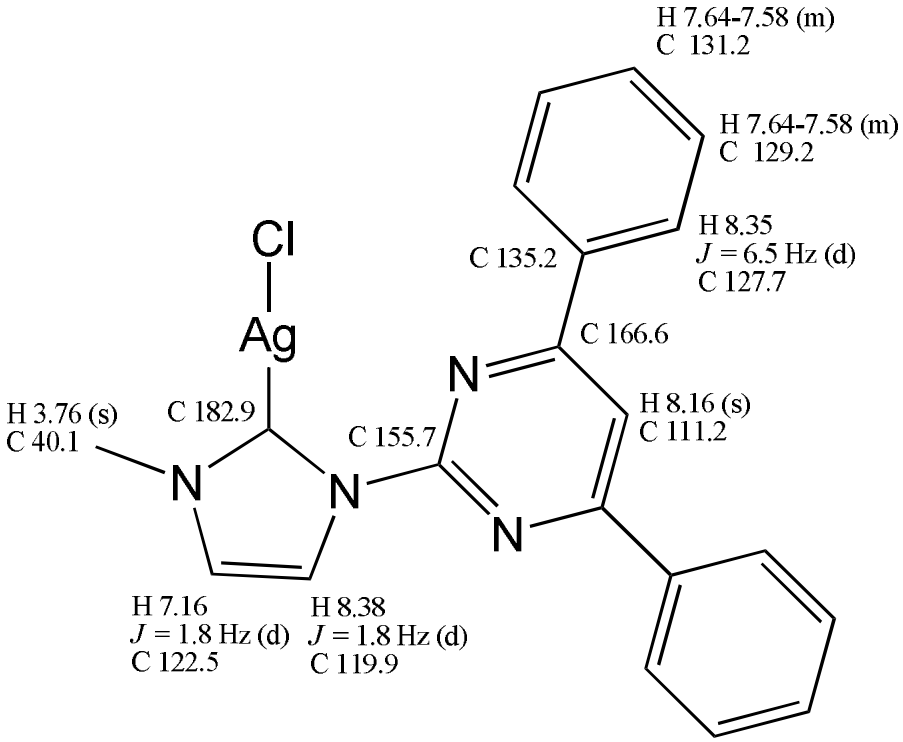

gCOSY
7.16 ⇔ 8.38 7.62 ⇔ 8.35

gHMBC		
3.76 <3> 122.5 3.76 <3> 182.9 7.62 <3> 127.7 7.62 <3> 135.2	8.16 <3> 135.2 8.16 <2> 166.6	8.35 <2> 122.5 8.35 <3> 131.9

*Carbene carbon resonance chemical shift = δ 182.9 ppm was identified by its HMBC crosspeak, because the resonance was not seen in 1D ^{13}C NMR spectra.

Figure 56. Figure with corresponding data on **8-Ph-AgCl**, taken in $CDCl_3$.

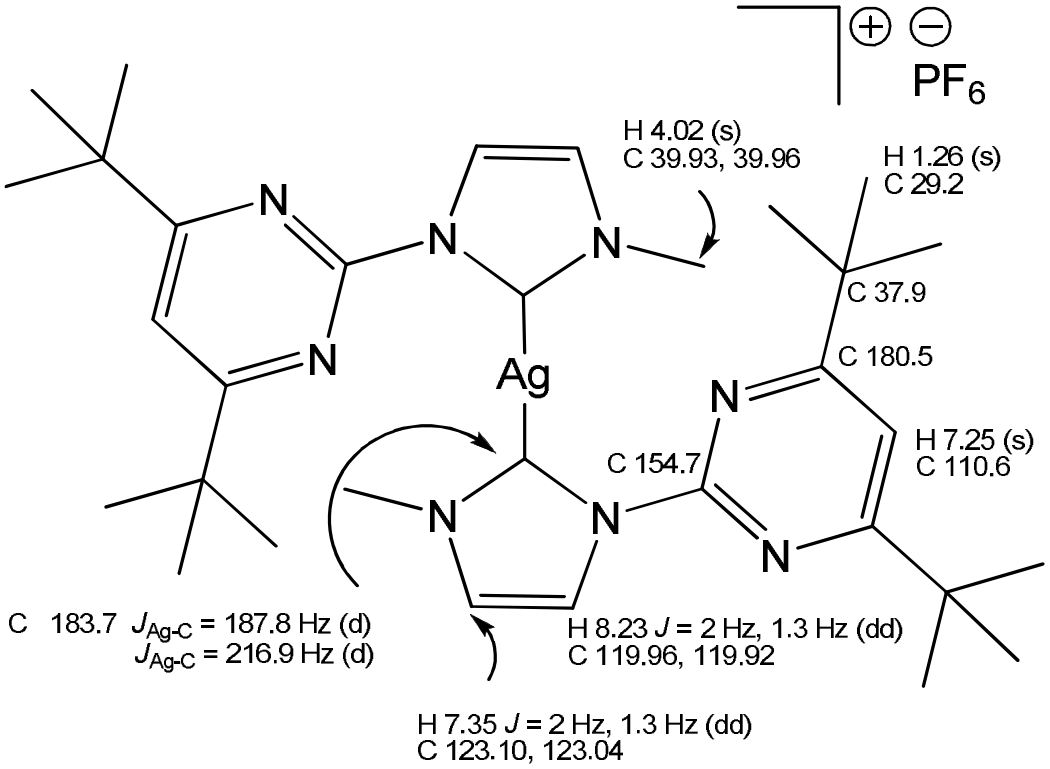

gCOSY
7.35 ⇔ 8.23

gHMBC		
183.7<3> 4.02	119.92 <2> 7.35	123.10 <2> 8.23
123.10 <3> 4.02	119.96 <2> 7.35	123.04 <2> 8.23
123.04 <3> 4.02		
	37.9 <2> 1.26	180.5 <2> 7.25
	37.9 <3> 7.25	

*For this compound several resonances showed two peaks of nearly equal intensity, which we ascribe to isotopic perturbation by ^{107}Ag and ^{109}Ag (51.8 and 48.2% natural abundance, respectively).[205-206]

Figure 57. Figure with corresponding data on **13-tBu-Ag**, taken in $CDCl_3$.

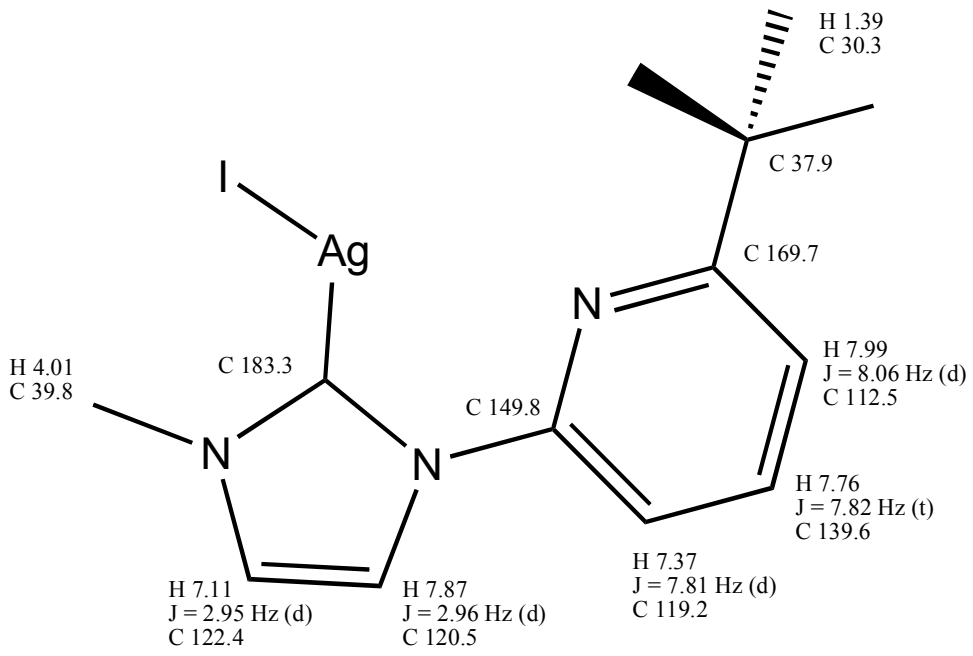

G HMBC		
1.39 <2> 37.9	7.11 <1> 122.4	7.76 <2> 112.5
1.39 <3> 30.3	7.11 <2> 120.5	7.76 <3> 149.8
1.39 <3> 169.7		7.76 <3> 169.7
	7.37 <3> 112.5	
4.01 <3> 122.4	7.37 <4> 169.7	7.87 <1> 120.5
4.01 <3> 183.3		
		7.99 <1> 112.5
		7.99 <3> 119.2

Figure 58. Figure with corresponding data on compound **16-AgI** in $CDCl_3$.

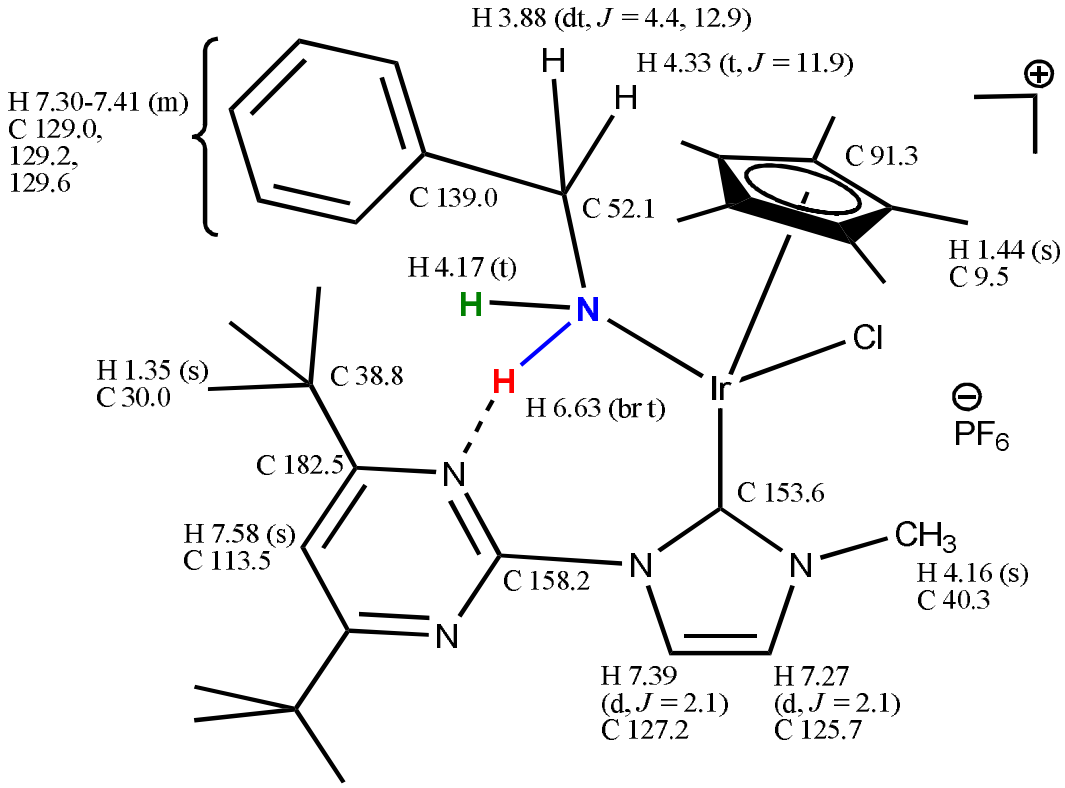

gCOSY		
3.88 ⇔ 4.33 3.88 ⇔ 6.63	4.33 ⇔ 6.63 4.33 ⇔ 7.37	7.25 ⇔ 7.39 7.30 – 7.41 ⇔ 7.30 - 7.41

gHSQC		
1.35 ⇔ 30.0 1.44 ⇔ 9.5 4.16 ⇔ 40.3	4.33 ⇔ 52.1 7.27 ⇔ 125.7 7.39 ⇔ 127.2	7.30 – 7.41 ⇔ 129.0, 129.2, 129.6

gHMBC		
1.35 <2> 182.5 1.35 <3> 38.8 1.44 <2> 91.3 1.44 <4> 153.6 3.88 <2> 139.0 3.88 <3> 129.0 3.88 <4> 153.6	4.16 <3> 125.7 4.16 <3> 153.6 4.33 <2> 139.0 4.33 <3> 129.2 7.27 <2> 127.2 7.27 <3> 40.3 7.27 <3> 153.6	7.39 <2> 125.7 7.39 <3> 153.6 7.39 <3> 158.2 7.58 <2> 182.5 7.58 <3> 38.8

Figure 59. Figure with corresponding data on compound **5c-BA**, taken in CD_2Cl_2 at 30°C.

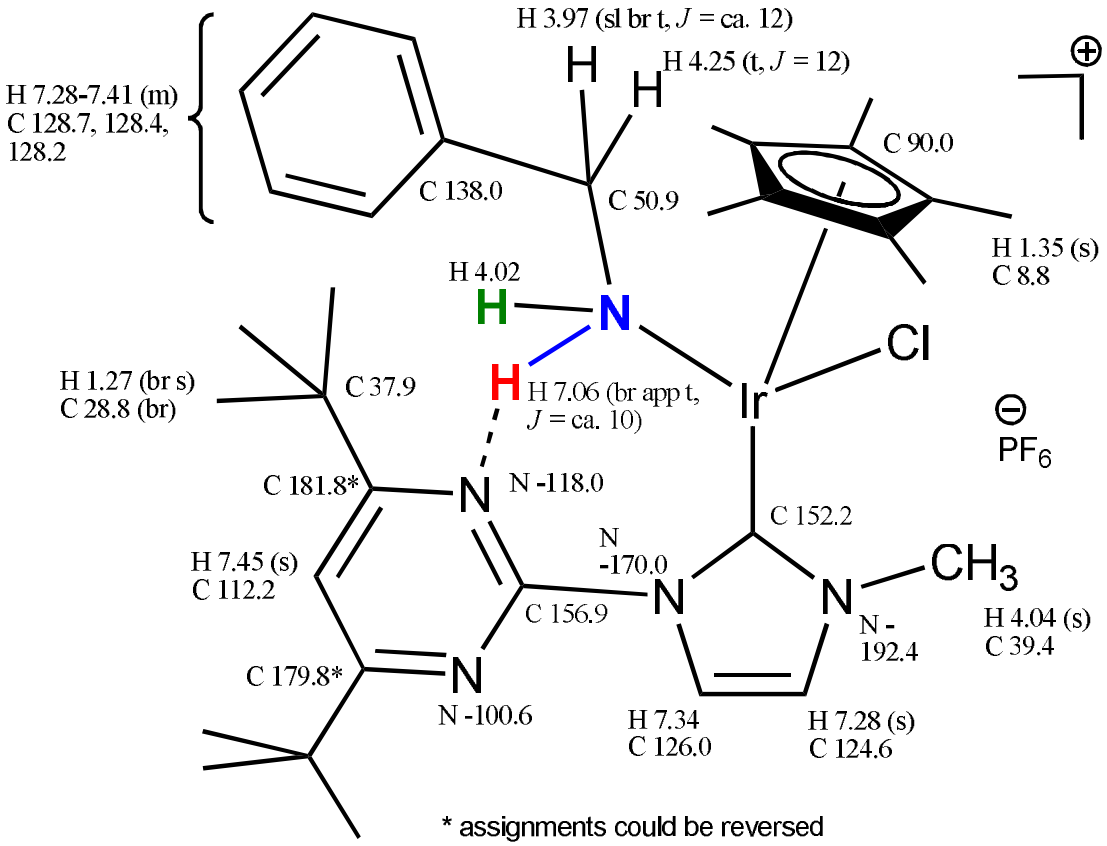

^{1}H-^{15}N gHMBC	
7.45 ⇔ -100.6 7.45 ⇔ -118.0 7.45 ⇔ -170.0 7.34 ⇔ -170.0	7.34 ⇔ -192.4 7.28 ⇔ -192.4 4.04 ⇔ -192.4

Figure 60. Figure with corresponding data on compound **5c-BA** in CD_2Cl_2 at -60°C.

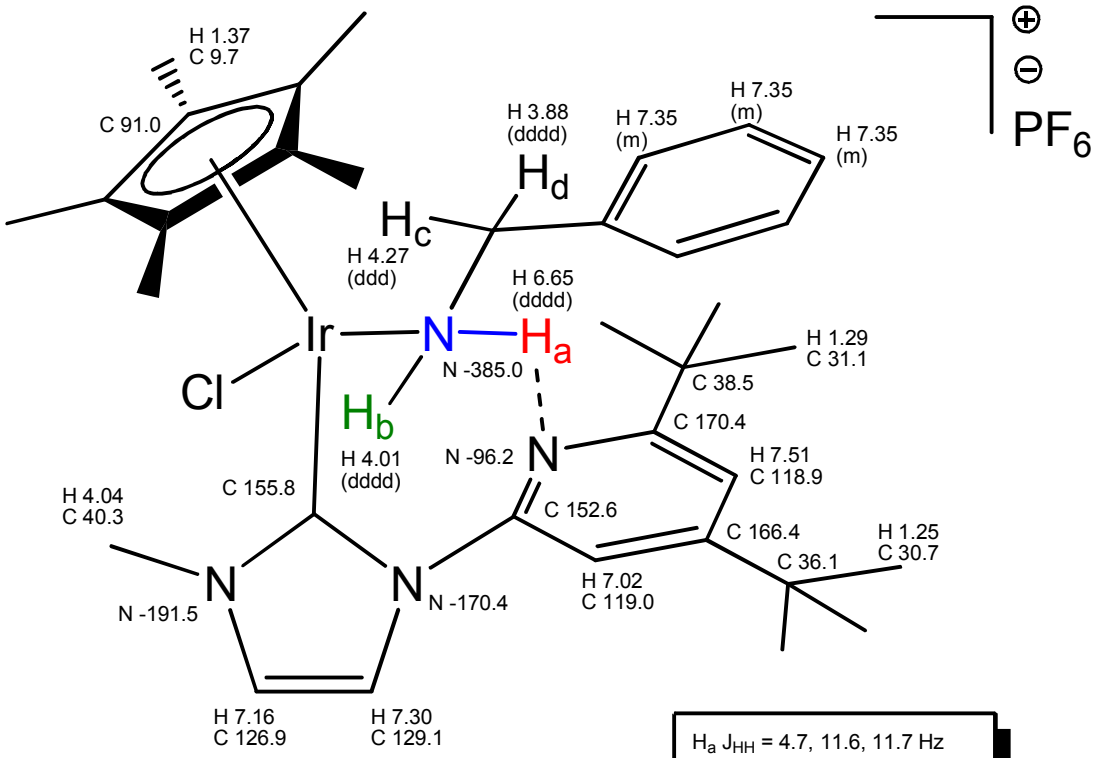

G COSY
7.51 <4> 7.02

G HSQC	
1.25 ⇔ 31.1	7.02 ⇔ 119.0
1.29 ⇔ 30.7	7.16 ⇔ 126.9
1.37 ⇔ 9.7	7.30 ⇔ 129.1
4.04 ⇔ 40.3	7.51 ⇔118.9

G HMBC ^{15}N		
4.01 <1> -385.0	4.04 <2> -191.5	7.16 <3> -170.4
4.04 <5> -385.0	7.16 <2> -191.5	7.33 <2> -170.4
7.02 <5> -385.0	7.30 <3> -191.5	7.51 <3> -96.2
7.16 <5> -385.0		

Figure 61. Figure with corresponding data on compound **5z-BA**, taken in CD_2Cl_2 at -60°C.

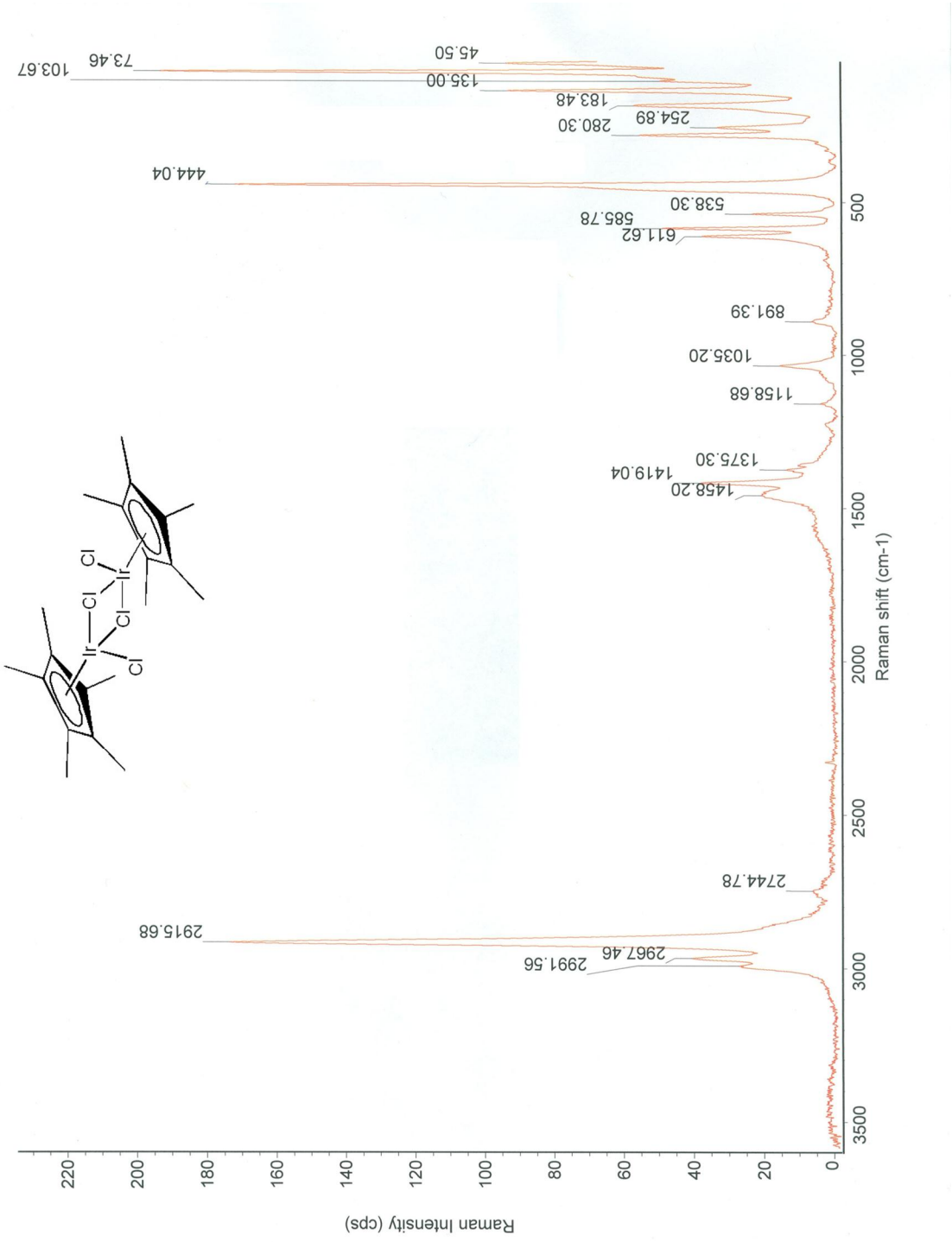

Figure 62. Raman spectrum of compound $[Cp^*Ir(\mu\text{-}Cl)Cl]_2$, taken of the solid sample.

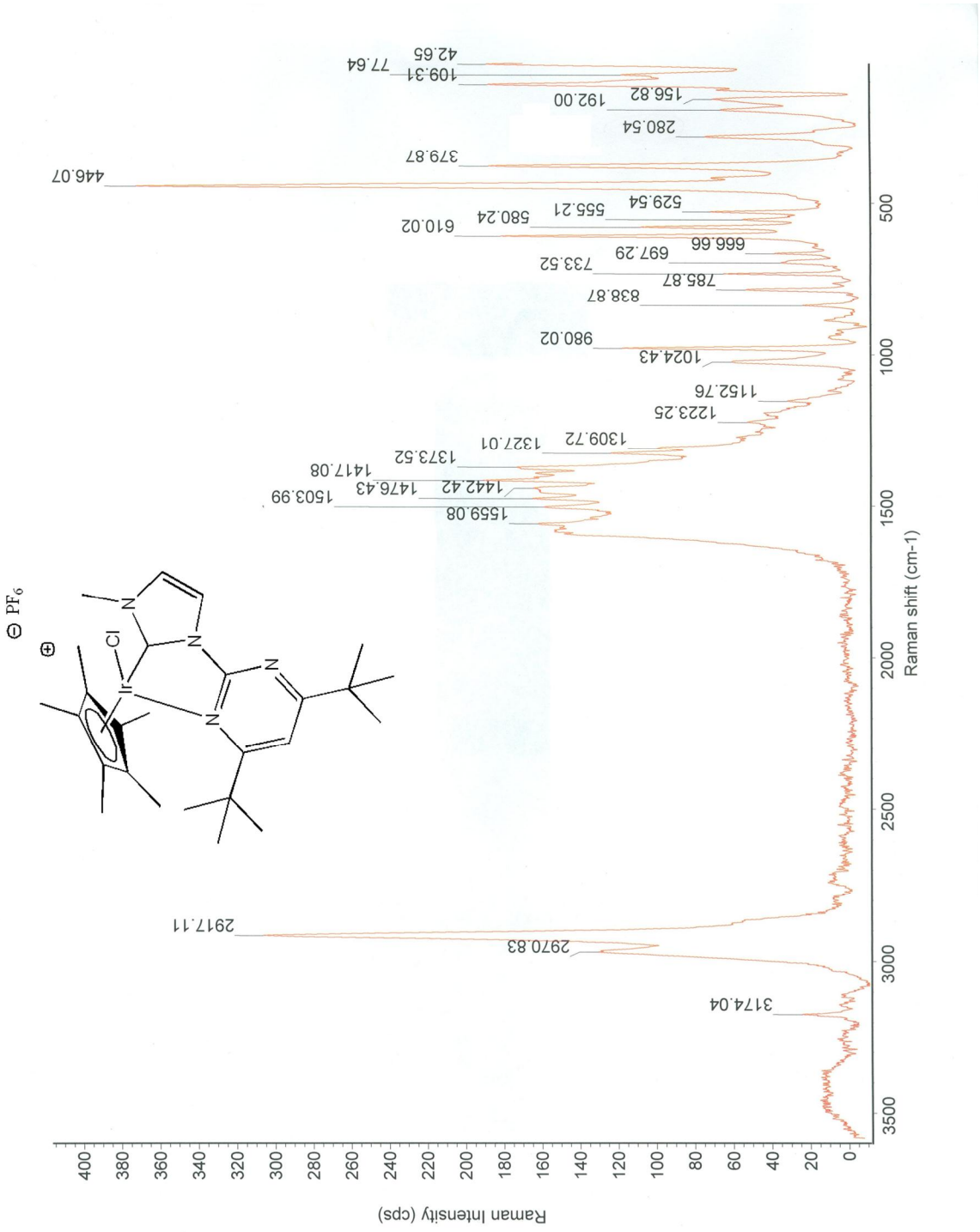

Figure 63. Raman spectrum of compound **5c**, taken of the solid sample.

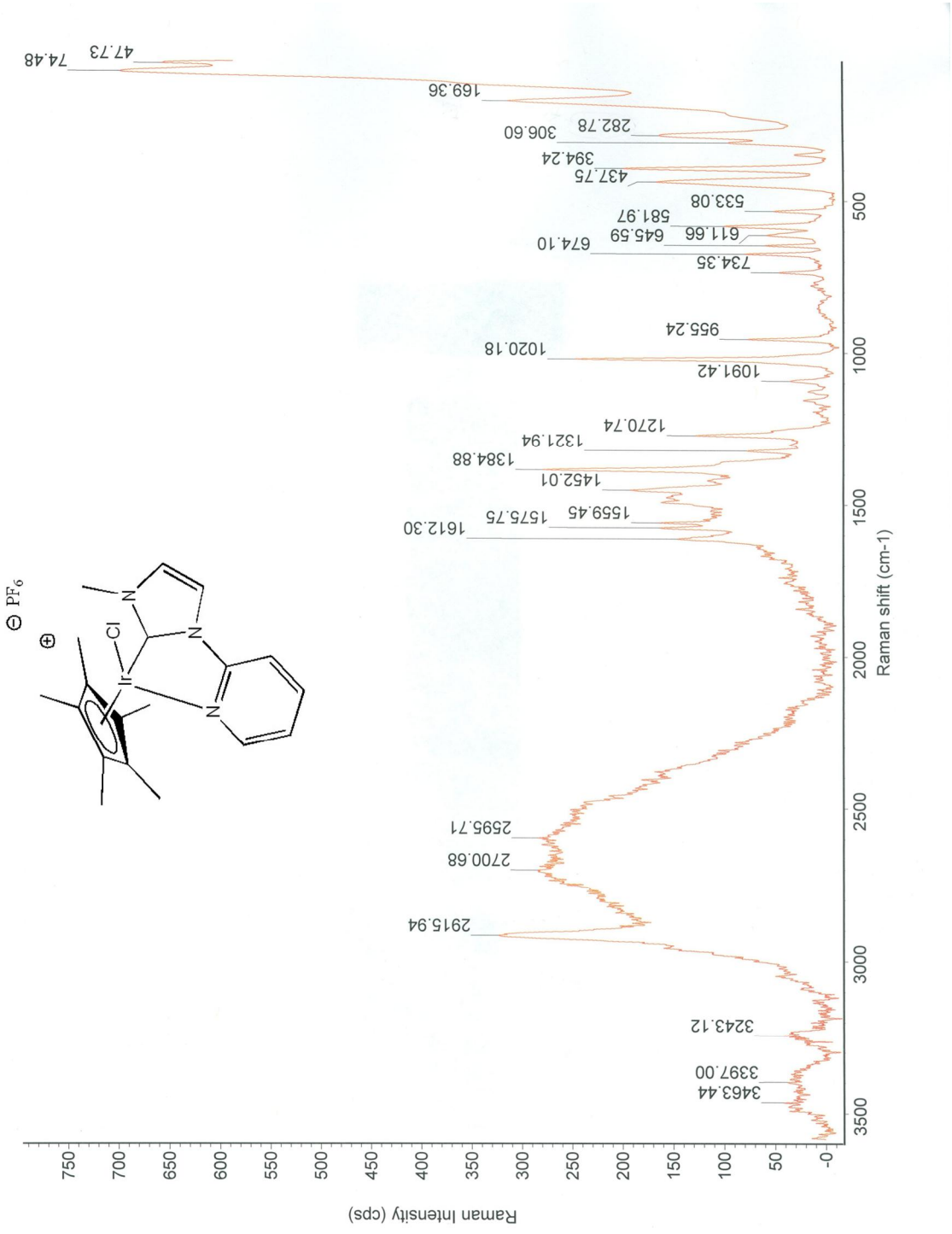

Figure 64. Raman spectrum of compound **5w**, taken of the solid sample.

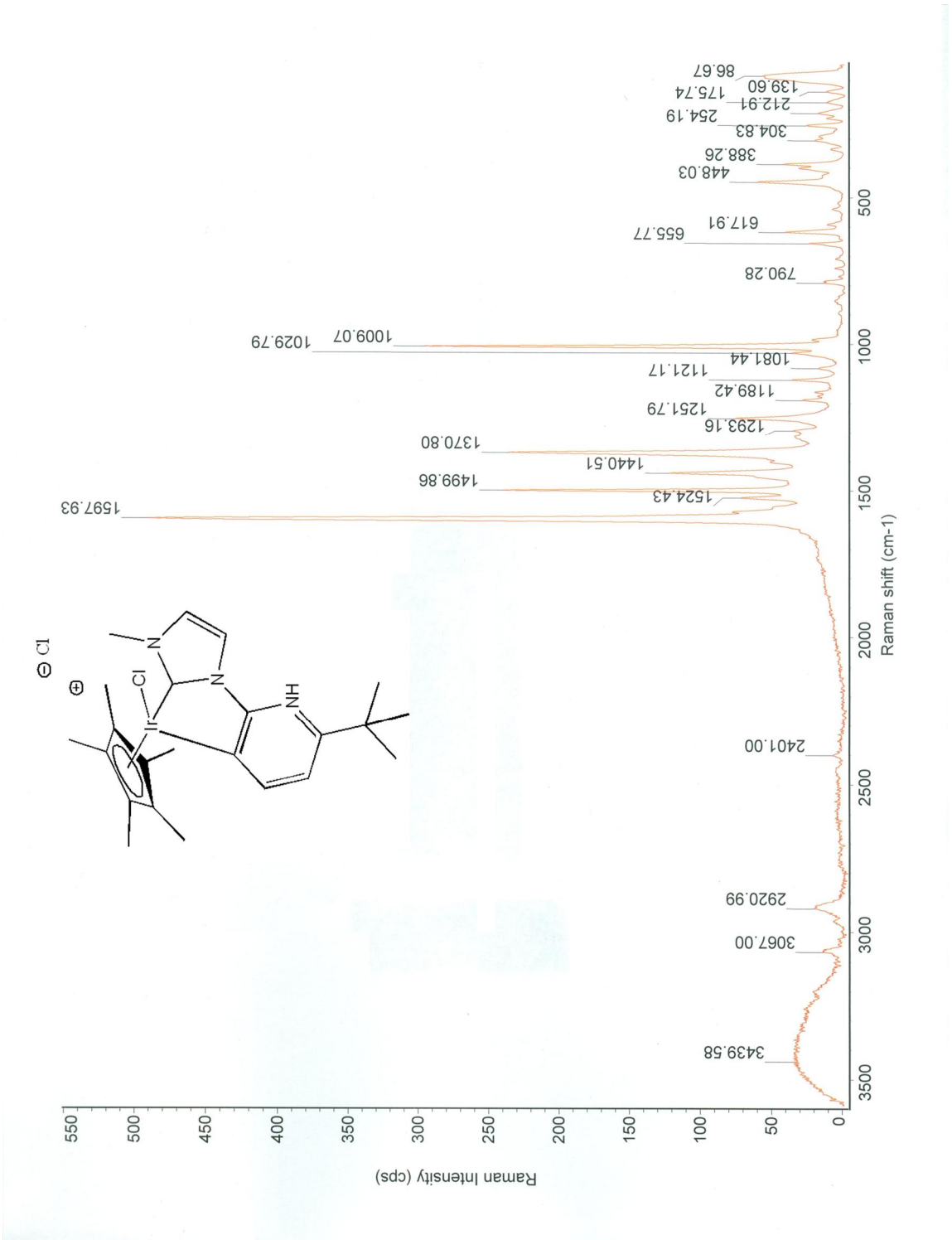

Figure 65. Raman spectrum of compound **5x**, taken of the solid sample.

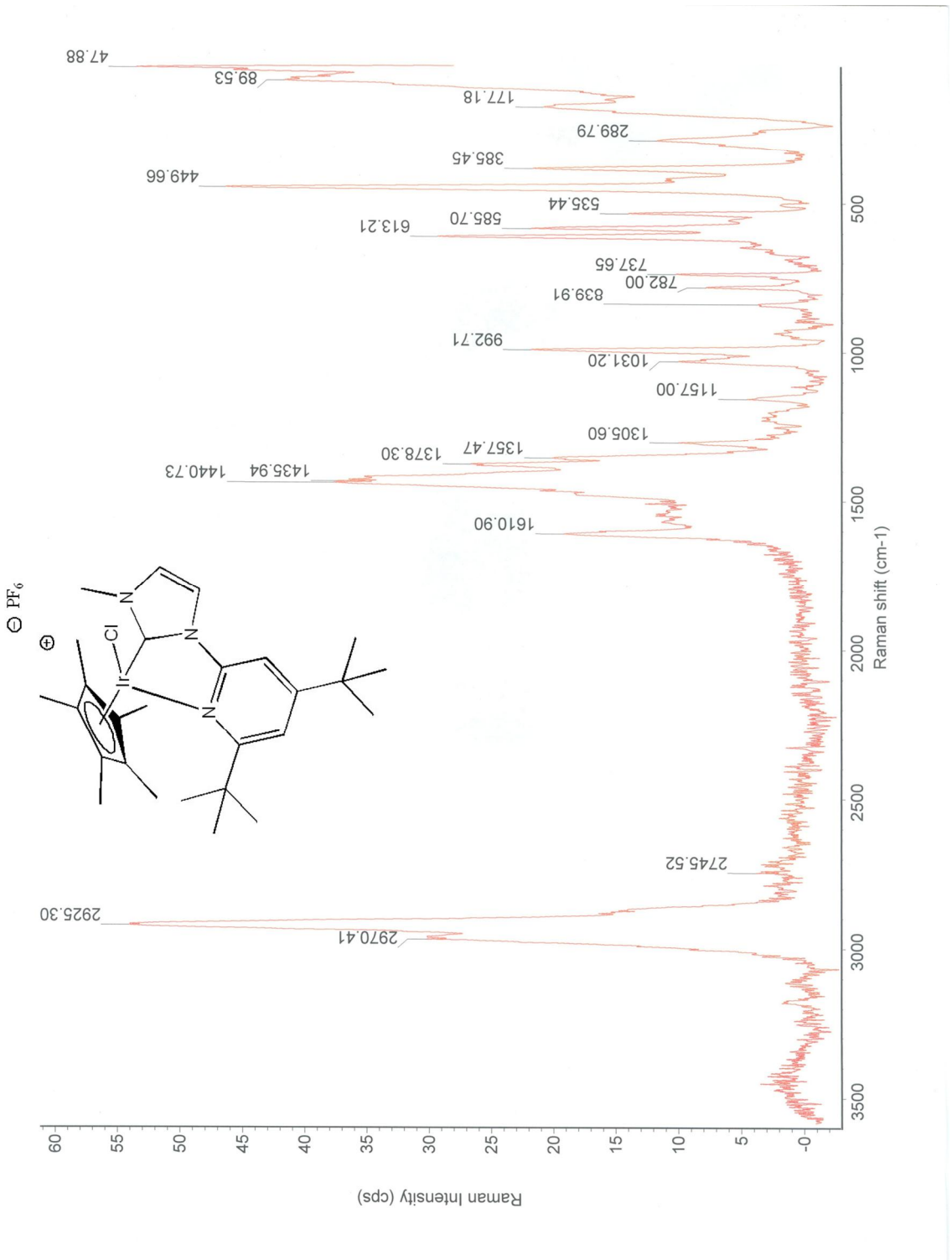

Figure 66. Raman spectrum of compound **5z**, taken of the solid sample.

Graph 1. The Arrhenius plot for **5b**, with *d*-chloroform as the solvent.

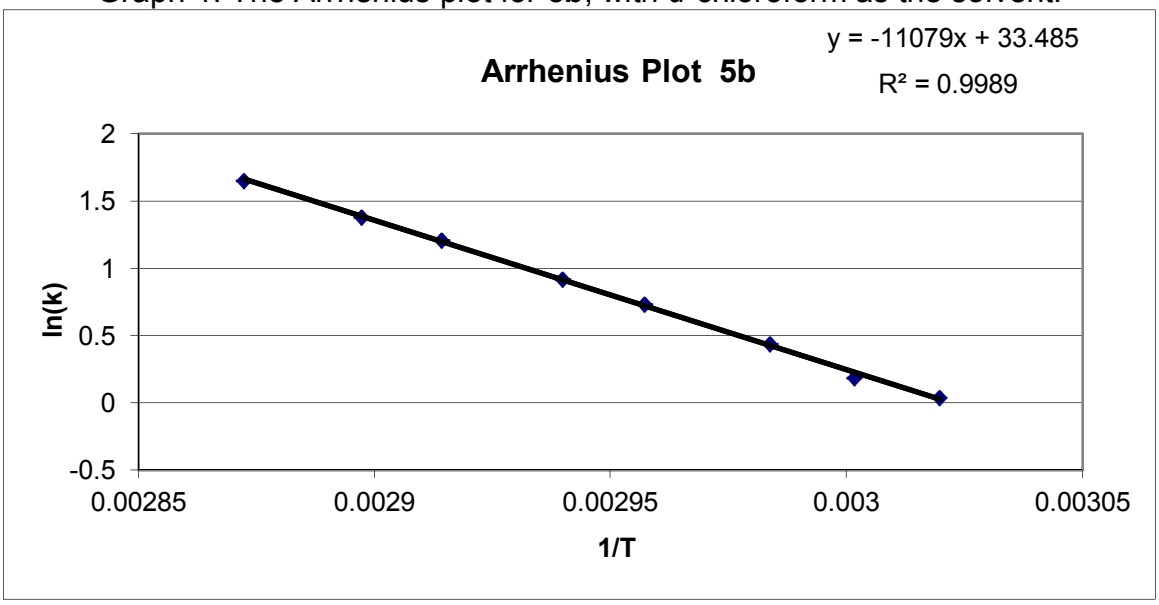

Graph 2. The Erying plot for **5b**, with *d*-chloroform as the solvent.

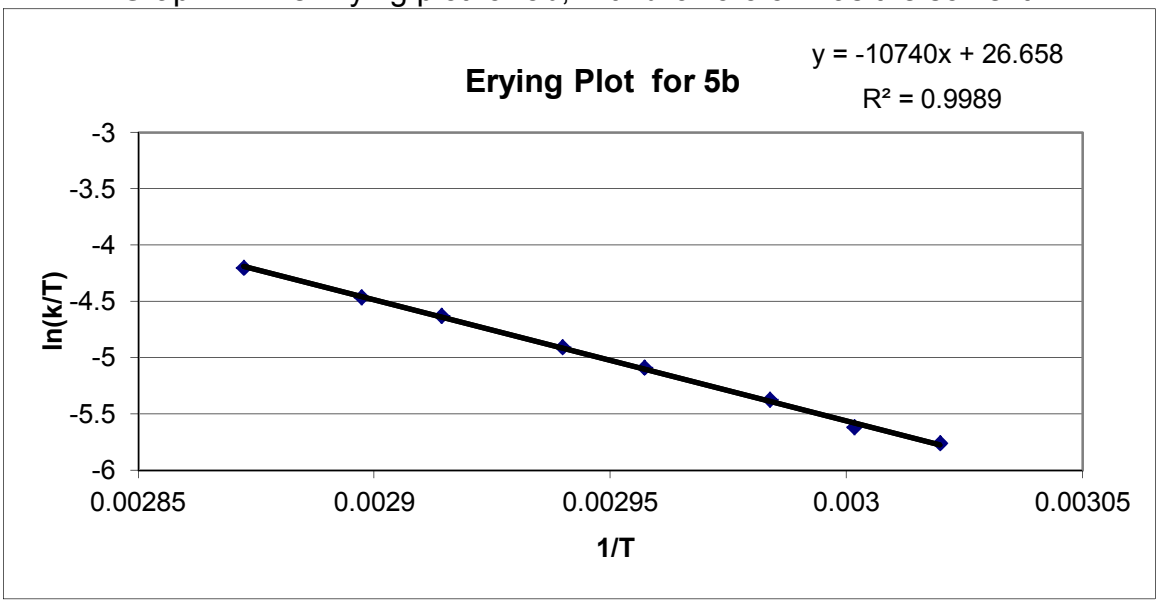

Graph 3. The Arrhenius plot for Crabtree's iridium NHC complex[88], with *d*-DMF as the solvent.

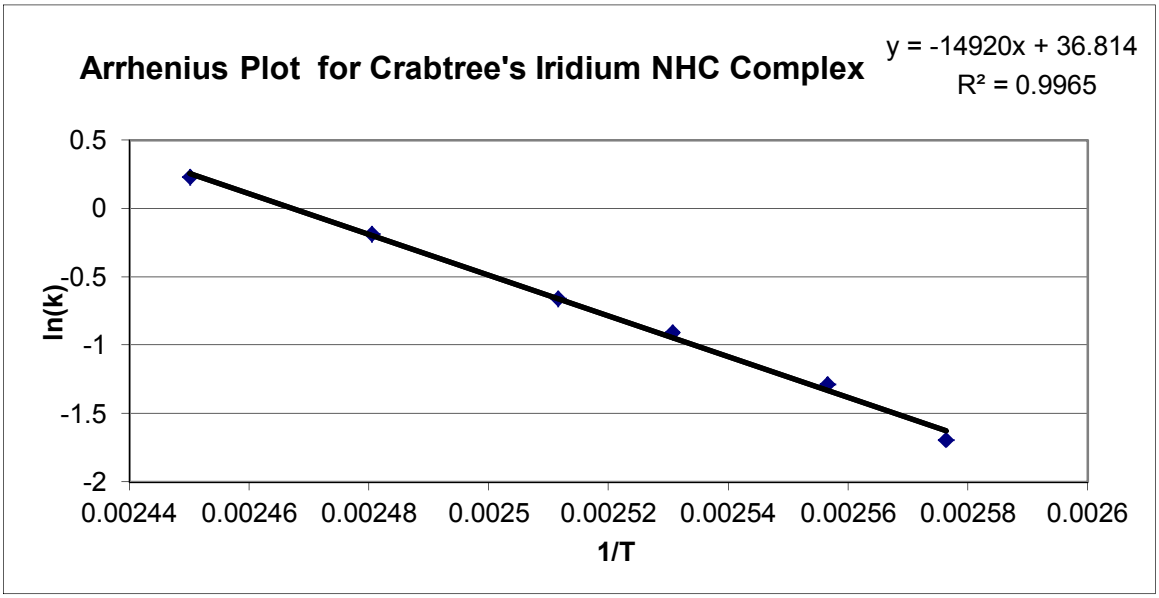

Graph 4. The Erying plot for Crabtree's iridium NHC complex, with *d*-DMF as the solvent.

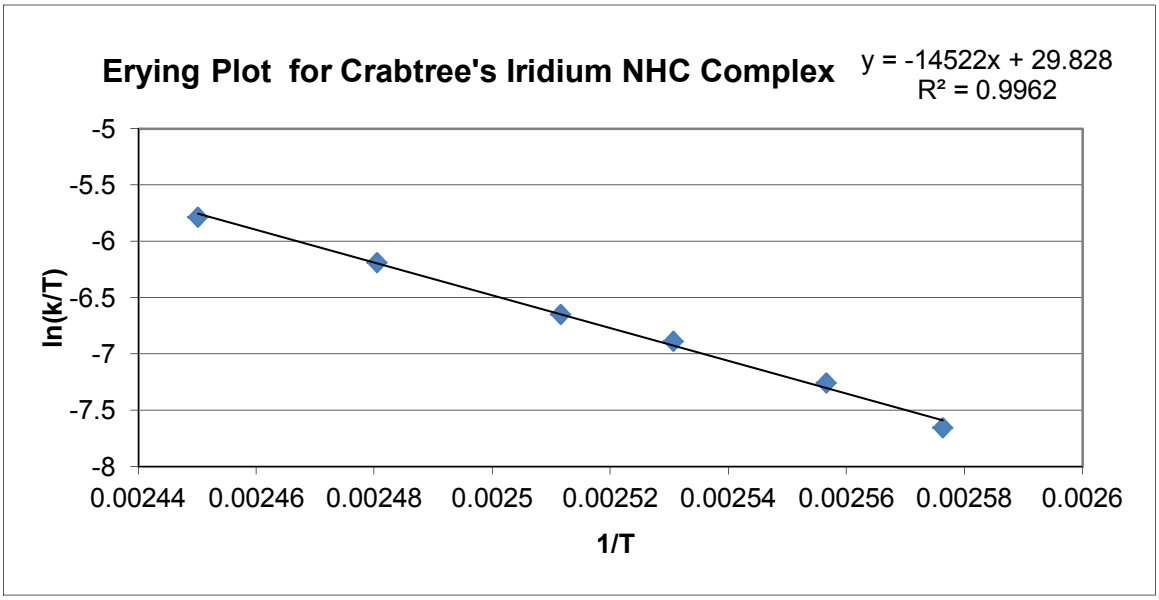

Under Standing General Orbital Shape Properties

The goal of today's lesson is to understand how electron orbitals may look based on where we are most likely to find the electrons around an atom. It is not precisely correct to refer to atomic orbitals as having a specific "shape." The regions of highest electron density appear to describe areas in space, and it is useful for us to remember those shapes when thinking about atomic properties and chemical bonding.

---

1. The way that we will be viewing these different regions of electron density will be to make a map of an atom on paper #1. Under this piece of paper you will place a piece of carbon paper. The nucleus will be drawn at the center and you will find the electron density around the atom by dropping a marble on to the paper from 1 meter above the paper. Drop a marble from 1 meter high, **30 times.**

Draw what this shape looks like:

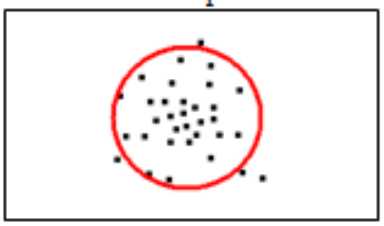

Would you say that is pattern is Sharp?

---

2. On paper number 2, fold once in the center, and then once on either side of the center, so that there is a one inch ridge down the center of the paper. Use a paper clip to hold the ridge together; at the circle in the center of the paper. Then place the carbon paper under this piece of paper. Again, drop a marble from 1 meter high, **30 times**.

Draw what this shape looks like:

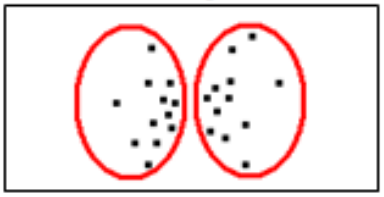

Scientists called this a Principal shape

---

3 and 4. On paper number 3, fold the paper so that it has two ridges, one going from top to bottom and the other running side to side through the center. Now cut the center of the paper along the shape of an "**I**", so that the ridges can overlap at the same time. Then place the carbon paper and paper clip on the paper just as before. Again, drop a marble from 1 meter high, **50 times**.

Draw what this shape looks like:

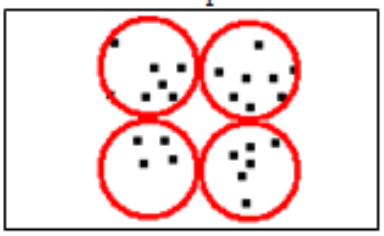

Would you call that a Diffuse pattern?

If you could then fold the paper so that it had three ridges all intersecting in the center it might give what would be called a Fundamental pattern. What might that look like

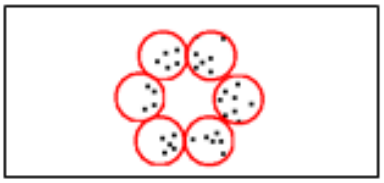

Figure 67. The answer key for the student handout for the mapping of electron density experient, discussed in chapter 4.

Questions

4. Define what an electron cloud is.

The region of negative charge surrounding an atomic nucleus that is associated with an atomic orbital.

5. Define what a node is.

An area where there is zero electron density around the nucleus.

6. How was density important in today's lab?

An electron orbit can be located by studying the electron density of an atom, which is related to the probability of finding an electron around a nucleus of an atom.

Draw the following electron orbitals:

S orbital **Px orbital** **Py orbital** **Pz orbital**

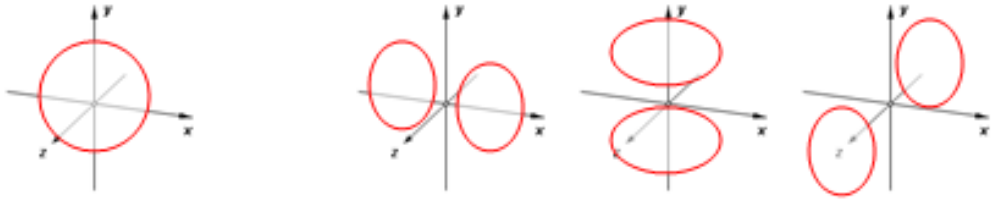

Dxy orbital **Dyz orbital** **Dxz orbital** **Dx^2-y^2 orbital** **Dz^2 orbital**

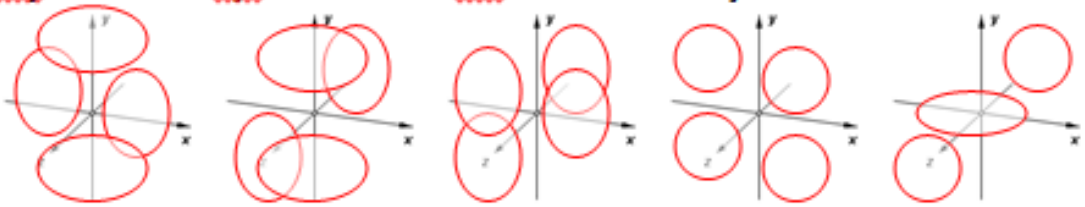

Write the electron configuration for each atom:

C: $1s^2 2s^2 2p^2$ **Al:** $1s^2 2s^2 2p^6 3s^2 3p^1$ **Ca:** $1s^2 2s^2 2p^6 3s^2 3p^6 4s^2$

Fill in all of the orbitals for the following atoms:

Carbon **Aluminum** **Calcium**

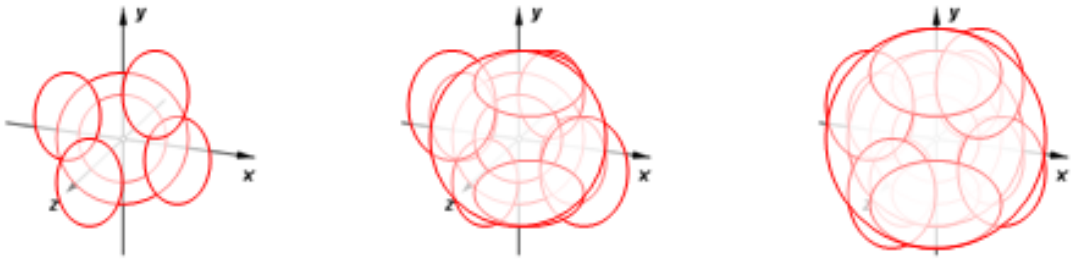

Figure 67. Continued

3.) Front

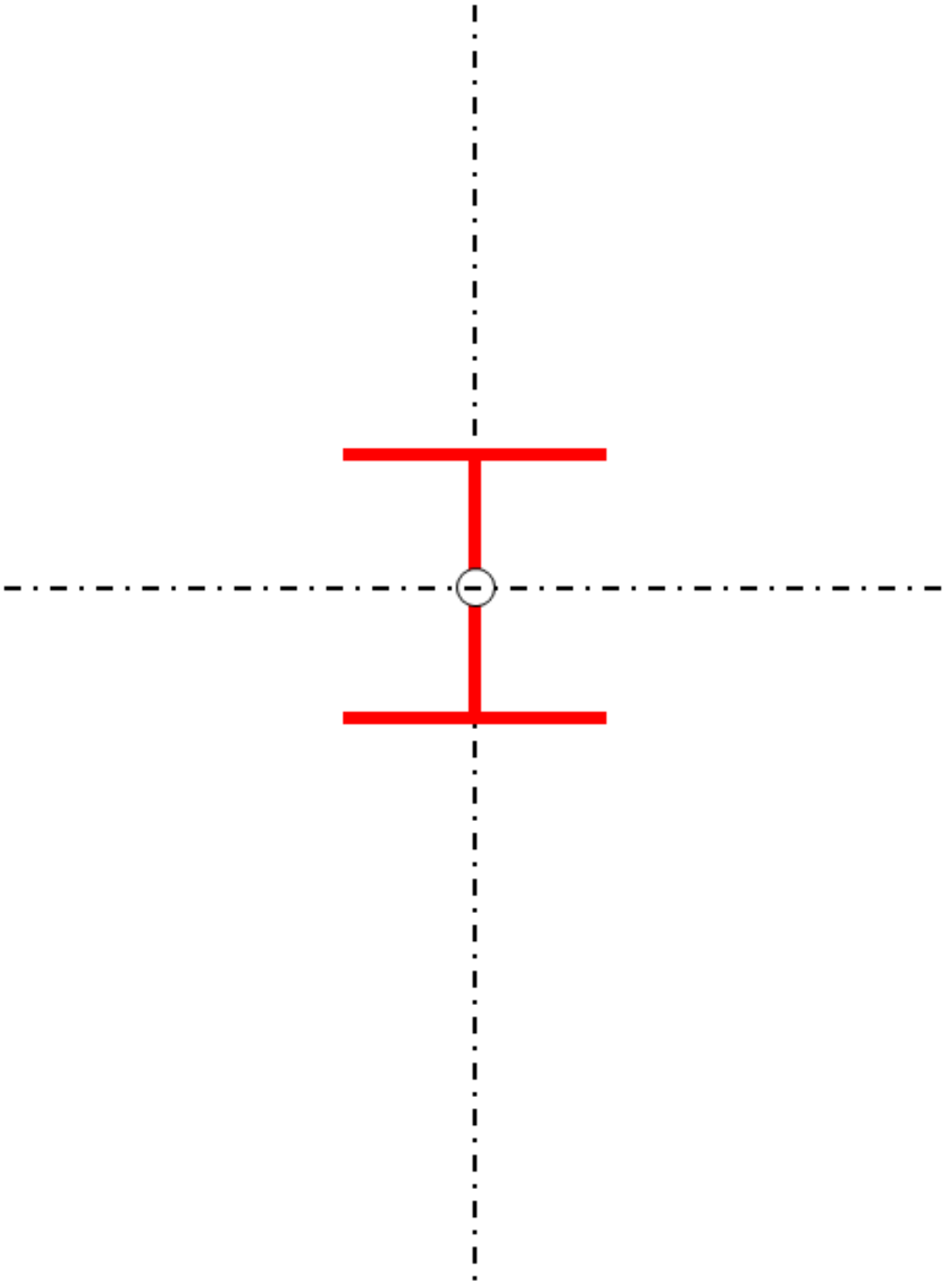

Figure 68. The template used for mapping the electron orbitals s, p, and d. The pages are intended to be printed back-to-back and are labeled accordingly.

3.) Back

Figure 68. Continued

2.) Front

Figure 68. Continued

2.) Back

Figure 68. Continued

1.) Front

Figure 68. Continued

References

1. Busacca, C. A.; Fandrick, D. R.; Song, J. J.; Senanayake, C. H., *Adv. Synth. Catal.* **2011,** *353* (11-12), 1825–1864.

2. Anon, *R&D Magazine* **September 2005**, 20.

3. Khodakov, A. Y.; Chu, W.; Fongarland, P., *Chem. Rev.* **2007,** *107* (5), 1692-1744.

4. Corradini, P.; Guerra, G.; Cavallo, L., *Acc. Chem. Res.* **2004,** *37* (4), 231-241.

5. Trnka, T. M.; Grubbs, R. H., *Acc. Chem. Res.* **2001,** *34* (1), 18-29.

6. Nobel Prize Home Page: http://nobelprize.org/nobel_prizes/chemistry/laureates

7. Martin, R.; Buchwald, S. L., *Acc. Chem. Res.* **2008,** *41* (11), 1461-1473.

8. Hayashi, T.; Kanehira, K.; Tsuchiya, H.; Kumada, M., *J. Chem. Soc., Chem. Commun.* **1982,** (20), 1162-1164.

9. Noyori, R.; Yamakawa, M.; Hashiguchi, S., *J. Org. Chem.* **2001,** *66* (24), 7931–7944.

10. Noyori, R.; Ohkuma, T., *Angew. Chem., Int. Ed.* **2001,** *40* (1), 40-73.

11. Grotjahn, D., *Chem. Eur. J.* **2005,** *11*, 7147-7153.

12. Grotjahn, D. B.; Gong, Y.; Zakharov, L.; Golen, J. A.; Rheingold, A. L., *J. Am. Chem. Soc.* **2006,** *128*, 438−453.

13. Grotjahn, D. B.; Gong, Y.; DiPasquale, A. G.; Zakharov, L. N.; Rheingold, A. L., *Organometallics* **2006,** *25* (24), 5693-5695.

14. Grotjahn, D. B.; Zeng, X.; Cooksy, A. L.; Kassel, W. S.; DiPasquale, A. G.; Zakharov, L. N.; Rheingold, A. L., *Organometallics* **2007,** *26* (14), 3385-3402.

15. Miranda-Soto, V. n.; Grotjahn, D. B.; DiPasquale, A. G.; Rheingold, A. L., *J. Am. Chem. Soc.* **2008,** *130* (40), 13200-13201.

16. Grotjahn, D. B.; Lev, D. A., *J. Am. Chem. Soc.* **2004,** *126* (39), 12232–12233.

17. Grotjahn, D. B.; Larsen, C. R.; Gustafson, J. L.; Nair, R.; Sharma, A., *J. Am. Chem. Soc.* **2007,** *129* (31), 9592-9593.

18. Arduengo, A. J., III; Harlow, R. L.; Kline, M., *J. Am. Chem. Soc.* **1991,** *113*, 361-363.

19. Arduengo, A. J., III; Dias, H. V. R.; Harlow, R. L.; Kline, M., *J. Am. Chem. Soc.* **1992,** *114*, 5530-5534.

20. Kirmse, W., *Angew. Chem., Int. Ed.* **2004,** *43* (14), 1767-1769.

21. Lavallo, V.; Mafhouz, J.; Canac, Y.; Donnadieu, B.; Schoeller, W. W.; Bertrand, G., *J. Am. Chem. Soc.* **2004,** *126*, 8670-8671.

22. Canac, Y.; Soleilhavoup, M.; Conejero, S.; Bertrand, G., *J. Organomet. Chem.* **2004,** *689* (24), 3857-3865.

23. Bourissou, D.; Guerret, O.; Gabbaie, F. P.; Bertrand, G., *Chem. Rev.* **2000,** *100* (1), 39-91.

24. Enders, D.; Balensiefer, T., *Acc. Chem. Res.* **2004,** *37* (8), 534-541.

25. Johnson, J. S., *Angew. Chem., Int. Ed.* **2004,** *43* (11), 1326-1328.

26. Sohn, S. S.; Rosen, E. L.; Bode, J. W., *J. Am. Chem. Soc.* **2004,** *126*, 14370-14371.

27. Nair, V.; Bindu, S.; Sreekumar, V., *Angew. Chem., Int. Ed.* **2004,** *43* (39), 5130-5135.

28. Hahn, F. E.; Jahnke, M. C., *Angew. Chem. Int. Ed.* **2008,** *47* (17), 3122-3172.

29. Nolan, S. P.; Diez-Gonzalez, S., *Coord. Chem. Rev.* **2007,** *251*, 874-883.

30. Hahn, F. E., *Angew. Chem., Int. Ed.* **2006,** *45* (9), 1348-1352.

31. Crabtree, R. H., *J. Organomet. Chem.* **2005,** *690* (24-25), 5451-5457.

32. Scott, N. M.; Nolan, S. P., *Eur. J. Inorg. Chem.* **2005,** (10), 1815-1828.

33. Herrmann, W. A., *Angew. Chem., Int. Ed. Engl.* **2002,** *41* (8), 1290-1309.

34. Weskamp, T.; Bohm, V. P. W.; Herrmann, W. A., *J. Organomet. Chem.* **2000,** *600* (1-2), 12-22.

35. Diez-Gonzalez, S.; Nolan, S. P., *Coord. Chem. Rev.* **2007,** *251*, 874-883.

36. Vougioukalakis, G. C.; Grubbs, R. H., *Organometallics* **2007,** *26* (9), 2469-2472.

37. Hong, S. H.; Grubbs, R. H., *J. Am. Chem. Soc.* **2006,** *128* (11), 3508-3509.

38. Castarlenas, R.; Esteruelas, M. A.; Onate, E., *Organometallics* **2005,** *24* (18), 4343-4346.

39. Ung, T.; Hejl, A.; Grubbs, R. H.; Schrodi, Y., *Organometallics* **2004,** *23* (23), 5399-5401.

40. Jafarpour, L.; Hillier, A. C.; Nolan, S. P., *Organometallics* **2002,** *21* (2), 442-444.

41. Sanford, M. S.; Love, J. A.; Grubbs, R. H., *Organometallics* **2001,** *20* (25), 5314-5318.

42. Scholl, M.; Ding, S.; Lee, C. W.; Grubbs, R. H., *Org. Lett.* **1999,** *1* (6), 953-956.

43. Weskamp, T.; Kohl, F. J.; Hieringer, W.; Gleich, D.; Herrmann, W. A., *Angew. Chem., Int. Ed.* **1998,** *38* (16), 2416-2419.

44. Weskamp, T.; Schattenmann, W. C.; Spiegler, M.; Herrmann, W. A., *Angew. Chem., Int. Ed.* **1998,** *37* (18), 2490-2493.

45. Corberán, R.; Peris, E., *Organometallics* **2008,** *27* (8), 1954-1958.

46. Voutchkova, A. M.; Gnanamgari, D.; Jakobsche, C. E.; Butler, C.; Miller, S. J.; Parr, J.; Crabtree, R. H., *Organometallics* **2008,** *693* (10), 1815-1821.

47. Poyatos, M.; McNamara, W.; Incarvito, C.; Peris, E.; Crabtree, R. H., *Chem. Commun. (Cambridge, U. K.)* **2007,** (22), 2267-2269.

48. Gnanamgari, D.; Moores, A.; Rajaseelan, E.; Crabtree, R. H., *Organometallics* **2007,** *26* (5), 1226-1230.

49. Herrmann, W. A.; Kohlpaintner, C. W., *Angew. Chem. Int. Ed.* **1993,** *32*, 1524-1544.

50. Herrmann, W. A.; Kulpe, J. A.; Konkol, W.; Bahrmann, H., *J. Organomet. Chem.* **1990,** *389*, 85-101.

51. Jimenez, M. V.; Perez-Torrente, J. J.; Bartolome, M. I.; Gierz, V.; Lahoz, F. J.; Oro, L. A., *Organometallics* **2008,** *27* (2), 224-234.

52. Poyatos, M.; Maisse-Francois, A.; Bellemin-Laponnaz, S.; Gade, L. H., *Organometallics* **2006,** *25* (10), 2634-2641.

53. Liu, Z.; Zhang, T.; Shi, M., *Organometallics* **2008,** *27* (11), 2668-2671.

54. Xi, Z.; Liu, B.; Chen, W., *J. Org. Chem.* **2008,** *73* (10), 3954-3957.

55. Dragutan, V.; Dragutan, I.; Delaude, L.; Demonceau, A., *Coord. Chem. Rev.* **2007,** *251* (5+6), 765-794.

56. Nonnenmacher, M.; Kunz, D.; Rominger, F.; Oeser, T., *J. Organomet. Chem.* **2007,** *692* (12), 2554-2563.

57. Matsubara, K.; Ueno, K.; Koga, Y.; Hara, K., *J. Org. Chem.* **2007,** *72* (14), 5069-5076.

58. Hahn, F. E.; Jahnke, M. C.; Pape, T., *Organometallics* **2007,** *26* (1), 150-154.

59. Taige, M. A.; Zeller, A.; Ahrens, S.; Goutal, S.; Herdtweck, E.; Strassner, T., *J. Organomet. Chem.* **2007,** *692* (7), 1519-1529.

60. Wang, R.; Twamley, B.; Shreeve, J. n. M., *J. Org. Chem.* **2006,** *71* (1), 426-429.

61. Navarro, O.; Marion, N.; Oonishi, Y.; Kelly, R. A., III; Nolan, S. P., *J. Org. Chem.* **2006,** *71* (2), 685-692.

62. Ackermann, L.; Althammer, A., *Synlett* **2006,** (18), 3125-3129.

63. Huynh, H. V.; Neo, T. C.; Tan, G. K., *Organometallics* **2006,** *25* (5), 1298-1302.

64. Scherg, T.; Schneider, S. K.; Frey, G. D.; Schwarz, J.; Herdtweck, E.; Herrmann, W. A., *Synlett* **2006,** (18), 2894-2907.

65. Kremzow, D.; Seidel, G.; Lehmann, C. W.; Fuerstner, A., *Chem. Eur. J.* **2005,** *11* (6), 1833-1853.

66. Lee, H. M.; Lu, C. Y.; Chen, C. Y.; Chen, W. L.; Lin, H. C.; Chiu, P. L.; Cheng, P. Y., *Tetrahedron* **2004,** *60*, 5807-5825.

67. Loch, J. A.; Albrecht, M.; Peris, E.; Mata, J.; Faller, J. W.; Crabtree, R. H., *Organometallics* **2002,** *21* (4), 700-706.

68. Viciu, M. S.; Germaneau, R. F.; Nolan, S. P., *Org. Lett.* **2002,** *4* (23), 4053-4056.

69. Herrmann, W. A.; Elison, M.; Fischer, J.; Koecher, C.; Artus, G. R. J., *Angew. Chem., Int. Ed.* **1995,** *34* (21), 2371-2374.

70. Gardiner, M. G.; Herrmann, W. A.; Reisinger, C.-P.; Schwarz, J.; Spiegler, M., *J. Organomet. Chem.* **1999,** *572*, 239-247.

71. Danopoulos, A. A.; Tsoureas, N.; Macgregor, S. A.; Smith, C., *Organometallics* **2007,** *26*, 253 - 263.

72. Kantchev, E. A. B.; O'Brien, C. J.; Organ, M. G., *Angew. Chem., Int. Ed.* **2007,** *46* (16), 2768-2813.

73. Pugh, D.; Wright, J. A.; Freeman, S.; Danopoulos, A. A., *Dalton Trans.* **2006,** (6), 775-782.

74. Mas-Marza, E.; Sanau, M.; Peris, E., *J. Organomet. Chem.* **2005,** *690* (24-25), 5576-5580.

75. Mas-Marza, E.; Sanau, M.; Peris, E., *Inorg. Chem.* **2005,** *44* (26), 9961-9967.

76. Stylianides, N.; Danopoulos, A. A.; Tsoureas, N., *J. Organomet. Chem.* **2005,** *690* (24-25), 5948-5958.

77. Chiu, P. L.; Lai, C.-L.; Chang, C.-F.; Hu, C.-H.; Lee, H. M., *Organometallics* **2005,** *24* (25), 6169-6178.

78. Winston, S.; Stylianides, N.; Tulloch, A. A. D.; Wright, J. A.; Danopoulos, A. A., *Polyhedron* **2004,** *23* (17), 2813-2820.

79. Danopoulos, A. A.; Tsoureas, N.; Wright, J. A.; Light, M. E., *Organometallics* **2004,** *23* (12), 166-168.

80. Danopoulos, A. A.; Wright, J. A.; Motherwell, W. B.; Ellwood, S., *Organometallics* **2004,** *23* (21), 4807-4810.

81. Catalano, V. J.; Malwitz, M. A.; Etogo, A. O., *Inorg. Chem.* **2004,** *43* (18), 5714-5724.

82. Tulloch, A. A. D.; Winston, S.; Danopoulos, A. A.; Eastham, G.; Hursthouse, M. B., *Dalton Trans.* **2003,** (4), 699-708.

83. Tulloch, A. A. D.; Danopoulos, A. A.; Tizzard, G. J.; Coles, S. J.; Hursthouse, M. B.; Hay-Motherwell, R. S.; Motherwell, W. B., *Chem. Commun. (Cambridge, U.K.)* **2001**, 1270-1271.

84. Lee, K.-M.; Chen, J. C. C.; Lin, I. J. B., *J. Organomet. Chem.* **2001,** *617-618*, 364-375.

85. Chen, J. C. C.; Lin, I. J. B., *Dalton Trans.* **2000**, 839-840.

86. Tulloch, A. A. D.; Danopoulos, A. A.; Cafferkey, S. M.; Kleinhenz, S.; Hursthouse, M. B.; Tooze, R. P., *Chem. Commun. (Cambridge, U.K.)* **2000**, 1247-1248.

87. Meyer, D.; Taige, M. A.; Zeller, A.; Hohlfeld, K.; Ahrens, S.; Strassner, T., *Organometallics* **2009,** *28* (7), 2142-2149.

88. Gnanamgari, D.; Sauer, E. L. O.; Schley, N. D.; Butler, C.; Incarvito, C. D.; Crabtree, R. H., *Organometallics* **2009,** *28* (1), 321-325.

89. Chen, C.; Qiu, H.; Chen, W.; Wang, D., *J. Organomet. Chem.* **2008,** *693* (20), 3273-3280.

90. Zhou, Y.; Chen, W., *Organometallics* **2007,** *26* (10), 2742-2746.

91. Wang, R.; Zeng, Z.; Twamley, B.; Piekarski, M. M.; Shreeve, J. n. M., *Eur. J. Org. Chem.* **2007,** (4), 655-661.

92. Zeng, F.; Yu, Z., *J. Org. Chem.* **2006,** *71* (14), 5274-5281.

93. Chiu, P. L.; Chen, C. Y.; Lee, C.-C.; Hsieh, M.-H.; Chuang, C.-H.; Lee, H. M., *Inorg. Chem.* **2006,** *45* (6), 2520-2530.

94. Scheele, U. J.; Dechert, S.; Meyer, F., *Chem. Eur. J.* **2008,** *14* (17), 5112-5115.

95. Herrmann, W. A.; Gooben, J.; Spiegler, M., *J. Organomet. Chem.* **1997,** *547*, 357-366.

96. Gade, L. H.; Bellemin-Laponnaz, S., *Coord. Chem. Rev.* **2007,** *251* (5+6), 718-725.

97. Schneider, N.; Cesar, V.; Bellemin-Laponnaz, S.; Gade, L. H., *Organometallics* **2005,** *24* (21), 4886-4888.

98. Cesar, V.; Bellemin-Laponnaz, S.; Gade, L. H., *Organometallics* **2002,** *21* (24), 5204-5208.

99. Houghton, J.; Dyson, G.; Douthwaite, R. E.; Whitwood, A. C.; Kariuki, B. M., *Dalton Trans.* **2007,** (28), 3065-3073.

100. Flahaut, A.; Baltaze, J.-P.; Roland, S.; Mangeney, P., *J. Organomet. Chem.* **2006,** *691* (16), 3498-3508.

101. Alcarazo, M.; Roseblade, S. J.; Alonso, E.; Fernandez, R.; Alvarez, E.; Lahoz, F. J.; Lassaletta, J. M., *J. Am. Chem. Soc.* **2004,** *126* (41), 13242-13243.

102. Dastgir, S.; Coleman, K. S.; Cowley, A. R.; Green, M. L. H., *Organometallics* **2006,** *25* (1), 300-306.

103. Bonnet, L. G.; Douthwaite, R. E.; Kariuki, B. M., *Organometallics* **2003,** *22* (21), 4187-4189.

104. Coleman, K. S.; Chamberlayne, H. T.; Turberville, S.; Green, M. L. H.; Cowley, A. R., *Dalton Trans.* **2003,** (14), 2917-2922.

105. Liao, C.-Y.; Chan, K.-T.; Zeng, J.-Y.; Hu, C.-H.; Tu, C.-Y.; Lee, H. M., *Organometallics* **2007,** *26* (7), 1692-1702.

106. Arnold, P. L.; Liddle, S. T., *Chem. Commun. (Cambridge, U.K.)* **2006**, 3959-3971.

107. Spencer, L. P.; Winston, S.; Fryzuk, M. D., *Organometallics* **2004,** *23* (14), 3372-3374.

108. Roseblade, S. J.; Ros, A.; Monge, D.; Alcarazo, M.; Alvarez, E.; Lassaletta, J. M.; Fernandez, R., *Organometallics* **2007,** *26* (10), 2570-2578.

109. Huynh, H. V.; Yeo, C. H.; Tan, G. K., *Chem. Commun. (Cambridge, U.K.)* **2006**, 3833-3835.

110. Cabeza, J. A.; Del Rio, I.; Sanchez-Vega, M. G.; Suarez, M., *Organometallics* **2006,** *25* (7), 1831-1834.

111. Ros, A.; Monge, D.; Alcarazo, M.; Alvarez, E.; Lassaletta, J. M.; Fernandez, R., *Organometallics* **2006,** *25* (26), 6039-6046.

112. Seo, H.; Park, H.-j.; Kim, B. Y.; Lee, J. H.; Son, S. U.; Chung, Y. K., *Organometallics* **2003,** *22* (4), 618-620.

113. Espinet, P.; Soulantica, K., *Coord. Chem. Rev.* **1999,** *193-195*, 499-556.

114. Chikkali, S.; Gudat, D.; Niemeyer, M., *Chem. Commun. (Cambridge, U.K.)* **2007**, 981-983.

115. Chen, G.; Lam, W. H.; Fok, W. S.; Lee, H. W.; Kwong, F. Y., *Chem. Asian J.* **2007,** *2* (2), 306-313.

116. Moxham, G. L.; Randell-Sly, H. E.; Brayshaw, S. K.; Woodward, R. L.; Weller, A. S.; Willis, M. C., *Angew. Chem., Int. Ed.* **2006,** *45* (45), 7618-7622.

117. Grotjahn, D. B.; Gong, Y.; Zakharov, L. N.; Golen, J. A.; Rheingold, A. L., *J. Am. Chem. Soc.* **2006,** *128*, 438-453.

118. Christmann, U.; Vilar, R., *Angew. Chem. Int. Ed.* **2005,** *44*, 366 -374.

119. Yu, H.-Z.; Jiang, Y.-Y.; Fu, Y.; Liu, L., *J. Am. Chem. Soc.* **2010,** *132* (51), 18078-18091.

120. *N-Heterocyclic Carbenes in Transition Metal Catalysis and Organocatalysis*. 1st Edition ed.; Springer: 2010; Vol. 32.

121. Hintermann, L.; Dang, T.; Labonne, A.; Kribber, T.; Xiao, L.; Naumov, P., *Chem. Eur. J.* **2009,** *15*, 7167-7179.

122. Grotjahn, D. B., *Dalton Trans.* **2008**, 6497-6508.

123. Tran, H. N.; Cortes-Llamas, S. A.; Rancudo, K. T.; Moore, C.; Rheingold, A. L.; Grotjahn, D. B. In *Bifunctional imidazolyl-substituted N-heterocyclic carbene complexes of iridium, ruthenium, and copper*, Abstracts of Papers, 239th ACS National Meeting, San Francisco, CA, United States, March 21-25, 2010, 2010; pp ORGN-1013

124. Smith, D. L.; Elving, P. J., *J. Am. Chem. Soc.* **1962,** *84* (14), 2741–2747.

125. Krygowski, T. M.; Szatyłowicz, H.; Zachara, J. E., *J. Org. Chem.* **2005,** *70* (22), 8859–8865.

126. Martin, R. B., *Science* **1963,** *139*, 1198-1203.

127. Specht, Z.; Lev, D. A.; Grotjahn, D. B.; Rheingold, A. L.; DiPasquale, A. G., Synthesis, characterization, and catalytic properties of bifunctional N-heterocyclic carbene complexes In *236th ACS National Meeting* Philadelphia, PA, United States, August 17-21, 2008, 2008; pp INOR-093.

128. Specht, Z.; Lev, D. A.; Grotjahn, D. B.; Rheingold, A. L.; DiPasquale, A. G., Synthesis and Characterization of Bifunctional N-Heterocyclic Carbene Complexes In *41st Western Regional Meeting of the American Chemical Society*, San Diego, CA, United States, October 9-13 2007 2007; pp GEN-089.

129. Specht, Z. G.; Cortes-Llamas, S. A.; Tran, H. N.; Niekerk, C. J. v.; Rancudo, K. T.; Golen, J. A.; Moore, C. E.; Rheingold, A. L.; Dwyer, T. J.; Grotjahn, D. B., *Chemistry--A European Journal* **2011,** *17* (24), 6606-6609.

130. Schomaker, J. M.; Delia, T. J., *J. Org. Chem.* **2001,** *66* (21), 7125-7128.

131. Hintermann, L.; Xiao, L.; Labonne, A., *Angew. Chem. Int. Ed.* **2008,** *47* (43), 8246-8250.

132. Frémont, P. d.; Scott, N. M.; Stevens, E. D.; Ramnial, T.; Lightbody, O. C.; Macdonald, C. L. B.; Clyburne, J. A. C.; Abernethy, C. D.; Nolan, S. P., *Organometallics* **2005,** *24* (26), 6301–6309.

133. Chianese, A. R.; Li, X.; Janzen, M. C.; Faller, J. W.; Crabtree, R. H., *Organometallics* **2003,** *22* (8), 1663-1667.

134. Sikorski, W. H.; Sanders, A. W.; Reich, H. J., *J. Magn. Res.* **1998,** *36*, S118-S124.

135. Perrin, C. L.; Dwyer, T. J., *Chem. Rev.* **1990,** *90*, 935-967.

136. Brown, K. C.; Tyson, R. L.; Weil, J. A., *J. Chem. Ed.* **1998,** *75* (12), 1632-1635.

137. Grotjahn, D. B., *Pure Appl. Chem.* **2010,** *82* (3), 635-647.

138. Bdour, H. M.; Kao, J. L.-F.; Taylor, J.-S., *J. Org. Chem.* **2006,** *71* (4), 1640-1646.

139. Fristrup, P.; Tursky, M.; Madsen, R., *Org. Biomol. Chem.* **2012,** *10*, 2569-2577.

140. Ken-ichi Fujita; Yamaguchi, R., *Synlett* **2005,** *2005* (4), 0560-0571.

141. Owston, N. A.; Parker, A. J.; Williams, J. M. J., *Org. Lett.* **2007,** *9* (1), 73-75.

142. Whitney, S.; Grigg, R.; Derrick, A.; Keep, A., *Org. Lett.* **2007,** *9* (17), 3299-3302.

143. Corbera, R.; Sanau, M.; Peris, E., *J. Am. Chem. Soc.* **2006,** *128* (12), 3974-3979.

144. Yung, C. M.; Skaddan, M. B.; Bergman, R. G., *J. Am. Chem. Soc.* **2004,** *126* (40), 13033-13043.

145. Hanasaka, F.; Fujita, K.; Yamaguchi, R., *Organometallics* **2005,** *24*, 3422-3433.

146. Fujita, K.-i.; Asai, C.; Yamaguchi, T.; Hanasaka, F.; Yamaguchi, R., *Org. Lett.* **2005,** *7* (18), 4017-4019.

147. Chang, X.; Chuan, L. W.; Yongxin, L.; Pullarkat, S. A., *Tetrahedron Lett.* **2012,** *53* (12), 1450-1455.

148. Julian, L. D.; Hartwig, J. F., *J. Am. Chem. Soc.* **2010,** *132*, 13813-13822.

149. Hesp, K. D.; Tobisch, S.; Stradiotto, M., *J. Am. Chem. Soc.* **2010,** *132*, 413-426.

150. Kashiwame, Y.; Kuwata, S.; Ikariya, T., *Chem. Eur. J.* **2010,** *16*, 766-770.

151. Michon, C.; Medina, F.; Capet, F.; Roussel, P.; Agbossou-Niedercorn, F., *Adv. Synth. Catal.* **2010,** *352*, 3293-3305.

152. Shen, X.; Buchwald, S. L., *Angew. Chem. Int. Ed.* **2010,** *49*, 564-567.

153. Ohmiya, H.; Moriya, T.; Sawamura, M., *Org. Lett.* **2009,** *11*, 2145-2147.

154. Bauer, E. B.; Andavan, G. T. S.; Hollis, T. K.; Rubio, R. J.; Cho, J.; Kuchenbeiser, G. R.; Helgert, T. R.; Letko, C. S.; Tham, F. S., *Org. Lett.* **2008,** *10*, 1175-1178.

155. Cochran, B. M.; Michael, F. E., *J. Am. Chem. Soc.* **2008,** *130*, 2786-2792.

156. Liu, Z.; Hartwig, J. F., *J. Am. Chem. Soc.* **2008,** *130*, 1570-1571.

157. Kovacs, G.; Ujaque, G.; Lledos, A., *J. Am. Chem. Soc.* **2008,** *130*, 853-864.

158. Munro-Leighton, C.; Delp, S. A.; Blue, E. D.; Gunnoe, T. B., *Organometallics* **2007,** *26*, 1483-1493.

159. Ryu, J.; Li, G. Y.; Marks, T. J., *J. Am. Chem. Soc.* **2003,** *125*, 12584-12605.

160. Chemler, S. R., *Org. Biomol. Chem.* **2009,** *7*, 3009-3019.

161. Mueller, T. E.; Hultzsch, K. C.; Yus, M.; Foubelo, F.; Tada, M., *Chem. Rev.* **208,** *108*, 3795-3892.

162. Liu, C.; Bender, C. F.; Han, X.; Widenhoefer, R. A., *Chem. Commun. (Cambridge)* **2007**, 3607-3618.

163. Widenhoefer, R. A.; Han, X., *Eur. J. Org. Chem.* **2006**, 4555-4563.

164. Reznichenko, A. L.; Nguyen, H. N.; Hultzsch, K. C., *Angew. Chem. Int. Ed.* **2010,** *49*, 8984-8987.

165. Xiao, X.-Q.; Jin, G.-X., *J. Organomet. Chem.* **2008,** *693* (21-22), 3363-3368.

166. Grotjahn, D. B.; Sang Van, D. C.; Lev, D. A.; Schneider, C.; Rideout, M.; Meyer, C.; Hernandez, G.; Mejorado, L., *J. Org. Chem.* **2002,** *67*, 9200-9209.

167. Miller, M. J.; Lyttle, M. H.; Streitwieser, J. A., *J. Org. Chem.* **1981,** *46* (10), 1977-1984.

168. Singh, R., *Org. Process Res. Dev.* **2011,** *15*, 175-179.

169. Jimenez-Gonzalez, C.; Poechlauer, P.; Broxterman, Q. B.; Yang, B.-S.; Ende, D. a.; Baird, J.; Bertsch, C.; Hannah, R. E.; Dell'Orco, P.; Noorman, H.; Yee, S.; Reintjens, R.; Wells, A.; Massonneau, V.; Manley, J., *Org. Process Res. Dev.* **2011,** *15* (4), 900-911.

170. Meyer, H., *Org. Process Res. Dev.* **2011,** *15*, 180-188.

171. Dam, J. t.; Hanefeld, U., *ChemSusChem* **2011,** *4*, 1017-1034.

172. Corma, A.; Iborra, S.; Velty, A., *Chem. Rev.* **2007,** *107*, 2411-2502.

173. Thibault, M. E.; DiMondo, D. V.; Jennings, M.; Abdelnur, P. V.; Eberlinc, M. N.; Schlaf, M., *Green Chem.* **2011,** *13*, 357-366.

174. Knifton, J. F.; James, T. G.; Allen, K. D.; Weider, P. R.; Powell, J. B.; Slaugh, L. H.; Williams, T. One-step production of 1,3-propanediol from ethylene oxide and syngas with a catalyst with a N-heterocyclic ligand. US Pat. 6,903,044, 2005.

175. Haas, T.; Jaeger, B.; Weber, R.; Mitchell, S. F.; King, C. F., *Appl. Catal., A* **2005,** *280*, 83-88.

176. Cervin, M. A.; Soucaille, P.; Valle, F. Process for the biological production of 1,3-propanediol with high yield. US 416192 P 2002.

177. Chaminand, J.; Djakovitch, L.; Gallezot, P.; Marion, P.; Pinel, C.; Rosier, C., *Green Chem.* **2004,** *6*, 359-361.

178. Mane, R. B.; Rode, C. V., *Org. Process Res. Dev.* **2012,** *Article ASAP*.

179. Ueda, N.; Nakagawa, Y.; Tomishige, K., *Chem. Lett.* **2010,** *39*, 506-507.

180. Alhanash, A.; Kozhevnikova, E. F.; Kozhevnikov, I. V., *Catalysis Letters* **2008,** *120*, 307-311.

181. Schlaf, M.; Ghosh, P.; Fagan, P. J.; Hauptman, E.; Bullocka, R. M., *Adv. Synth. Catal.* **2009,** *351*, 789-800.

182. Taher, D.; Thibault, M. E.; Mondo, D. D.; Jennings, M.; Schlaf, M., *Chem. Eur. J.* **2009,** *15*, 10132-1143.

183. Arnold, L. P.; Pearson, S., *Coor. Chem. Rev.* **2007,** *251*, 596-609.

184. Deffeyes, K., *Hubbert's Peak: The Impending World Oil Shortage*. Princeton University Press: Princeton, New Jersey, 2009; p 224

185. Obama, B. H. Transcript of Remarks by Obama on Energy Security *The Washington Post.* [Online], March 31 2010. http://projects.washingtonpost.com/obama-speeches/speech/210/.

186. Pahl, G., *Biodiesel: Growing a New Energy Economy*. Second Edition ed.; Chelsea Green Publishing Company: White River Junction, Vermont, 2008.

187. Lynd, L. R.; Woods, J., *Nature* **2011,** *474*, S20.

188. Biodiesel Production and Quality. National Biodiesel Board April 26 2007. http://www.biodiesel.org/pdf_files/fuelfactsheets/prod_quality.pdf.

189. Gerpen, J. V., *Fuel Processing Tech.* **2005,** *86*, 1097.

190. Vicente, G.; Martinez, M.; Aracil, J., *Bioresource Tech.* **2004,** *92*, 297.

191. Otera, J., *Chem. Rev.* **1993,** *93*, 1449.

192. Ainsworth, S., *C&EN News* **12 Sept. 2011,** *89* (37), 51 - 53.

193. Specht, Z.; Raley, D., *J. Chem. Ed.* **Submitted April 2012**.

194. *National Science Education Standard*. National Academy Press: 2101 Constitution Avenue, NW, Washington, DC, February 1998; Vol. fifth printing

195. Taber, K. S., *Chem. Ed.: Research and Practice In Europe* **2002,** *3*, 145-158.

196. Purser, G. H., *J. Chem. Educ.* **2001,** *78*, 981-983.

197. Kong, B. R. P. C., *J. Chem. Educ.* **1995,** *72*, 406-408.

198. Jue, T., *Quantum Mechanic Basic to Biophysical Methods. Fundamental Concepts in Biophysics*. Humana Press: New York, 2009; p 33.

199. Tsaparlis, G., *J. Chem. Educ.* **1997,** *74*, 922-925.

200. Coll, R. K., *Metaphor and Analogy in Science Education: The Role of Models, Mental Models and Analogies in Chemistry Teachin*. Springer: Netherlands, 2006; p 65-77.

201. Cardellini, L., *J. Chem. Educ.* **2010,** *87*, 482-486.

202. Orofino, H.; Faria, R. B., *J. Chem. Educ.* **2010,** *87*, 1451-1454.

203. Gillespie, R. J.; Matta, C. F., *Chem. Ed.: Research And Practice In Europe* **2001,** *2*, 73-90.

204. Pritchard, H. O., *J. Chem. Educ.* **2012,** *89*, 301-303.

205. Arduengo, A. J.; Dias, H. V. R.; Calabrese, J. C.; Davidson, F., *Organometallics* **1993,** *12*, 3405-3409.

206. Wang, H. M. J.; Lin, I. J. B., *Organometallics* **1998,** *17*, 972-975.